

Theoretical prediction and experimental verification
of SEI composition
formed on negative electrodes
in lithium ion batteries

Yasuhito Aoki

March 2023

Contents

Chapter 1

General Introduction

- 1.1 Increasing demands for lithium ion batteries
- 1.2 Working principle of LIBs and the importance of electrolyte solutions
- 1.3 Advances in solvent developments
- 1.4 Advances in electrolyte salt development
- 1.5 New dimension for electrolyte solution, concentration and dilution
- 1.6 Computational approach for electrolyte solutions
- 1.7 Outline of this work

References

Chapter 2

Quantitative analysis of solid electrolyte interphase and its correlation with the electrochemical performance of lithium ion batteries using concentrated LiPF₆/propylene carbonate

2.1 Introduction

2.2 Experimental section

2.3 Results and discussions

2.3.1 Charge and discharge properties of Li | graphite cells

2.3.2 Composition analysis of surface films on graphite electrode

2.3.3 Charge and discharge properties of Li|NCM523 cells

2.3.4 Charge and discharge properties of Full cells, Graphite | NCM523

2.4 Conclusions

References

Chapter 3

Predictive characterization of SEI formed on graphite negative electrodes for efficiently designing an effective electrolyte solutions

3.1 Introduction

3.2 Experimental

3.2.1. Electrolyte solutions

3.2.2. Charge and discharge tests

3.3 Results and discussions

3.3.1. Charge and discharge properties of graphite

3.3.2. Solution structure analysis

3.3.3. Correlations between theoretical calculation and irreversible capacity

3.4 Conclusions

References

Chapter 4

Effective approach by computational chemical prediction and experimental verification to elucidate SEI formation mechanism in LiPF_6 , LiFSI and LiBF_4 -containing electrolyte solutions

3.1 Introduction

3.2 Experimental

3.3 Results and discussions

3.4 Conclusions

References

Chapter 5

General conclusions and publication lists

5.1 General conclusions

5.2 Publication list

5.3 Other published works by the author

Chapter 1

General introduction

1.1 Increasing demands for lithium ion batteries

Currently, it is one of the global environmental issues to reduce greenhouse gas emissions for the realization of a carbon-neutral and decarbonized society. A number of policies and roadmaps have been formulated¹, and various kinds of technologies and services are being developed, not only in Japan but also all over the world. Lithium ion batteries (LIBs) are one of the promising devices that can serve as a large scale storage for renewable energy such as solar-power and wind-power electric generation, as well as an essential power source for electric vehicles. In Japan, CO₂ emissions from the transportation division account for about 20% of the total domestic CO₂ emissions, and hence electrification of automobiles is considered to offer a significant contribution to the reduction of CO₂ emissions².

Since the introduction of LIBs into commercial use in 1990s^{3,4,5}, great improvements have been achieved in their performance such as energy density,

durability, and safety. However, there still remain many technical issues, including safety issues, to meet the increasing demands for a longer driving range of electric vehicles, a larger storage for renewable energy. Research and development of electrode active materials are extensively progressing to respond those market needs, and those for electrolyte solutions are also active in order to utilize the fullest extent of the newly developed electrode materials^{6,7}.

Various kinds of characteristics are required for electrolyte solutions in LIBs³. One is a high ionic conductivity, which is generally achieved through high solubility and dissociation of lithium salts. Since the electromotive force of LIBs is typically as high as ca. 4 V, the electrolyte solution is exposed to very low and high potentials at negative and positive electrodes, respectively. Therefore, ideally, the electrochemical stability in a wide potential range is needed to allow LIBs efficiently rechargeable. Actually, however, almost all electrolyte solutions reductively decompose on negative electrodes such as graphite, and then the decomposition products precipitate on the electrode to form a protective surface film, which is referred to as SEI (solid electrolyte interphase). SEI functions as both an electronic insulator and a lithium ion conductor, and hence further decomposition of the electrolyte solution is suppressed. As the nature of SEI is influenced by chemical structures of electrolyte solutions, the solvents and

lithium salts need to be combined properly to realize LIBs with better performance.

A typical electrolyte solution used in commercial LIBs is about 1 mol/l LiPF_6 dissolved in carbonate ester solvents⁸. LiPF_6 shows well balanced properties in its solubility, chemical stability, and compatibility with negative and positive electrodes. The concentration is optimized at around 1 mol/l to maximize an ionic conductivity. Although the conventional electrolyte solutions show satisfactory performance to some extent, there still remains some disadvantages; LiPF_6 is instable against moisture and temperature, which causes performance degradation when exposed over a long period of time. In addition, carbonate ester solvents are volatile and flammable, which results in high risk for ignition of LIBs. Great efforts have been made all over the world to overcome those disadvantages in the conventional electrolyte solutions, for example, utilization of ionic liquid⁹, polymer electrolytes¹⁰ and inorganic solid state electrolytes¹¹. Among them, one of the most promising candidates is the highly concentrated electrolyte solution; an increase in the concentration of lithium salts to far higher than the conventional one and to almost saturation¹². Though the increased concentration results in a higher viscosity and a lower ion conductivity, the concentrated electrolyte solutions are thermally stable and possess higher stability against oxidation, which is quite important features for LIBs with long-term durability and high energy density.

Based on these background, Chapter 1 describes the working principle of LIBs and the history of research and development of electrolyte solutions. Electrolyte solutions are generally designed by selecting electrolyte salts, organic solvents, and additives through trial and error of battery performance tests. The concentration of electrolyte salts were typically set to ca. 1 mol/l, while the degree of freedom in designing electrolyte solutions can be remarkably broadened by adding the concentration as a new criterion. The author studied the stability of electrolyte solutions against reduction and SEI formation mechanism from the viewpoints of analytical chemistry, electrochemistry, and physical chemistry, based on the solvation structure and electron affinity of solvates, and tried to find guiding principles to select appropriate solvents, lithium salts, and the concentrations.

1.2 Working principle of LIBs and the importance of electrolyte solutions

Lithium ions in a positive electrode move back and forth between positive and negative electrodes through an electrolyte solution in charge and discharge reactions of LIBs^{13,14}. Figure 1-1 shows a schematic diagram of charge and discharge processes using a graphite negative-electrode and a lithium transition metal oxide positive-electrode as an example. The charge and discharge reactions proceed at positive and

negative electrode as follows, where M denotes transition metal (e.g. Ni, Mn, and Co).

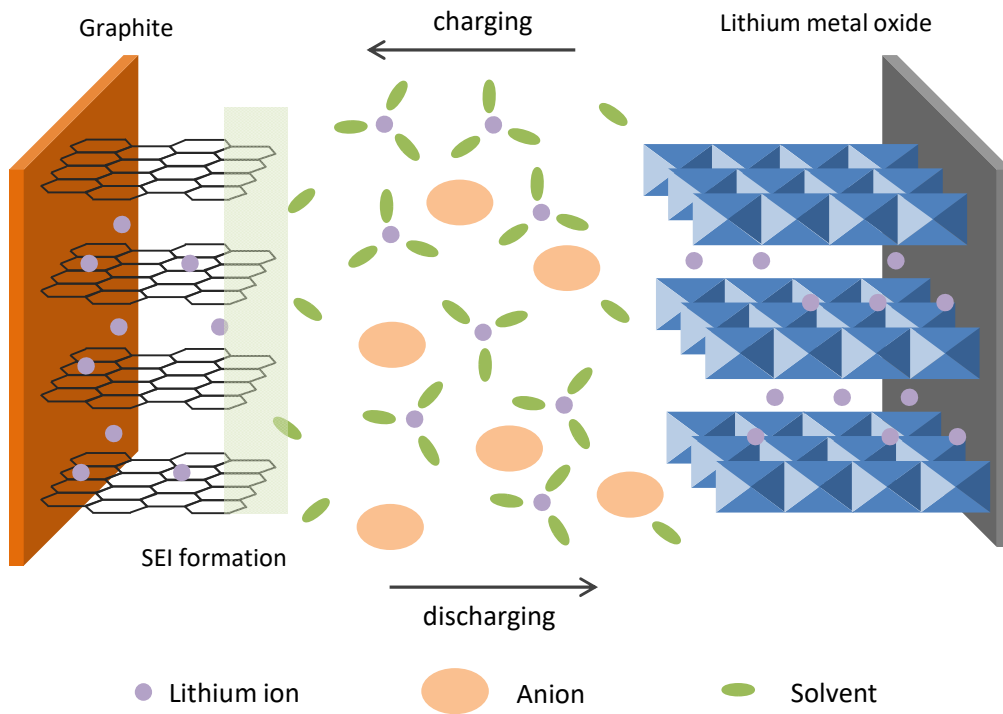
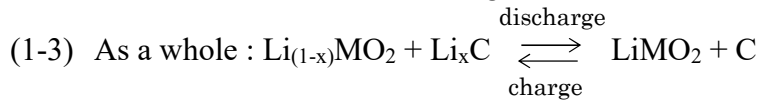
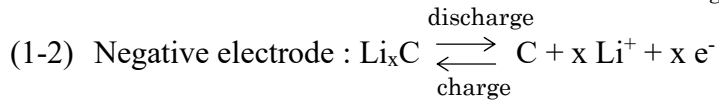
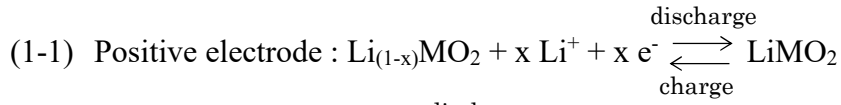


Figure 1.1 Schematic diagram of Lithium Ion Battery (LIB)

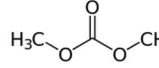
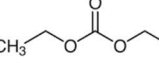
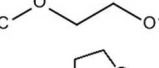
The charge reaction proceeds when a LIB is connected to an external power source, and lithium ions are released from the crystal structure of lithium transition metal oxide into an electrolyte solution to be intercalated into graphite layers. In the discharge reaction, a current is consumed through the external circuit while accompanying de-intercalation of

lithium ions from graphite and insertion of them into crystal structure of $\text{Li}_{(1-x)}\text{MO}_2$ through an electrolyte solution. Thus, the electrolyte solution is responsible for lithium ion transfer between active materials, and determines the charge and discharge performance of them. Ideally, electrolyte solutions should be electrochemically stable to positive and negative electrodes. However, it is difficult to fully satisfy the requirements thermodynamically, particularly for a negative electrode, and indeed the electrolyte solutions reductively decomposed to kinetically achieve a stable interface through the formation of SEI. Thus, the electrochemical stability of SEI, in addition to the active materials themselves, play a critical role in LIBs. The historical background of material research for electrolyte solutions is described in the following sections, including the selection of lithium salts and solvents, and the influence of electrolyte concentration, which has attracted much attention recently.

1.3 Advances in solvent developments

Solvents need to have the following characteristics, which is, of course, similar to the performance requirements for electrolyte solutions¹⁵. First, they are polar solvents with high dielectric constants to ensure the solubility of electrolyte salts. Second, they need to be electrochemically stable in a wide potential range from 0 to 4.5 V (v.s. Li⁺/Li) to achieve sufficient charge and discharge performance.

Table 1.1 organic carbonates and Esters as electrolyte solvents, modified for simplification from ref 3

Solvent	Structure	MW	Tm/°C	Tb/°C	η/cP @ 25°C	ϵ @ 25°C
EC		88	36.4	248	1.90 @ 40 °C	89.78
PC		102	-48.8	242	2.53	64.92
γ BL		86	-53	204	1.73	39
DMC		90	4.6	91	0.59 @ 20 °C	3.107
DEC		118	-74.3	126	0.75	2.805
DME		90	-58	84	0.46	7.2
THF		72	-109	66	0.46	7.4

Various kinds of carbonate solvents have been investigated for LIBs so far. Among them, propylene carbonate (PC) attracted much attention because it is in a liquid state at room temperature with a high dielectric constant, and has been commercially

used in lithium primary batteries^{16,17}. PC-based electrolyte solutions were compatible with non-graphitizable carbon negative-electrodes in LIBs. Several types of non-graphitizable carbon showed higher reversible capacities than graphite ($\sim 372 \text{ mAh g}^{-1}$), while they have serious shortcomings such as a wide difference in potential between charge and discharge reactions, and a high irreversible capacity, which is defined as a capacity that cannot be recovered in the subsequent discharge process. In addition, PC-based electrolyte solutions did not allow lithium ions to intercalate into graphite negative-electrodes; co-intercalation of lithium ions with PC molecules into graphite results in the ceaseless exfoliation of graphene sheets¹⁸. This fundamental problem was resolved by the use of ethylene carbonate (EC); in EC-based electrolyte solutions, lithium ions can be successfully released from EC molecules to be intercalated into graphite electrodes. Graphite negative-electrodes show an acceptably small difference in charge/discharge potentials and low irreversible capacities, unlike non-graphitizable carbon. Hence, graphite and EC have been most commonly used as a negative electrode and a main solvent for an electrolyte solution in commercial LIBs. EC differs only slightly in molecular structure from PC. EC is a cyclic carbonate that is solid at room temperature and EC-based electrolyte solutions are highly viscous. Accordingly, EC is usually mixed with liquid carbonates such as PC¹⁹, low-viscosity dimethyl carbonate

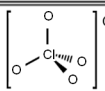
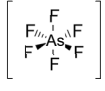
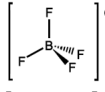
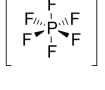
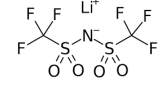
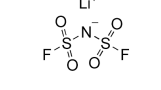
(DMC)²⁰ and diethyl carbonate (DEC)²¹, which improves the solubility of lithium salts and reduce the viscosity of electrolyte solutions.

Ethers were also investigated as a main solvent for LIBs, but ether-based electrolyte solutions did not show satisfactory charge/discharge performance due to severe oxidative decomposition at positive electrodes²². In addition, ether is readily co-intercalated into graphite due to the strong solvation ability. Its high vapor pressure also causes a safety issue, and ethers have gradually become out of the research scope for practical electrolyte solutions.

1.4 Advances in electrolyte salt development

The properties required for lithium salts are quite similar to those for solvents. The high solubility and dissociation of lithium salts are considered to enhance the lithium ion conductivity of electrolyte solutions³. The dissociation constant varies greatly depending on the counter anions; e.g., ClO₄⁻, BF₄⁻, AsF₆⁻, PF₆⁻, and imide anions such as (FSO₂)₂N⁻ and (CF₃SO₂)₂N⁻. Both electrochemical and thermal stability of the counter anions are required, while the ability to form an SEI through the reductive decomposition is also needed, as is the case for solvents.

Table 1.2 Electrolyte salts as electrolyte solutes, modified for simplification from ref 3

Salt	Structure	MW	Tm/°C	Al corrosion	$\sigma/\text{mS cm}^{-1}$ 1.0 mol/l @ 25°C	
					in PC	in EC/DMC
LiClO ₄		236	236	N	5.6	8.4
LiAsF ₆	Li ⁺ 	195.9	340	N	5.7	11.1
LiBF ₄		93.9	293	N	3.4	4.9
LiPF ₆	Li ⁺ 	151.9	200	N	5.8	10.8
LiTFSI		286.9	234	Y	5.1	9.0
LiFSI		287.1	236	Y	-	12.1

From these perspectives, various kinds of lithium salts have been investigated so far. Historically, LiClO₄ was extensively studied in the 1970s and 1980s because of the high ionic conductivity, high solubility, high thermal and electrochemical stability²³. However, it did not reach practical application because it causes the corrosion of an Al current collector of positive electrodes. LiBF₄^{24,25} and LiAsF₆^{24,26} were considered as candidates at the same time to overcome the difficulty of LiClO₄. However, LiBF₄ had a low ionic conductivity due to its small dissociation constant, and hence it could not be

put into practical use. Though LiAsF_6 sufficiently has a high ion conductivity and a high stability against oxidation and reduction that can withstand the commercial use, it was not commercially practical because it contains As, which shows very high toxicity depending on its valence.

LiPF_6 is the most commonly used lithium salt in commercial LIBs²³. Almost 1 mol/l LiPF_6 dissolved in carbonate ester solvents exhibits a high ionic conductivity enough to use on commercial basis. LiPF_6 can be reductively decomposed on negative electrodes to form an acceptably stable SEI. Although the stability of LiPF_6 against hydrolysis and high temperatures are lower than those for the other lithium salts, it can deliver well-balanced performance in all characteristics. Therefore, LiPF_6 has established a position as a standard electrolyte for LIBs in practical use.

Recently, lithium salts with fluorine-containing molecular anions such as LiTFSI (lithium bis(trifluoromethanesulfonyl)imide, $\text{Li}(\text{CF}_3\text{SO}_2)_2\text{N}$) and LiFSI (lithium bis(fluorosulfonyl)imide, $\text{Li}(\text{FSO}_2)_2\text{N}$) have been attracting much attention^{27,28}; these imide-based electrolyte solutions exhibit a high ionic conductivity close to LiPF_6 -based ones, and have the high thermal stability and low reactivity with moisture. Though they have cost disadvantages, it is considered to be a promising candidate for next-generation LIBs.

1.5 New dimension for electrolyte solution, concentration

The concentration of lithium salts is usually set to almost 1 mol/l because the ionic conductivity of electrolyte solutions reaches the highest level. A further increase in the concentration results in a decrease in the ionic conductivity. However, the highly concentrated electrolyte solutions, close to saturating concentrations, exhibit high stability against oxidation and reduction, and deliver high safety due to low vapor pressure and high thermal stability^{12,29}. Due to these favorable characteristics, the highly concentrated electrolyte solutions are considered as a candidate for the next-generation ones that can achieve higher voltages, long-term durability, and higher safety. In addition, reactions at an interface between an electrode and a highly concentrated electrolyte solution differ from those for conventional electrolyte solutions. For example, lithium ion could not be intercalated into graphite layers due to their exfoliation when PC was used as a solvent at the typical concentration of ca. 1 mol/l, while the intercalation/de-intercalation reactions flawlessly proceed when the concentration increases significantly³⁰. The highly concentrated electrolyte solutions achieve high oxidative stability for 5 V-class high voltage positive electrode active materials³¹, and enable the charge/discharge reactions at high rates. On the other hand, there are significant challenges to their practical application; the high viscosity results in slow

permeation into the electrodes and separator, and very high cost due to the usage of a very large amount of lithium salts^{32,33}.

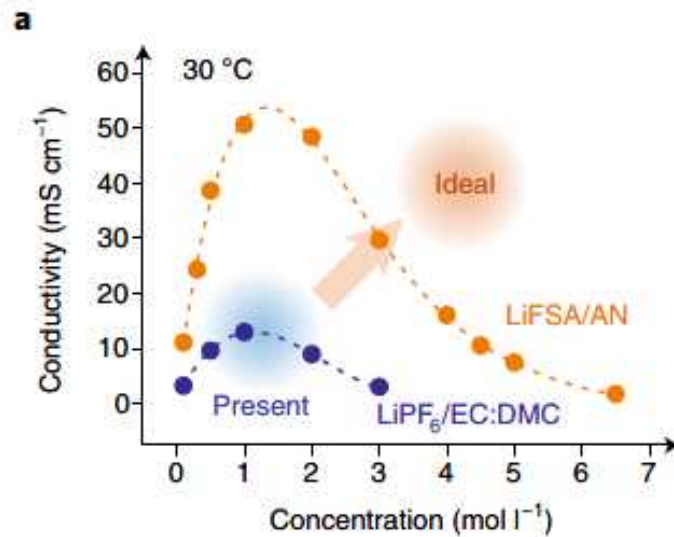


Figure 1.2 Variation of ionic conductivity with concentration of lithium salts of electrolyte solutions. The ionic conductivity is dependent on the electrolyte composition and concentration, excerpts from ref 29.

1.6 Computational approach for electrolyte solutions

Although various kinds of solvents, lithium salts and additives have been investigated to improve the performance of electrolyte solutions, the electrochemical reactions that occur at an interphase between an electrode and an electrolyte solution have not yet been fully elucidated. In particular, it is difficult to experimentally demonstrate the reduction and decomposition reactions of electrolyte solutions and the subsequent formation of SEI. Hence, theoretical calculations are often used to predict the reaction mechanism.

When estimating the electrochemical stability of electrolyte solutions by computational chemistry, *ab initio* calculation is often used to partially model the solvation structure in the electrolyte solution because of its computational accuracy and versatility³⁴. It is popular to use HOMO and LUMO energy levels to estimate the stability of solvation structures against oxidative and reduction, respectively^{35,36}, while the calculation values easily change depending on calculation methods and basis functions used in the calculations. To avoid these difficulties, electron affinity (EA) was used to evaluate the stability of solvation structures against reduction in this study³⁷.

Since electrolyte solutions consist of a number of molecules of solvents and lithium salts, molecular dynamics calculations combined with *ab initio* calculation (AIMD) are being used to elucidate the reactions at an electrolyte solution/electrode interface³⁸. Although the computational cost of AIMD is significantly high, it has provided detailed and plausible results to account for a part of experimental data, and is still developing to clarify a whole picture of SEI formation reactions. In AIMD simulations, EA is often used as a measure for the reduction stability of electrolyte solutions^{39,40}.

1.7 Outline of this work

It is important to elucidate the formation reactions and the chemical components of SEI qualitatively and quantitatively to design superior electrolyte solutions that can improve charge/discharge performance of LIBs. In Chapter 2, qualitative and quantitative analysis of surface films that formed on graphite negative electrodes during charge-discharge cycles was conducted using electrolyte solutions of different concentrations. The constituents of surface films were correlated with electrochemical properties such as irreversible capacity and surface film resistance.

In Chapter 3, the author aimed to establish a methodology for designing electrolyte solutions efficiently, which is the main subject of this study. Since the reductive decomposition of electrolyte solutions on the surface of graphite negative electrodes is considered to depend on the solution structure, especially the solvation structure of lithium ions, the structure of solvates in electrolyte solutions was estimated experimentally by laser Raman spectroscopy, and the structural optimization was performed by density functional theory. Then, EA and LUMO distribution of each solvate was evaluated by density functional theory (DFT) calculations, and was used as an indicator to assess the reductive stability. Furthermore, by considering the electrochemical performance of graphite electrodes and the composition of SEI, design

guidelines for electrolyte solutions were developed.

In Chapter 4, the validity of computational approaches discussed above was verified using electrolyte solutions with different lithium salts. The theoretical predictions of the reductive stability of electrolyte solutions were contrasted with the results of the compositional analysis of the surface films formed on graphite negative electrodes. As is the case in Chapter 3, the solvation structure was estimated by laser Raman spectroscopy and EA and LUMO distributions were calculated by DFT to predict the reductive stability and the starting point of decomposition reaction in the solvation structure. To verify the predictions experimentally, cyclic voltammetry of graphite electrodes and composition analysis of the surface films on them were conducted. As a result, this study showed that the formation mechanism and electrochemical properties of SEI can be elucidated by an appropriate combination of experimental estimation of solvation structures, structural optimization by DFT at a laboratory level, and quantitative analysis of the surface films formed on graphite negative electrode.

In Chapter 5, this study was summarized, and an outlook for future research and development of electrolyte solutions was described.

References

- [1] Ministry of Economy, Trade and Industry, Green Growth Strategy Through Achieving Carbon Neutrality in 2050,
<https://www.meti.go.jp/press/2020/12/20201225012/20201225012-1.pdf>
- [2] Ministry of Land, Infrastructure, Transport and Tourism,
https://www.mlit.go.jp/sogoseisaku/environment/sosei_environment_tk_000007.html
- [3] Xu, K.; Nonaqueous Liquid Electrolytes for Lithium-Based Rechargeable Batteries, *Chem. Rev.* **2004**, 104, 4303-4417
- [4] Nishi, Y.; Azuma, H.; Omaru, A. *U.S. Patent*, **1990**, 4,959,281.
- [5] Dahn, J. R.; von Sacken, U.; Fong, R. Extended Abstracts of the 178th Electrochemical Society Meeting, Seattle, WA, Oct. 14-19, 1990; Abstract No. 42; Electrochemical Society: Pennington, NJ.
- [6] Li, X.; Colclasure, M.; Finegan, P.; Ren, D.; Feng, X.; Cao, L.; Yang, Y.; Smith, K. Degradation mechanisms of high capacity 18650 cells containing Si graphite anode and nickel-rich NCM cathode, *Electrochim. Acta.*, **2019**, 297, 1109–1120

- [7] Liu, W.; Oh, P.; Liu, X.; Lee, J.; Cho, W.; Chae, C.; Kim, Y.; Cho, J. Nickel-rich layered lithium transition-metal oxide for high-energy lithium-ion batteries, *Angew. Chem. Int. Ed.* **2015**, 54, 4440 – 4457.
- [8] Xu, K. Electrolytes and interphases in Li-ion batteries and beyond. *Chem.Rev.* **2014**, 114, 11503–11618.
- [9] Watanabe, M. Application of ionic liquids to energy storage and conversion materials and devices. *Chem. Rev.* **2017**, 117, 7190–7239.
- [10]. Hallinan, T.; Balsara, P. Polymer electrolytes. *Annu. Rev. Mater. Res.* **2013**, 43, 503–525.
- [11]. Manthiram, A.; Yu, X.; Wang, S. Lithium battery chemistries enabled by solid-state electrolytes. *Nat. Rev. Mater.* **2017**, 2, 16103
- [12] Yamada, Y.; Yamada, A. Review - Superconcentrated Electrolytes for Lithium Batteries, *J. Electrochem. Soc.*, **2015**, 162, A2406-A2423
- [13] Goodenough, B.; Park, S. The Li-Ion Rechargeable Battery: A Perspective, *J. Am. Chem. Soc.* **2013**, 135, 1167–1176

- [14] Goodenough, B.; Kim, Y. Challenges for Rechargeable Li Batteries, *Chem. Mater.* **2010**, *22*, 587–603
- [15] Ue, M. Electrolytes: nonaqueous, In Encyclopedia of electrochemical power sources; Garche, J.; Dyer, C.; Moseley, P.; Ogumi, Z.; Rand, D.; Scrosati, B., Eds.; Elsevier, Amsterdam, Netherlands, 2009; vol.5; 71-84.
- [16] Selim, R.; Bro, P. Some Observations on Rechargeable Lithium Electrodes in a Propylene Carbonate Electrolyte, *J. Electrochem. Soc.* **1974**, *121*, 1457.
- [17] Rauh, D.; Brummer, B. The effect of additives on lithium cycling in propylene carbonate, *Electrochim. Acta*, **1977**, *22*, 75
- [18] Fong, R.; von Sacken, U.; Dahn, J. R. Studies of Lithium Intercalation into Carbons Using Nonaqueous Electrochemical Cells, *J. Electrochem. Soc.*, **1990**, *137*, 2009.
- [19] Yamaura, J.; Ozaki, Y.; Morita, A.; Ohta, A. High voltage, rechargeable lithium batteries using newly-developed carbon for negative electrode material, *J. Power Sources*, **1993**, *43*, 233.

- [20] Guyomard, D.; Tarascon, J. M. Rechargeable $\text{Li}_{1+x}\text{Mn}_2\text{O}_4$ / Carbon Cells with a New Electrolyte Composition: Potentiostatic Studies and Application to Practical Cells, *J. Electrochem. Soc.* **1993**, 140, 3071
- [21] Aurbach, D.; Ein-Eli, Y.; Markovsky, B.; Zaban, A.; Luski, S.; Carmeli, Y.; Yamin, H. The Study of Electrolyte Solutions Based on Ethylene and Diethyl Carbonates for Rechargeable Li Batteries: II . Graphite Electrodes, *J. Electrochem. Soc.* **1995**, 142, 2882.
- [22] Campbell, S. A.; Bowes, C.; McMillan, R. S. The electrochemical behaviour of tetrahydrofuran and propylene carbonate without added electrolyte *J. Electroanal. Chem.* **1990**, 284, 195
- [23] Tarascon, J. M.; Guyomard, D. New electrolyte compositions stable over the 0 to 5 V voltage range and compatible with the $\text{Li}_{1+x}\text{Mn}_2\text{O}_4$ /carbon Li-ion cells, *Solid State Ionics*, **1994**, 69, 293
- [24] Koch, V. R.; Young, J. H. The Stability of the Secondary Lithium Electrode in Tetrahydrofuran - Based Electrolytes, *J. Electrochem. Soc.* **1978**, 125, 1371
- [25] Takata, K.; Morita, M.; Matsuda, Y. Cycling Characteristics of Secondary Li Electrode in LiBF_4 / Mixed Ether Electrolytes, *J. Electrochem. Soc.* **1985**, 132, 126

- [26] Rauh, R. D.; Reise, T. F.; Brummer, S. B. Efficiencies of Cycling Lithium on a Lithium Substrate in Propylene Carbonate *J. Electrochem. Soc.* **1978**, 125, 186
- [27] Krause, L. J.; Lamanna, W.; Summerfield, J.; Engle, M.; Korba, G.; Loch, R.; Atanasoski, R. Corrosion of aluminum at high voltages in non-aqueous electrolytes containing perfluoroalkylsulfonyl imides; new lithium salts for lithium-ion cells, *J. Power Sources*, **1997**, 68, 320
- [28] Foropoulos, J.; DesMarteau, D. D. Synthesis, properties, and reactions of bis((trifluoromethyl)sulfonyl) imide, $(\text{CF}_3\text{SO}_2)_2\text{NH}$, *Inorg. Chem.* **1984**, 23, 3720
- [29] Yamada, Y.; Wang, J.; Ko, S.; Watanabe, E.; Yamada, A. Advances and issues in developing salt-concentrated battery electrolytes, *Nature Energy*, **2019**, 4, 269
- [30] Doi, T.; Masuhara, R.; Hashinokuchi, M.; Shimizu, Y.; Inaba, M. Concentrated LiPF_6/PC electrolyte solutions for 5-V $\text{LiNi}_{0.5}\text{Mn}_{1.5}\text{O}_4$ positive electrode in lithium-ion batteries. *Electrochim. Acta*, **2016**, 209, 219–224.
- [31] Superconcentrated electrolytes for a high-voltage lithium-ion battery, Wang, J.; Yamada, Y.; Sodeyama, K.; Chiang, H.; Tateyama, Y.; Yamada, A. Superconcentrated electrolytes for a high-voltage lithium-ion battery, *Nat. Commun.* **2016**, 7, 12032.

- [32] Zheng, H.; Li, J.; Song, X.; Liu, G.; Battaglia, S. A comprehensive understanding of electrode thickness effects on the electrochemical performances of Li-ion battery cathodes. *Electrochim. Acta*, **2012**, *71*, 258–265.
- [33] Sander, S.; Erb, R.; M., Li.; L., Gurijala, A.; Chiang, M. High performance battery electrodes via magnetic templating. *Nat. Energy*, **2016**, *1*, 16099
- [34] Seo, D.; Reininger, S.; Kutcher, M.; Redmond, K.; Euler, W.; Lucht, B. Role of Mixed Solvation and Ion Pairing in the Solution Structure of Lithium Ion Battery Electrolytes. *J. Phys. Chem. C* **2015**, *119*, 14038-14046.
- [35] Borodin, O.; Smith, G. Quantum Chemistry and Molecular Dynamics Simulation Study of Dimethyl Carbonate: Ethylene Carbonate Electrolytes Doped with LiPF₆. *J. Phys. Chem. B* **2009**, *113*, 1763-1776.
- [36] Xing, L.; Zheng, X.; Schroeder, M.; Alvarado, J.; Cresce, A. W.; Xu, K.; Li, Q.; Li, W. Deciphering the Ethylene Carbonate–Propylene Carbonate Mystery in Li-Ion Batteries. *Acc. Chem. Res.* **2018**, *51*, 282-289.
- [37] Ue, M.; Murakami, A.; Nakamura, S. Anodic Stability of Several Anions Examined by Ab Initio Molecular Orbital and Density Functional Theories. *J. Electrochem. Soc.* **2002**, *149*, A1572-A1577.

- [38] Tateyama, Y. First-Principles Calculation Study on Solid Electrolyte Interphase (SEI) in Lithium Ion Battery. *J. Comput. Chem. Jpn.* **2019**, *18*, 18-28.
- [39] Okuno, Y.; Ushirogata, K.; Sodeyama, K.; Tateyama, Y. Decomposition of the fluoroethylene carbonate additive and the glue effect of lithium fluoride products for the solid electrolyte interphase : an ab initio study. *Phys. Chem. Chem. Phys.* **2016**, *18*, 8643-8653.
- [40] Sodeyama, K.; Yamada, Y.; Aikawa, K.; Yamada, A.; Tateyama, Y. Sacrificial Anion Reduction Mechanism for Electrochemical Stability Improvement in Highly Concentrated Li-Salt Electrolyte. *J. Phys. Chem. C* **2014**, *118*, 14091-14097.

Chapter 2

Quantitative analysis of solid electrolyte interphase and its correlation with the electrochemical performance of lithium ion batteries using concentrated LiPF₆/propylene carbonate

2.1. Introduction

Lithium ion batteries (LIB) have been used not only as power sources for portable devices, but also as large-scale batteries for automobile and stationary applications¹. Many studies are seeking to further increase their energy density and durability for use in electric vehicles. To achieve a higher energy density, two approaches are mainly taken: one is to use active materials with higher capacity, such as LiNi_{0.8}Mn_{0.1}Co_{0.1}O₂ (NCM811) positive electrode^{2,3} and Si negative electrode,^{4,5} and the other is to use higher voltage cathode materials such as LiCoPO₄ and spinel-type LiNi_{0.5}Mn_{1.5}O₄ which have charge/discharge potentials of 5 V (vs. Li/Li⁺).⁶⁻⁸ For realizing LIBs using these materials, it is important to develop stable electrolyte solutions with a wide electrochemical potential window. Many studies have reported the use of a surface

coating on the cathode and additives to enhance durability against oxidative decomposition.⁹⁻¹¹

Recently, it has been reported that concentrated electrolyte solution possesses a wide electrochemical potential window,^{12,13} and we have demonstrated low irreversible capacity and high coulombic efficiency of a 5-V $\text{LiNi}_{0.5}\text{Mn}_{1.5}\text{O}_4$ cathode in PC-based concentrated electrolyte solutions.^{14,15} Decomposition of electrolyte solutions proceeds during the charge and discharge processes to form solid electrolyte interphase (SEI, often referred to as CEI, Cathode Electrode Interphase, for positive electrode) on both the negative and positive electrodes, which plays an important role in achieving stable battery performance. The composition of the SEI and CEI might change depending on the electrolyte salt concentration, and this could affect the electrochemical performance.¹⁶⁻¹⁸ In this study, we qualitatively and quantitatively elucidated the SEI compositions on graphite negative and CEI composition on $\text{LiNi}_{0.5}\text{Co}_{0.2}\text{Mn}_{0.3}\text{O}_2$ (NCM523) positive electrodes in a conventional 1 mol/l ethylene carbonate (EC)-based and a concentrated electrolyte solution, and tried to correlate quantitatively the amount and composition of the SEI with electrochemical performance such as irreversible capacity and electrochemical impedance in each solution.

2.2. Experimental

The charge and discharge performance of Li|graphite and Li|NCM523 two-electrode cells was investigated using 2032 coin-type cells. The graphite electrode was composed of graphite powder as an active material, and styrene-butadiene rubber (SBR) and carboxymethyl cellulose (CMC) as binders (98:1:1 by weight). The NCM523 electrode consisted of NCM523 powder as an active material, polyvinylidene difluoride as a binder, and acetylene black as a conductive agent (92:5:3 by weight). Electrolyte solutions of two different concentrations were prepared for comparison: one was a conventional electrolyte solution of 1 mol/l LiPF₆ dissolved in a mixture of EC and DMC (1:2 by vol.), and the other was a highly concentrated electrolyte solution of 4.45 mol/kg LiPF₆/PC (nearly saturated). Charge/discharge tests were performed at a 0.1 C rate between 0.01 and 1.5 V and between 3.0 and 4.6 V for Li|graphite and Li|NCM523 cell, respectively, for 15 cycles at 30 °C.

AC impedance measurements of the Li|graphite and Li|NCM523 coin cells were conducted using a VSP potentiostat/galvanostat (Biologics Inc.) after the 2nd and 15th cycles. Potential was set to 0.2 V vs Li/Li⁺ for the Li|graphite cells, and 3.8 V vs Li/Li⁺ for Li|NCM523 cells. Measurement frequency ranges and potential modulation were set to from 100 kHz to 10 mHz and ±10 mV, respectively.

After the charge/discharge test, the coin cell was disassembled in an Ar-filled glove box to take out the working electrode, which was then rinsed in DMC to remove the electrolyte solution and dried under vacuum at room temperature. The composition and amount of the formed surface films were investigated by X-ray photoelectron spectroscopy (Quanta SXM, ULVAC-PHI) and extraction analysis. In XPS measurements, the acceleration voltage and the emission current of monochromatic Al $K\alpha$ X-ray gun were set at 15 kV and 3 mA, respectively. Depth profiles were collected after Ar ion etching¹⁹. The etching rate was presumed to be 5.2 nm/min for SiO₂ equivalents. For the extraction analysis, D₂O extraction was conducted to collect the surface films formed on the graphite and NCM523 electrodes. The addition of D₂O to the electrodes decomposed the surface film into various chemical species, and the extracts that are soluble in D₂O were analyzed by H-NMR and ion chromatography (IC) to identify organic and inorganic components, respectively.²⁰ Raman spectra were obtained by a Model PDP 320 (Photon Design) using a spectrometer equipped with a grating of 1800 gr/mm with a 320 mm focus length and a 514.5 nm Ar ion laser as an excitation source.

2.3. Results and Discussions

2.3.1 Charge and discharge properties of Li | graphite cells

Charge/discharge curves and cycle performances of Li|graphite cells are shown in Figure 2.1. Figure 2.1 (b) clearly indicates that PC-based electrolyte solution can be used for charge/discharge of the graphite negative electrode with high coulombic efficiency when the LiPF₆ concentration is high²¹⁻²³. The coulombic efficiency reached almost 100% for both the conventional and concentrated electrolyte solutions within the initial a few charge/discharge cycles, as shown in Figure 2.2 and Table 2.1. These results suggest that solid electrolyte interphase (SEI) was effectively formed through reductive decomposition of each electrolyte solution to stabilize the electrode/electrolyte interface, regardless of the concentration of LiPF₆. The total irreversible capacities over the 15 cycles were evaluated to be 83.1 and 71.3 mAh/g for the conventional and concentrated electrolyte solution, respectively. Thus, the electrolyte decomposition was slightly suppressed in the highly concentrated electrolyte solution (Table 2.1).

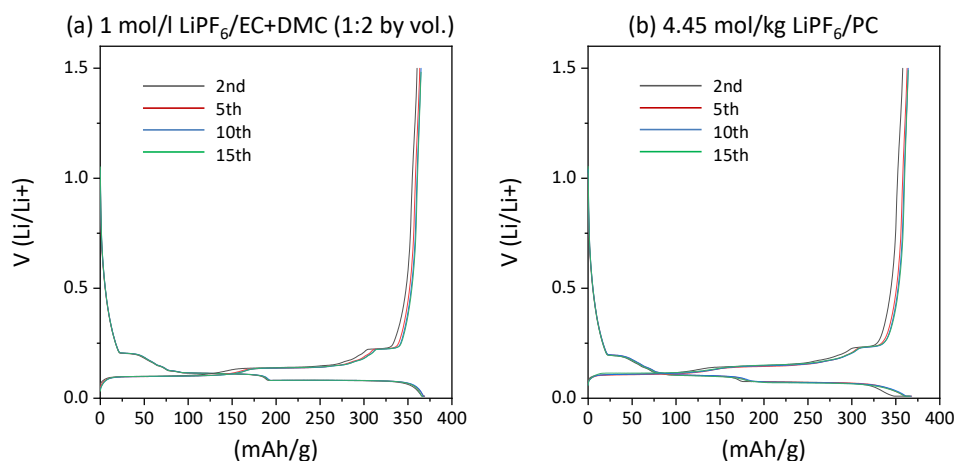


Figure 2.1 Charge and discharge curves of Li | graphite cells with (a) conventional 1 mol/l LiPF₆/EC+DMC (1:2 by vol) and (b) nearly saturated 4.45 mol/kg LiPF₆/PC electrolyte solutions.

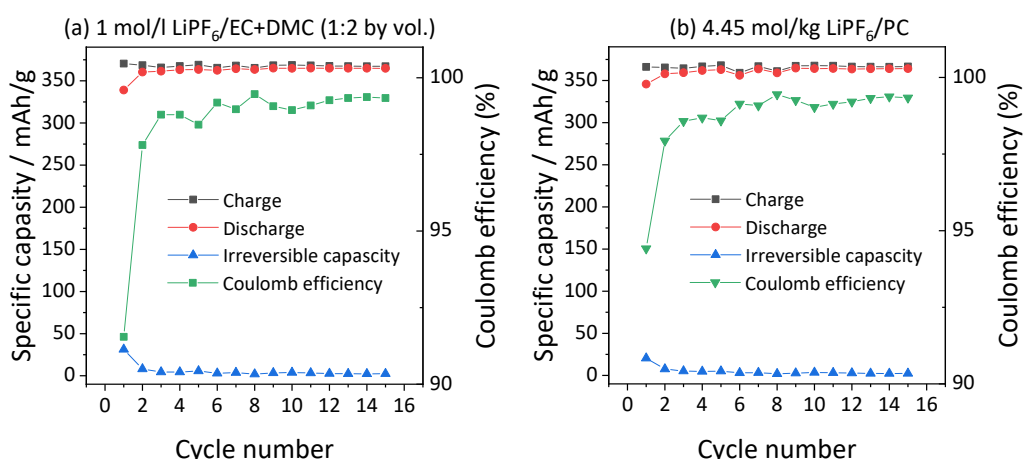


Figure 2.2 Variation of charge, discharge and irreversible capacities, and coulomb efficiencies with cycle number for Li | graphite cells with (a) conventional 1 mol/l LiPF₆/EC+DMC (1:2 by vol) and (b) nearly saturated 4.45 mol/kg LiPF₆/PC.

To elucidate the correlation between surface film- and interfacial-resistance for the graphite negative electrode, electrochemical AC impedance measurements were performed using the Li|graphite coin-type cell, and the results are shown in Figure 2.3.

In the conventional electrolyte solution (Figure 2.3 (a)), two semi-circles were

observed; the semi-circles in the high- and low-frequency regions are identified as impedances for the surface film and the interfacial Li^+ transfer at the graphite/electrolyte interface, respectively.^{24,25} The total interfacial resistance was 34.7Ω at the 15th cycle (Table 2.2). On the other hand, only one depressed semicircle was seen for the concentrated electrolyte solution, suggesting overlapping of the two semicircles (Figure 2.3 (b)). The total interfacial resistance (123Ω) was about 3.6 times as high as that in the conventional electrolyte solution (Table 2.2). The difference in irreversible capacity between the conventional and concentrated electrolyte solutions was small as shown in Table 2.1, and therefore the increase in interfacial resistance should result not only from an increase in the amount of surface film formed, but also from the difference in chemical composition.

Table 2.1 Total irreversible capacities and average coulomb efficiencies of Li | graphite cells in 15 cycles.

	Total irreversible capacity (mAh/g)	Average coulomb efficiency (%)
1 mol/l $\text{LiPF}_6/\text{EC}+\text{DMC}$ (1:2 by vol.)	83.1	98.5
4.45 mol/kg LiPF_6/PC	71.3	98.7

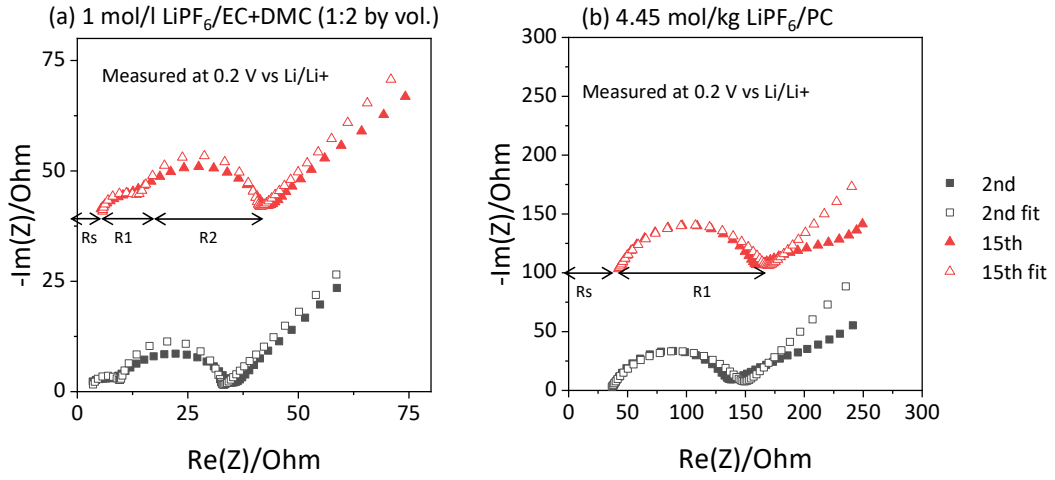


Figure 2.3 Nyquist plots and the numerical fitting of graphite electrodes in (a) conventional 1 mol/l LiPF₆/EC+DMC (1:2 by vol) and (b) nearly saturated 4.45 mol/kg LiPF₆/PC after the 2nd and the 15th cycle.

Table 2.2 Fitting results for Nyquist plots of graphite electrodes in Figure 2.2.

		Rs (Ω)	R1 (Ω)	R2 (Ω)
1 mol/l LiPF ₆ /EC:DMC=1:2	2 nd	3.2	6.6	22.3
	15 th	5.6	8.5	26.2
		Rs (Ω)	R1 (Ω)	
4.45mol/kg LiPF ₆ /PC	2 nd	35	112	
	15 th	41	123	

To confirm the increase in the impedance, we have also checked the rate capability of the Li | graphite cells. The graphite electrode was charged to 0.01 V to discharge to 1.5 V with different C-rate from 0.1 C to 2 C. Figure 2.4 shows that the decrease in the capacity is much more pronounced at the cell with the concentrated electrolyte solution than the conventional one, as expected from the impedance measurement. This shows

that the surface film with higher resistance exists at the surface of the graphite electrode in the concentrated electrolyte solution.

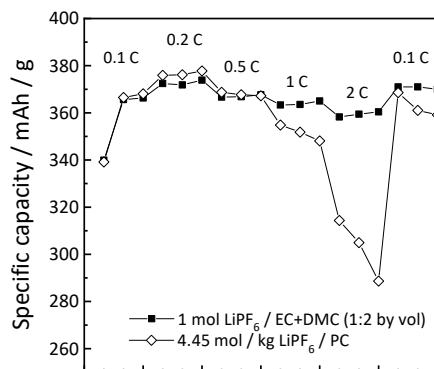


Figure 2.4 Rate capability of graphite electrodes in (a) conventional 1 mol/l LiPF₆/EC+DMC (1:2 by vol) and (b) nearly saturated 4.45 mol/kg LiPF₆/PC.

2.3.2 Composition analysis of surface films on graphite electrode

XPS F1s and C1s spectra of the surfaces of graphite electrodes after 15 cycles in the conventional and concentrated electrolyte solutions are shown in Figure 2.5. The F1s spectrum for the conventional electrolyte solution exhibited two peaks at 685 and 687 esV, which derived from LiF and LiPF₆, respectively (Figure 2.5 (a)). LiPF₆ is a residue on the graphite electrode after rinsed with DMC. On the other hand, the use of the concentrated electrolyte solution resulted in a strong peak of LiF with a weak shoulder due to the residual LiPF₆, which suggests that LiPF₆ decomposed preferentially and the resultant LiF was easily deposited on the electrode because of the

nearly saturated conditions. The C1s spectrum for the conventional electrolyte solution showed three peaks (Figure 2.5 (b)); one at 284.5 eV was identified as C=C of graphite, and another at 286 eV was ether C–O component. The other strongest peak at 289 eV was assigned to ester C=O and carbonate (Li_2CO_3). The atomic concentrations, which were evaluated from Li1s, C1s, O1s, F1s, and P2s spectra, are summarized in Table 2.3. The amount of ester C=O and carbonate precipitated on the graphite electrode in the conventional electrolyte solution (12.0 atomic%) was 7 times larger than that of LiF (1.7 atomic%). These results suggest that the decomposition products of EC and/or DMC solvent molecules dominantly gave an effective surface film in the conventional electrolyte solution. On the other hand, C1s spectrum for the concentrated electrolyte solution showed a strong peak at 284.5 eV due to graphite along with a shoulder peak at 286 eV for ether C–O component (Figure 2.5 (b)). Notably, almost no peak was detected at 289 eV for ester C=O or carbonate. Based on these results, the reductive decomposition of LiPF_6 preferentially occurred in preference to PC solvent molecules in the concentrated electrolyte solution to form a LiF-rich surface film with a high resistance.

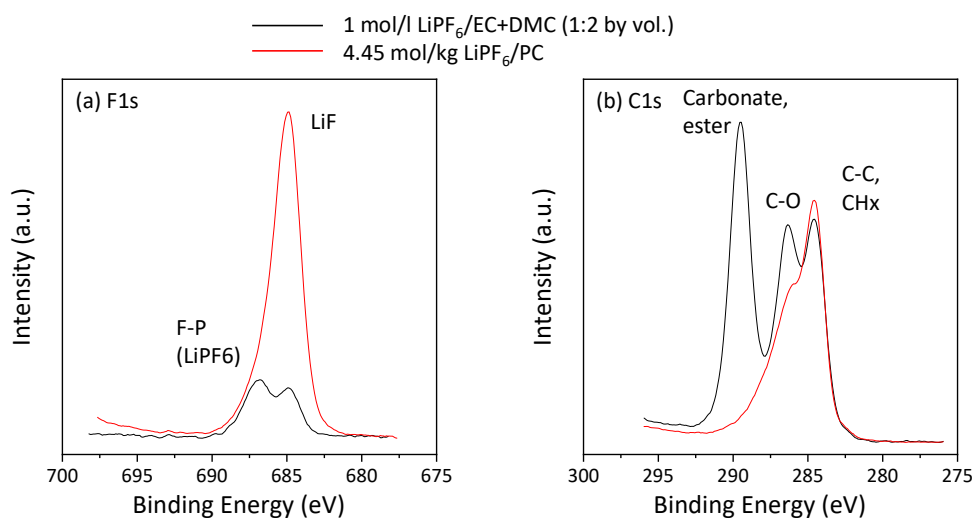


Figure 2.5 (a) F1s and (b) C1s spectra of the graphite electrode surface after 15 cycles in conventional 1 mol/l LiPF₆/EC+DMC (1:2 by vol) and nearly saturated 4.45 mol/kg LiPF₆/PC.

Table 2.3 Atomic composition percentages of (a) whole surface films, and (b) C- and (c) F-containing compounds in the surface films of graphite electrode that formed by conventional 1 mol/l LiPF₆/EC+DMC (1:2 by vol) and nearly saturated 4.45 mol/kg LiPF₆/PC.

(a) Whole surface films					
	(atomic%)				
	Li	C	O	F	P
1 mol/l LiPF ₆ /EC+DMC (1:2 by vol.)	21.6	30.1	41.4	4.4	0.6
4.45 mol/kg LiPF ₆ /PC	23.4	33	14	24.6	3.5

(b) C-containing compounds				
	(atomic%)			
	Carbonate, Ester	carboxylic acid / salt	C-O	C-C, CHx
1 mol/l LiPF ₆ /EC+DMC (1:2 by vol.)	12.0	1.5	8.1	8.5
4.45 mol/kg LiPF ₆ /PC	0	3.8	10.3	18.9

(c) F-containing compounds		
	(atomic%)	
	F-P	F- (LiF)
1 mol/l LiPF ₆ /EC+DMC (1:2 by vol.)	2.7	1.7
4.45 mol/kg LiPF ₆ /PC	3.3	21.3

The elemental distribution in the direction of depth of the surface film on graphite electrode was obtained by XPS measurements using an Ar ion etching technique. When the conventional electrolyte solution was used, the atomic concentration of C atom increased within 50 nm from the surface, and a strong signal was detected in the interior deeper than 50 nm (Figure 2.6 (a)). These results suggest that the surface film should be thoroughly etched by Ar ion at a depth of ca. 50 nm to expose the surface of graphite. In the same depth range, the signals of O and Li decreased significantly. Therefore, the thickness of the surface film was estimated to be about 50 nm and it should be mainly composed of O- and Li-rich compounds, such as ester C=O and carbonate, which is consistent with the results in Figure 2.5 (b). As for the concentrated electrolyte solution, strong F and Li signals were detected at the surface, and these gradually decreased to a depth of about 100 nm (Figure 2.6 (b)). A strong signal of C due to graphite was detected in the interior deeper than 100 nm. These results indicate that a LiF-rich surface film of about 100 nm thickness was formed on the graphite electrode. Thus, the surface film formed in the concentrated electrolyte solution was thicker than that formed in the conventional electrolyte solution.

To quantitate the constituents of the surface films, we tried to extract them with D₂O. It is difficult to extract compounds on the active material as they are because

hydrolysis reactions proceed during D₂O extraction, especially for organic ones. However, we can use the hydrolyzed species of organic compounds and the ionized species of inorganic compounds to estimate the original structures in the surface films.

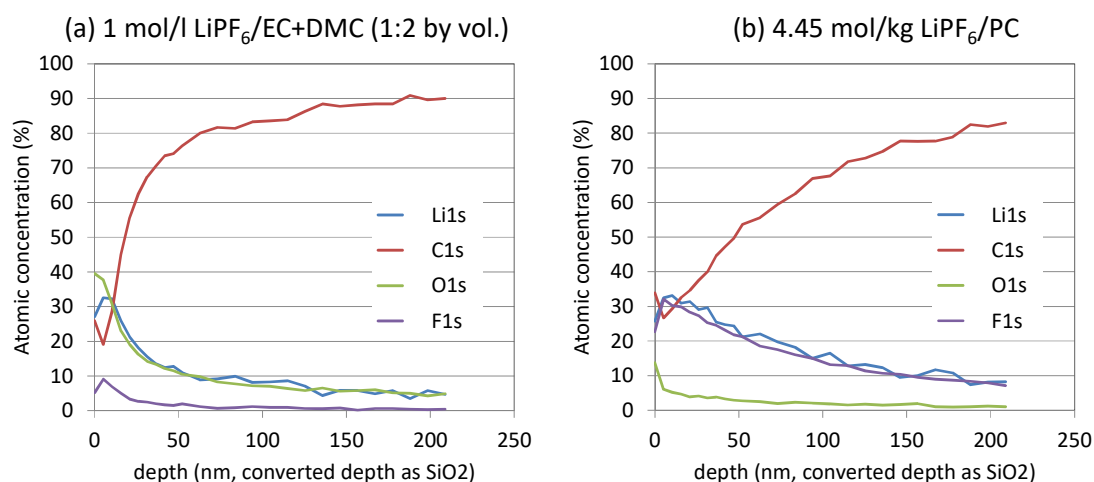


Figure 2.6 Atomic distribution in a depth direction from the surface of graphite electrodes after 15 cycles in the (a) conventional 1 mol/l LiPF₆/EC+DMC (1:2 by vol) and (b) nearly saturated 4.45 mol/kg LiPF₆/PC.

¹H NMR spectra of the D₂O extracts from the graphite electrode after 15 cycles are shown in Figure 2.7. The extract from the electrode cycled in the conventional electrolyte solution showed distinct peaks at 3.7 ppm (ethylene glycol structure), 3.3 ppm (methoxy group), 1.3 ppm (ethoxy group), and 2.9 ppm (acetic acid), and 8.4 ppm (oxalic acid). As for the concentrated electrolyte solution, almost the same peaks were detected, while the peak intensities were weaker than those obtained for the conventional electrolyte solution. These results indicate that a smaller amount of

organic compounds was deposited on the graphite electrode in the concentrated electrolyte solutions than that in the conventional electrolyte solution.

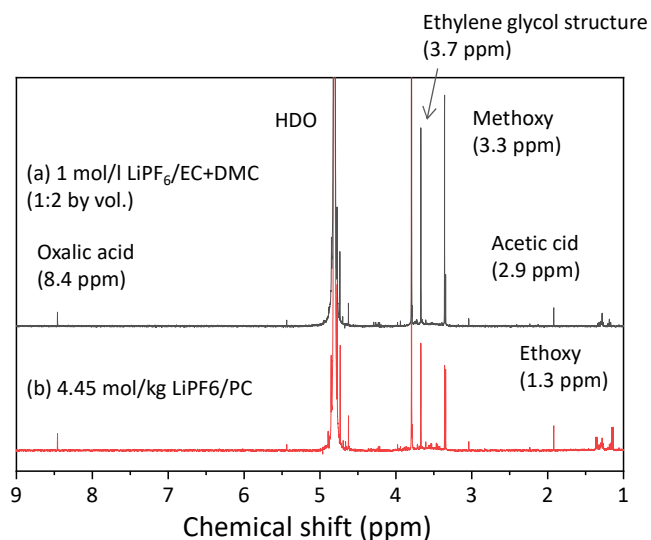


Figure 2.7 ^1H NMR spectra of D_2O extracts from graphite electrodes after 15 charge / discharge cycles in (a) conventional 1 mol/l $\text{LiPF}_6/\text{EC}+\text{DMC}$ (1:2 by vol) and (b) nearly saturated 4.45 mol/kg LiPF_6/PC .

The results of extraction analysis are summarized in Figure 2.8. In the conventional electrolyte solution, carbonates and organic compounds, which are decomposition products of EC and/or DMC solvent molecules, were dominant in the SEI. In the concentrated electrolyte solution, the amount of F^- detected was much greater than that in the conventional electrolyte solution, which means that the decomposition products of LiPF_6 was dominant in the SEI over those of PC solvent molecules. Thus, the conventional and the concentrated electrolyte solutions gave solvent-derived and salt-derived SEIs, respectively, of totally different compositions; however, they were both

stable on the graphite electrode.

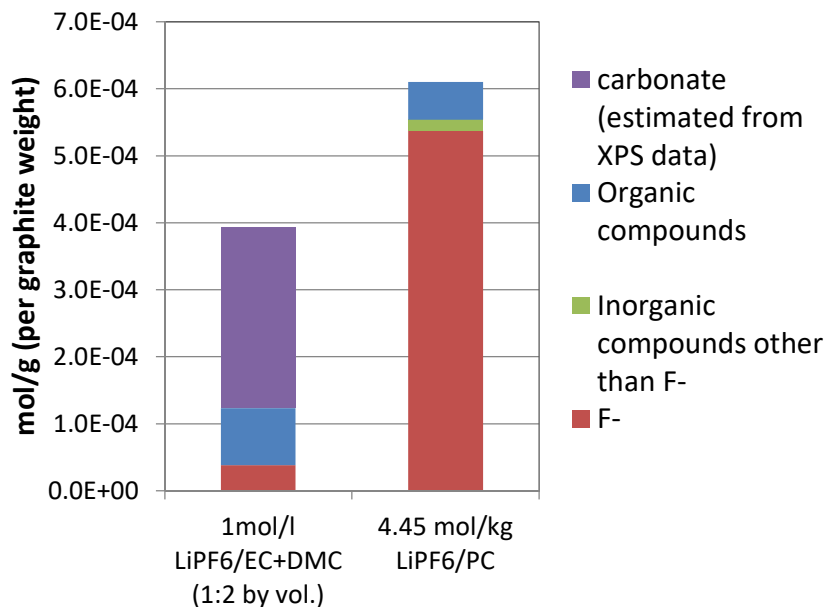


Figure 2.8 Constituents of surface films on graphite electrodes after 15 cycles in conventional 1 mol/l LiPF₆/EC+DMC (1:2 by vol) and nearly saturated 4.45 mol/kg LiPF₆/PC.

Here, the total irreversible capacity is correlated with the quantitative analysis data of the surface film precipitated on the graphite electrode. First, we calculated the total number of electrons consumed to produce the surface film on the electrode based on the quantitative analysis data. We hypothesized that methoxy, ethoxy compound, carboxylic acids and LiF are formed through one-electron reduction, while carbonate compounds through two-electron reduction.^{24,25} On this basis, the mole number of chemical species in surface film of the conventional electrolyte, 3.9×10^{-4} mol/g (per graphite weight), can be converted to 6.6×10^{-4} mol/g, which equals to 3.97×10^{20} electrons. Since almost no

carbonate was detected and only one electron reduction can be assumed for the concentrated electrolyte, the mole number of the surface film in the concentrated electrolyte, 6.1×10^{-4} mol/g, directly corresponds to the number of electrons, that is, 3.67×10^{20} electrons. A trace amount of FPO_3^{2-} and PO_4^{3-} was ignored in the calculation. The total number of electrons consumed to form the surface film in the concentrated electrolyte was by 8% less than that in the conventional electrolyte.

Next we separate the irreversible capacity into two component, the one contributing to produce surface film on the electrode, and the other dissolving into electrolyte solvent. The irreversible capacity of conventional electrolyte is 83.1 mAh/g, which corresponds to 1.87×10^{21} electrons assuming 1 C(coulomb) is 6.25×10^{18} electrons, and that of concentrated electrolyte, 71.3 mAh/g, corresponds to 1.60×10^{21} electrons. Here, we can estimate that the ratio of electrons consumed to produce the surface film is 23 % for the concentrated electrolyte, and 21 % for the conventional electrolyte, respectively. This means that about 20 % of irreversible capacity was consumed to form surface film both in the concentrated and conventional electrolyte solution. As for the residual 80 %, we are assuming following two possibilities. One is the component soluble to electrolyte solvent. Low molecular weight compounds generated during charge / discharge cycles can be soluble to the electrolyte solution. The other is the component

rinsed off in the process to remove the residual electrolyte solution. Since the chemical species correlated with the electrochemical impedance is thought to be insoluble to the electrolyte solvent, the residual 80 % has little contribution to the quantitative analysis shown in this section.

Since the total amount of electrons consumed to form the surface film in the concentrated electrolyte was by 8% less than that of the conventional electrolyte, and the irreversible capacity for the concentrated electrolyte solution was by 14% less than that of the conventional electrolyte solution, a quantitative correlation was found between the irreversible capacity and the total electrons to form the surface film. Though the mole numbers of chemical species of the surface film in the concentrated electrolyte is 1.5 times as large as that of the conventional electrolyte, the impedance of the SEI formed in the concentrated electrolyte solution was 3.6 times higher than that formed in the conventional one, as shown in Figure 2.3. This can be explained by a difference in the quality of SEI; that is, the inorganic (LiF)-based SEI had a higher impedance than organic-based SEI.

2.3.3 Charge and discharge properties of Li|NCM523 cells

The same approach was adopted for the analysis of NCM523 electrodes. Charge

and discharge curves and the cycling performance of Li|NCM523 cells are shown in Figure 2.9 and Figure 2.10, respectively. When the concentrated electrolyte solution was used, coulombic efficiencies hovered at around 98 % after the 2nd cycle, and were relatively stable compared to those for the conventional electrolyte solution. These results suggest that the concentrated electrolyte solution was more durable against oxidation than the conventional one, and in fact, the former gave a lower irreversible capacity than the latter (Table 2.4). AC impedance measurements were performed at 3.8 V vs. Li/Li⁺ after the 2nd and 15th cycle. Two semi-circles appeared in the conventional electrolyte solution, as shown in Figure 2.11 (a); the semi-circles in the high- and low-frequency regions are assigned to the surface film and the interfacial Li⁺ transfer at NCM523/electrolyte, respectively.^{26,27} The sum of the two resistances was 67.9 Ω at the 15th cycle (Table 2.5). Similarly, two semi-circles are seen in the concentrated electrolyte solution (Figure 2.11 (b)). The total interfacial resistance (1,118 Ω) was about 16 times as high as that in the conventional electrolyte solution despite the rather low irreversible capacity as shown in Table 2.4. To understand the apparently contradictory results, XPS and D₂O extraction analysis were conducted for the NCM523 electrodes.

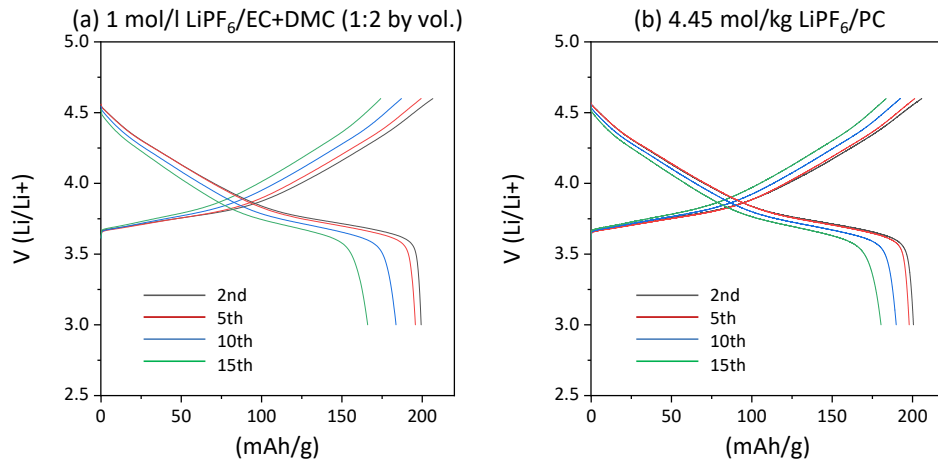


Figure 2.9 Charge and discharge curves of Li | NCM523 cells with (a) conventional 1 mol/l LiPF₆/EC+DMC (1:2 by vol) and (b) nearly saturated 4.45 mol/kg LiPF₆/PC electrolyte solutions.

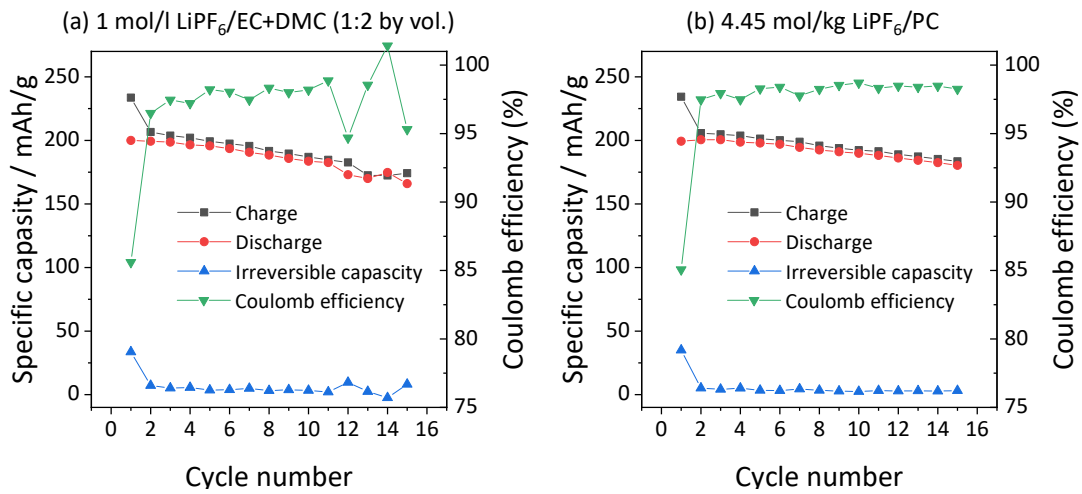


Figure 2.10 Variation of charge, discharge and irreversible capacities, and coulomb efficiencies with cycle number for Li | NCM523 cells with (a) conventional 1 mol/l LiPF₆/EC+DMC (1:2 by vol) and (b) nearly saturated 4.45 mol/kg LiPF₆/PC.

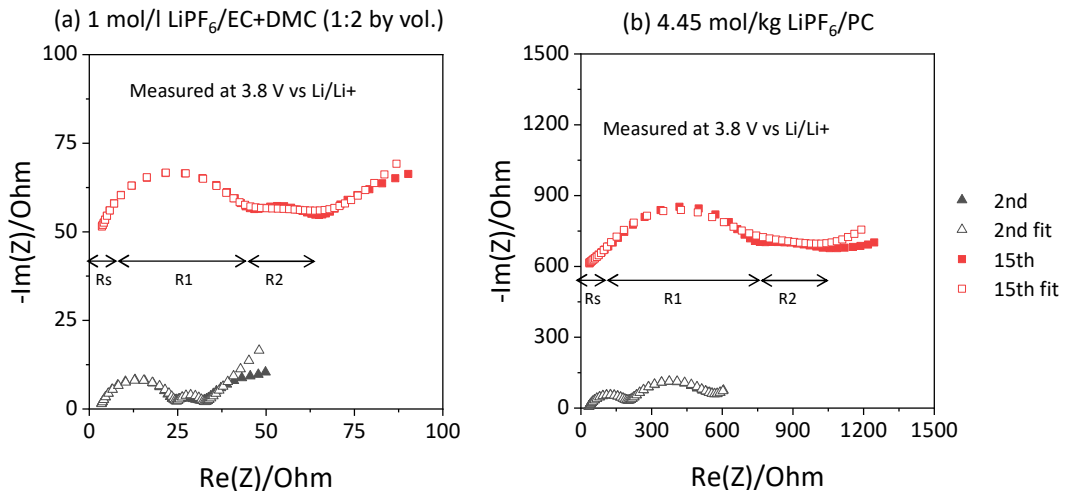


Figure 2.11 Nyquist plots and their numerical fitting of NCM523 electrodes in (a) conventional 1 mol/l LiPF₆/EC+DMC (1:2 by vol) and (b) nearly saturated 4.45 mol/kg LiPF₆/PC after the 2nd and 15th cycle.

Table 2.4 Total irreversible capacities and average coulomb efficiencies of Li | NCM523 cells in 15 cycles.

	Total irreversible capacity (mAh/g)	Average coulomb efficiency (%)
1 mol/l LiPF ₆ /EC+DMC (1:2 by vol.)	94.6	85.6
4.45 mol/kg LiPF ₆ / PC	84.6	97.5

Table 2.5 Fitting results for Nyquist plots of NCM523 electrodes in Figure 2.7.

		Rs (Ω)	R1 (Ω)	R2 (Ω)
1 mol/l LiPF ₆ /EC:DMC=1:2	2 nd	2.9	6.7	22.0
	15 th	2.4	36.7	31.2
		Rs (Ω)	R1 (Ω)	R2 (Ω)
4.45mol/kg LiPF ₆ /PC	2 nd	30.5	171	347
	15 th	13.0	599	519

To confirm the increase in the impedance, we have also checked the rate capability

of the Li | NCM523 cells, same as conducted for the Li | Graphite cells. The NCM523 electrode was charged to 4.6 V to discharge to 3.0 V with different C-rate from 0.1 C to 2 C. Figure 2.12 shows that the decrease in the capacity is much more pronounced at the cell with the concentrated electrolyte solution than the conventional one, as expected from the impedance measurement. Almost no capacity was detected at 2 C rate discharge in the NCM523 electrode with the concentrated electrolyte solution, which shows there exists the layer with much higher resistance than that of the graphite electrode.

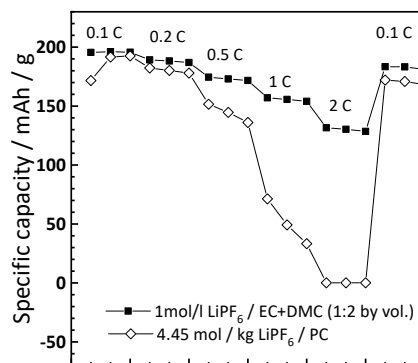


Figure 2.12 Rate capability of NCM523 electrodes in conventional 1 mol/l LiPF₆/EC+DMC (1:2 by vol) and nearly saturated 4.45 mol/kg LiPF₆/PC.

Figure 2.13 shows XPS Li1s, C1s, Ni3p, Co3p and Mn3p spectra of NCM523 electrodes after 15 cycles in the conventional and the concentrated electrolyte solutions. A large amount of Li was detected for the concentrated electrolyte solution, in

comparison with that for the conventional electrolyte solution (Figure 2.13 (a)), suggesting that the oxidative decomposition of LiPF_6 occurred dominantly. On the other hand, for the conventional electrolyte solution, relatively large amounts of carbonate, ester and ether components were observed on the C1s spectrum, which were derived from EC and DMC solvent molecules. These results are very similar to those obtained for the graphite electrode surfaces in Figure 2.5. Atomic composition percentages calculated from XPS spectra are summarized in Table 2.6.

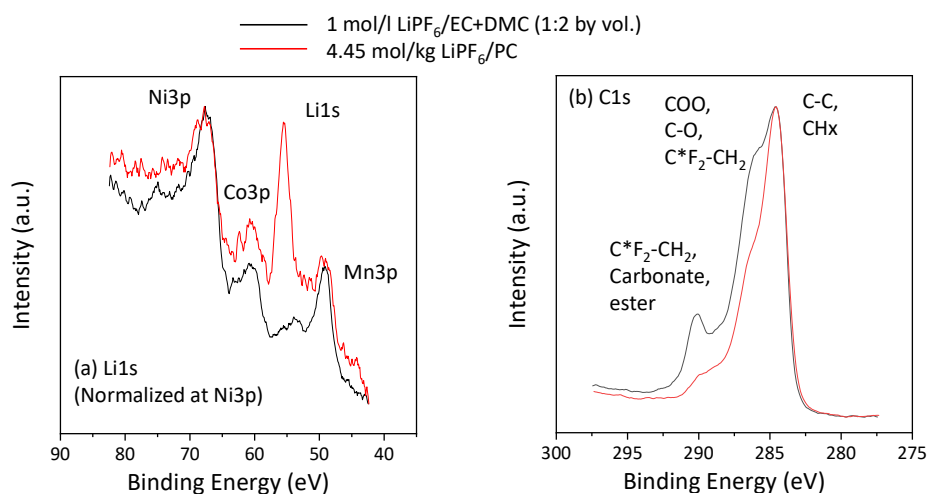


Figure 2.13 (a) $\text{Li}1s$, $\text{Ni}3p$, $\text{Co}3p$ and $\text{Mn}3p$, and (b) $\text{C}1s$ spectra of NCM523 electrode surface after 15th cycles in conventional 1 mol/l $\text{LiPF}_6/\text{EC}+\text{DMC}$ (1:2 by vol) and nearly saturated 4.45 mol/kg LiPF_6/PC .

Table 2.6 Atomic composition percentages of (a) whole surface films and (b) C-containing compounds in surface films on NCM523 electrode that formed by conventional 1 mol/l LiPF₆/EC+DMC (1:2 by vol) and nearly saturated 4.45 mol/kg LiPF₆/PC.

(a) whole surface films	(atomic%)							
	Li	C	O	F	P	Mn	Co	Ni
1mol/l LiPF ₆ /EC+DMC (1:2 by vol.)	1.1	57.9	20.7	14.5	1.3	0.8	0.3	1.1
4.45 mol/kg LiPF ₆ / PC	23.4	33	14	24.6	3.5	0.4	0.2	0.5

(b) C-containing compounds	(atomic%)			
	CH ₂ -C*F ₂ carbonate, ester	carboxylic acid / salt	CH ₂ -C*F ₂ C-O	C-C, CHx
1 mol/l LiPF ₆ /EC+DMC (1:2 by vol.)	6.3	8.7	18.4	24.6
4.45 mol/kg LiPF ₆ / PC	2.6	5.7	13.8	30.0

XPS depth profile analyses (Figure 2.14) revealed that the atomic percentage of Li, as well as that of F, was high at the surface for the concentrated electrolyte solution, suggesting that inorganic compounds containing Li and F, such as LiF, were present at the surface of the NCM523 electrode. On the other hand, for the conventional electrolyte solution, the relative intensity of C was higher than that for the concentrated electrolyte solution, which suggests that the surface films contained more organic compounds. In both cases, the transition metals of NCM523, including Ni, were detected at around 20 nm from the surface, and hence the surface films on the NCM523 electrodes were thinner than those for the graphite negative electrodes (Figure 2.6); No definite correlation with the LiPF₆ concentration of electrolyte solutions was seen in

Figure 2.14, unlike for the graphite electrode.

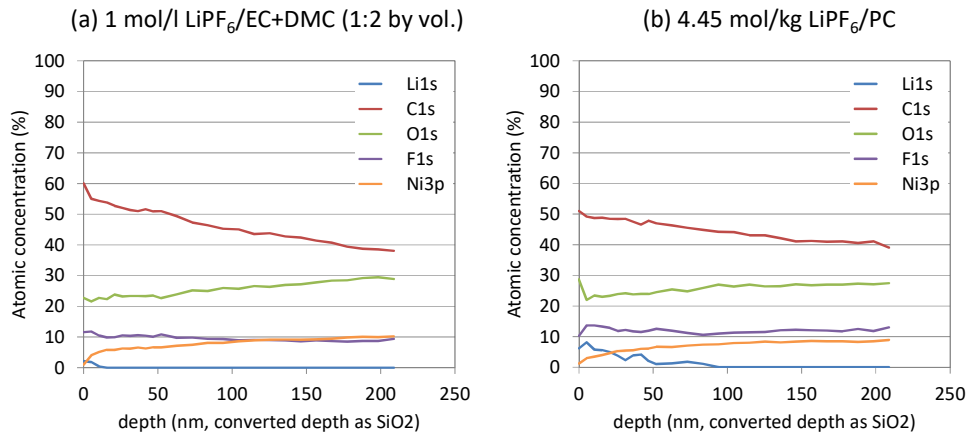


Figure 2.14 Atomic distribution in a depth direction from the surface of NCM523 electrodes after 15 cycles in the (a) conventional 1 mol/l LiPF₆/EC+DMC (1:2 by vol) and (b) nearly saturated 4.45 mol/kg LiPF₆/PC.

D₂O extraction analysis was performed for NCM523 electrodes after 15 cycles with Li|NCM523 cells, and the results are shown in Figure 2.15. The surface film formed in the highly concentrated electrolyte solutions was characterized by a high proportion of F⁻ and other inorganic compounds, and the total amount was three times as large as that for the conventional electrolyte solution.

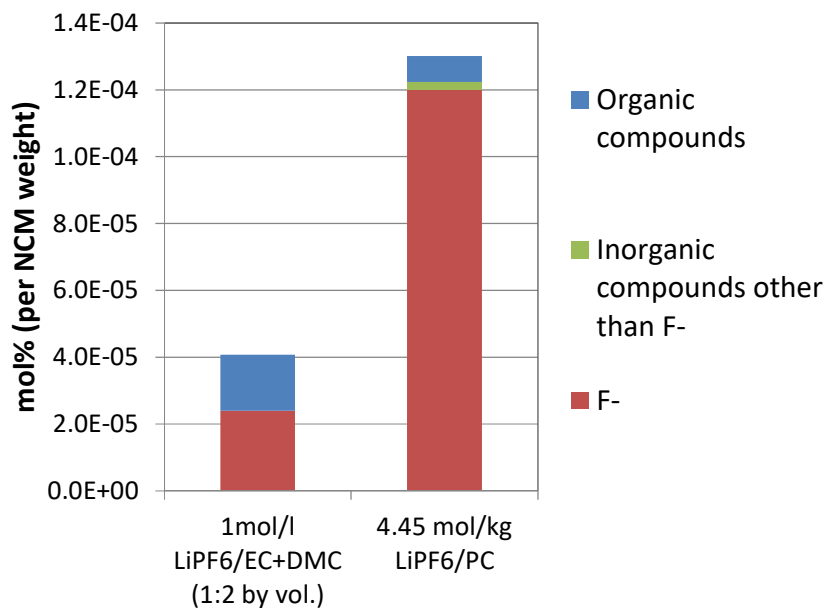


Figure 2.15 Constituents of surface films on NCM523 electrodes after 15 cycles in conventional 1 mol/l LiPF₆/EC+DMC (1:2 by vol) and nearly saturated 4.45 mol/kg LiPF₆/PC.

In summary, the concentrated electrolyte solution delivered a three times larger amount of surface film and a 16 times higher interfacial resistance, despite low irreversible capacities, as compared with the conventional electrolyte solution. These results imply that the inorganic surface film seems to be highly resistive. However, this does not sufficiently explain the fact that the interfacial resistance for the NCM523 electrode (1,118 Ω) was much higher than that for the graphite electrode (123 Ω), even though the amount of surface film for the NCM523 electrode was much smaller than that for the graphite electrode in the concentrated electrolyte solution. The inorganic surface film that formed on the NCM523 electrode might be thinner and denser than

that on the graphite electrode. In addition, the change in crystal structure at the surface of NCM523 might result in an increase in interfacial resistance. This assumption was verified by Raman spectroscopy. The Raman spectra of NCM523 electrodes before and after 15 cycles are shown in Figure 2.16. The detection depth is around 50 nm or less from the electrode surface in Raman spectroscopy, and hence a structural change of the NCM523 surface can be discussed. The A_{1g} and E_g modes derived from the layered rock-salt structure were observed at 600 and 500 cm^{-1} , respectively.^{28,29} After 15 cycles in the concentrated electrolyte solution, a spectral broadening, a change in intensity ratio, and a new band at around 580 cm^{-1} were observed. The results suggest the deterioration of the crystallinity of NCM523 and/or the formation of a transition metal oxide other than the initial structure. These seem to also be the reasons for the very high interfacial resistance at the NCM523 electrode in the concentrated electrolyte solution.

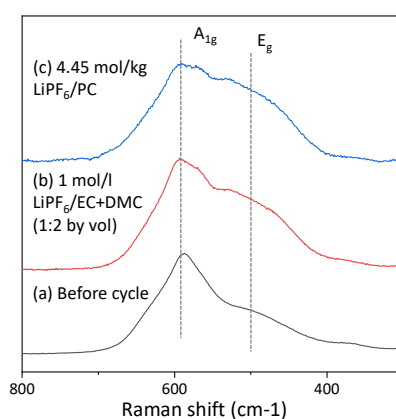


Figure 2.16 Raman spectra of NCM523 electrodes (a) before and after 15 cycles in (b) conventional 1 mol/l $\text{LiPF}_6/\text{EC}+\text{DMC}$ (1:2 by vol) and (c) nearly saturated 4.45 mol/kg LiPF_6/PC .

2.3.4 Charge and discharge properties of Graphite | NCM523 cells

Full cell battery performances were also checked using Graphite | NCM523 coin-type cells with the conventional and the concentrated electrolyte solutions. Charge/discharge tests were performed at a 0.1 C rate between 3.0 and 4.5 V for 15 cycles at 30 °C. Quantitative analysis data by D₂O extraction were summarized in Figure 2.17. We have found that there exists the surface film mainly composed from LiF on the graphite electrode with the concentrated electrolyte solution, as was found in the half cell experiment (Figure 2.8), and this would result in higher impedance in the conventional electrolyte solution. As for the NCM523 electrode, we found that higher amount of LiF exists in the surface film of the concentrated electrolyte solution, and the total amount is less than that on the graphite electrode. This is also similar result obtained from the half cell experiment.

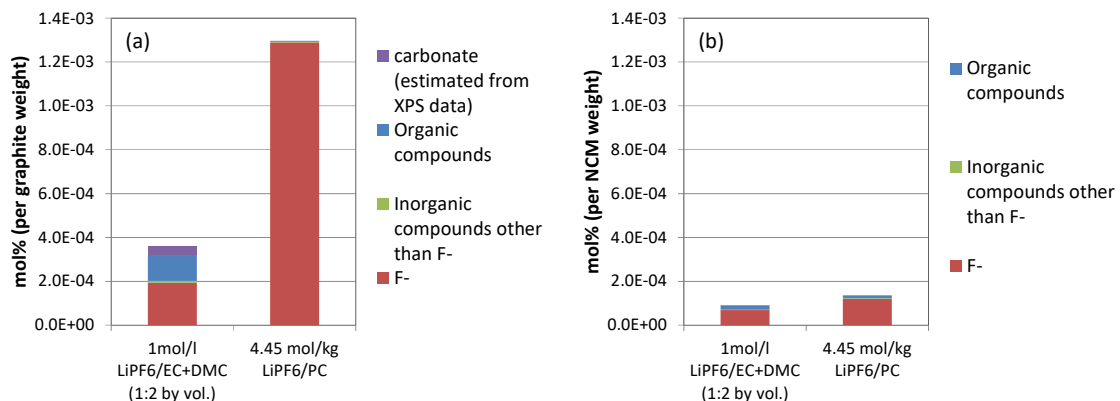


Figure 2.17 Constituents of surface films on (a) graphite electrode, and (b) NCM523 electrodes after 15 cycles in conventional 1 mol/l LiPF₆/EC+DMC (1:2 by vol) and nearly saturated 4.45 mol/kg LiPF₆/PC.

2.4. Conclusions

We compared the cycle performance of the graphite and the NCM523 electrodes in the conventional 1 mol/l LiPF₆ EC+DMC (1:2 by vol) and the nearly saturated 4.45 mol/kg LiPF₆/PC electrolyte solutions. For the graphite negative electrode, the reductive decomposition of solvent molecules and LiPF₆ salt preferentially proceeded in the conventional and concentrated electrolyte solutions respectively. A quantitative correlation between irreversible capacity and the total electrons consumed to form surface film deposited was clarified. The increase in the impedance of the CEI formed in the concentrated electrolyte was remarkable compared to the difference in the mole number of chemical species contained in the surface film. The inorganic-rich CEI that was formed in the concentrated electrolyte solution resulted in an increase in interfacial resistance after charge/discharge cycles. For the NCM523 positive electrode, the interfacial resistance drastically increased and a large amount of surface film, especially inorganic species, formed after charge/discharge cycles in the concentrated electrolyte solution. The large interfacial resistance could not be accounted for solely by the amount of surface films, which should be caused by degradation of the NCM523 surface structure.

References

- [1] J. B. Goodenough, “Evolution of Strategies for Modern Rechargeable Batteries”, *Acc. Chem. Res.*, 46, 1053–1061 (2013), <https://doi.org/10.1021/ar2002705>.
- [2] J. Sturm, A. Rheinfeld, I. Zilberman, F.B. Spingler, S. Kosch, F. Frie, A. Jossen, “Modeling and simulation of inhomogeneities in a 18650 nickel-rich, silicon graphite lithium-ion cell during fast charging”, *J. Power Sources*, 412, 204–223 (2019)
- [3] X. Li, A.M. Colclasure, D.P. Finegan, D. Ren, Y. Shi, X. Feng, L. Cao, Y. Yang, K. Smith, “Degradation mechanisms of high capacity 18650 cells containing Si graphite anode and nickel-rich NCM cathode”, *Electrochim. Acta.*, 297, 1109–1120 (2019)
- [4] X. Zuo, J. Zhu, P. Müller-Buschbaum, Y.J. Cheng, “Silicon based lithium-ion battery anodes: a chronicle perspective review”, *Nanomater. Energy*, 31, 113–143 (2017)
- [5] W. Liu, P. Oh, X. Liu, M.J. Lee, W. Cho, S. Chae, Y. Kim, J. Cho, “Nickel-rich layered lithium transition-metal oxide for high-energy lithium-ion batteries”, *Angew. Chem. Int. Ed.* 54, 4440–4457 (2015)
- [6] K. Amine, H. Yasuda, and M. Yamachi, “Olivine LiCoPO_4 as 4.8V electrode material for lithium batteries”, *Electrochem. Solid State Lett.*, 3, 178 (2000).
- [7] S. Okada, S. Sawa, M. Egashira, J. Yamaki, M. Tabuchi, H. Kageyama, T. Konishi, and A. Yoshino, “Cathode properties of phospho-olivine LiMPO_4 for lithium secondary

batteries,” *J. Power Sources*, 430, 97–98 (2001).

[8] K. Ariyoshi, Y. Iwakoshi, N. Nakayama, and T. Ohzuku, “Topotactic two-phase reactions of $\text{Li}[\text{Ni}_{1/2}\text{Mn}_{3/2}]\text{O}_4$ (P4332) in nonaqueous lithium cells,” *J. Electrochem. Soc.*, 151, A296 (2004).

[9] Y. K. Sun, K. J. Hong, J. Prakash, and K. Amine, “Electrochemical performance of nano-sized ZnO-coated $\text{LiNi}_{0.5}\text{Mn}_{1.5}\text{O}_4$ spinel as 5 V materials at elevated temperatures”, *Electrochem. Commun.*, 4, 344 (2002).

[10] J. Liu, A. Manthiram, and A. “Improved electrochemical performance of the 5 V spinel cathode $\text{LiMn}_{1.5}\text{Ni}_{0.42}\text{Zn}_{0.08}\text{O}_4$ by surface modification”, *J. Electrochem. Soc.*, 156, A66 (2009).

[11] M. Xu, L. Zhou, Y. Dong, Y. Chen, A. Garsuch, and B. L. Lucht, “Improving the performance of graphite/ $\text{LiNi}_{0.5}\text{Mn}_{1.5}\text{O}_4$ cells at high voltage and elevated temperature with added lithium bis(oxalato) borate (LiBOB)”, *J. Electrochem. Soc.*, 160, A2005 (2013)

[12] Y. Yamada and A. Yamada “Review - Superconcentrated Electrolytes for Lithium Batteries”, *J. Electrochem. Soc.*, 162 A2406-A2423 (2015)

[13] Y. Yamada, K. Usui, C. H. Chiang, K. Kikuchi, K. Furukawa, and A. Yamada, “General Observation of Lithium Intercalation into Graphite in Ethylene-Carbonate-

Free Superconcentrated Electrolytes”, ACS Appl. Mater. Interfaces, 6, 10892–10899

(2014)

[14] T. Doi, Y. Shimizu, M. Hashinokuchi, and M. Inaba, “LiBF₄-Based Concentrated Electrolyte Solutions for Suppression of Electrolyte Decomposition and Rapid Lithium-Ion Transfer at LiNi_{0.5}Mn_{1.5}O₄/Electrolyte Interface”, J. Electrochem. Soc., 163, A2211-A2215 (2016)

[15] T. Doi, Y. Shimizu, M. Hashinokuchi, and M. Inaba, “Dilution of Highly Concentrated LiBF₄/Propylene Carbonate Electrolyte Solution with Fluoroalkyl Ethers for 5-V LiNi_{0.5}Mn_{1.5}O₄ Positive Electrodes”, J. Electrochem. Soc., 164 (1) A6412-A6416 (2017)

[16] P. Verma, P. Maire, P. Novák, “A Review of the Features and Analyses of the Solid Electrolyte Interphase in Li-Ion Batteries”, Electrochim. Acta., 55, 6332–6341 (2010)

[17] E. Peled, “The Electrochemical Behavior of Alkali and Alkaline Earth Metals in Nonaqueous Battery Systems—The Solid Electrolyte Interphase Model”. J. Electrochem. Soc., 126, 2047–2051 (1979)

[18] Aurbach, D. “Review of Selected Electrode–Solution Interactions which Determine the Performance of Li and Li Ion Batteries”, J. Power Sources, 89, 206–218 (2000)

[19] Niehoff, P.; Passerini, S.; Winter, M. Interface Investigations of a Commercial

- Lithium Ion Battery Graphite Anode Material by Sputter Depth Profile X-ray Photoelectron Spectroscopy, *Langmuir* 29, 5806–5816 (2013)
- [20] M. Nie, D. P. Abraham, D. M. Seo, Y. Chen, A. Bose, B. L. Lucht, Role of Solution Structure in Solid Electrolyte Interphase Formation on Graphite with LiPF_6 in Propylene Carbonate, *J. Phys. Chem. C.*, 117, 25381–25389 (2013)
- [21] S. K. Jeong, H. Y. Seo, D. H. Kim, H. K. Han, J. G. Kim, Y. B. Lee, Y. Iriyama, T. Abe, and Z. Ogumi, Suppression of dendritic lithium formation by using concentrated electrolyte solutions, *Electrochem. Commun.*, 10, 635 (2008)
- [22] Y. Yamada, Y. Koyama, T. Abe, Z. Ogumi, Correlation between Charge–Discharge Behavior of Graphite and Solvation Structure of the Lithium Ion in Propylene Carbonate-Containing Electrolytes. *J. Phys. Chem. C.*, 113, 8948–8953 (2009)
- [23] S.-K. Jeong, M. Inaba, Y. Iriyama, T. Abe, Z. Ogumi, Interfacial Reactions Between Graphite Electrodes and Propylene Carbonate-Based Solutions: Electrolyte-Concentration Dependence of Electrochemical Lithium Intercalation Reaction, *J. Power Sources*, 175, 540–546 (2008)
- [24] Recent studies of the lithium-liquid electrolyte interface Electrochemical, morphological and spectral studies of a few important systems, D. Aurbach, A. Zaban, Y. Gofer, Y. E. Ely, I. Weissman, O. Chusid, O. Abramson, *J. Power Sources*, 54, 76-84

(1995)

[25] K. Tasaki, A. Goldberg, Jian-Jie Lian, M. Walker, A. Timmons, S J. Harris, Solubility of Lithium Salts Formed on the Lithium-Ion Battery Negative Electrode Surface in Organic Solvents, *J. Electrochem. Soc.*, 156, A1019-A1027 (2009),

[26] K. Dokko, M. Mohamedi, Y. Fujita, T. Itoh, M. Nishizawa, M. Umeda, I. Uchida, Kinetic Characterization of Single Particles of LiCoO_2 by AC Impedance and Potential Step Methods, *J. Electrochem. Soc.*, 148, A422-A426 (2001)

[27] D. Aurbach, M. D. Levi, E. Levi, H. Telier, B. Markovsky, G. Salitra, U. Heider, L. Hekier, Common Electroanalytical Behavior of Li Intercalation Processes into Graphite and Transition Metal Oxides, *J. Electrochem. Soc.*, 145, 3024 (1998)

[28] M. Inaba, Y. Iriyama, Z. Ogumi, Y. Todzuka, A. Tasaka, Raman study of layered rock-salt LiCoO_2 and its electrochemical lithium deintercalation, *J. Raman Spectrosc.* 28, 613 (1997)

[29] H. Koga, C. Laurence, M. Philippe, M. Michel, W. Francois, B. Lydie, D. Mathieu, S. Emmanuelle, D. Claude, $\text{Li}_{1.20}\text{Mn}_{0.54}\text{Co}_{0.13}\text{Ni}_{0.13}\text{O}_2$ with Different Particle Sizes as Attractive Positive Electrode Materials for Lithium-Ion Batteries: Insights into Their Structure., *J. Phys. Chem. C.*, 116, 13497–13506 (2012)

Chapter 3

Predictive characterization of SEI formed on graphite negative electrodes for efficiently designing an effective electrolyte solutions

3.1. Introduction

An electrolyte solution is reductively decomposed on a graphite negative electrode to form a solid electrolyte interphase (SEI) in initial charge/discharge cycles of lithium ion batteries (LIBs). The physicochemical properties of SEI determine the overall charge/discharge performance of LIBs¹⁻⁶. Hence, SEI has been extensively investigated by using various types of instrumental analysis such as FT-IR⁷, XPS^{8,9} and NMR^{10,11}. SEI consists of a mixture of organic and inorganic compounds, but the chemical composition has not yet been fully elucidated even after more than thirty years since the introduction of LIBs. In addition to experimental studies, quantum chemical calculations are opening the door to the further elucidation of SEI¹²⁻¹⁷. In general, the formation processes of SEI are divided into two steps to minimize the calculation cost;

one is the reductive decomposition of electrolyte solutions and the other is a subsequent precipitation of the decomposed products. The electrochemical stability of electrolyte solutions has been studied by density functional theory (DFT) calculations; i.e., the HOMO and LUMO energy levels, and their gaps are commonly used as criteria for the stability of electrolyte solutions against oxidation and reduction. The calculations have been conducted focusing mainly on the organic molecules in electrolyte solutions, i.e., solvents and additives that can form an effective SEI. The stability of these organic molecules against reduction is greatly affected by a structure of electrolyte solutions. In a conventional electrolyte solution containing ca. 1 mol/l LiPF_6 , LiPF_6 is generally dissociated and solvent molecules solvate a lithium ion to form a solvent separated ion pair (SSIP)¹⁸⁻²². When the LiPF_6 concentration increases, the association of lithium ions and PF_6^- anions progresses to form a contact ion pair (CIP) and/or aggregate (AGG) structures. Thus, electrolyte solutions are composed of solvates and associated ions depending on the LiPF_6 concentration. These complicated structures of electrolyte solutions prevent us from completely understanding the mechanism of SEI formation. In general, energetically optimized structures of SSIP consisting of a lithium ion and solvent molecules are determined to evaluate the HOMO and LUMO energy levels²²⁻²⁴. On the other hand, as for CIP and AGG, the counter anion such as PF_6^- needs to be

incorporated into the solvation structures, but few reports explicitly evaluate the electrochemical stability considering the anion by quantum chemical calculations²⁴. The calculated values vary depending on both calculation methods and basis functions, and hence a comparison with previous studies using different calculation methods is often difficult²⁵. To avoid these difficulties, ionization potential (IP) and electron affinity (EA) are used to compare the electrochemical stability of solvents and solvates^{15,16}. Recently, DFT calculations combined with molecular dynamics simulation, or AIMD (Ab Initio molecular dynamics calculation), have been used to study the electrochemical stability of electrolyte solutions and the reaction pathway for SEI formation. AIMD can incorporate counter anions, as well as lithium ions, and solvent and additive molecules at different concentrations, while the computational cost is quite high. AIMD has provided detailed and plausible results to account for a part of the experimental data²⁶⁻³¹, and is still developing to clarify a whole picture of the SEI formation mechanism. In AIMD simulations, EA is often used as a means of validation for the reductive stability of electrolyte solutions.

In this study, two kinds of highly concentrated LiPF₆/carbonate ester electrolyte solutions were used to obtain quite different types of SEI and different charge/discharge behavior of graphite negative electrodes. Solvation structures of the electrolyte solutions

were studied by Raman spectroscopy, and EA of the geometrically optimized solvation structures containing a PF_6^- counter anion was evaluated by DFT calculations. Based on the calculation results, we predicted not only the chemical species more vulnerable to reduction but also the reductive decomposition products of electrolyte solutions, i.e., a chemical composition of SEI, and supported the predictions by experimental results. Then, these results were correlated with the electrochemical performance of graphite electrodes to understand the stability of SEI against reduction.

3.2. Experimental

3.2.1. Electrolyte solutions

Electrolyte solutions were prepared using propylene carbonate (PC), ethylene carbonate (EC) and diethyl carbonate (DEC) as solvents and LiPF_6 as a salt (battery grade, Kishida Chemical) in an Ar-filled glove box (< 10 ppm O_2 , < 1 ppm H_2O). Four kinds of electrolyte solution were prepared: 1 mol/l LiPF_6 dissolved in a mixture of EC and DEC (1:1 by vol.) as a conventional electrolyte solution, and 3.3 mol/l $\text{LiPF}_6/\text{EC}+\text{DEC}$ (1:1 by vol.) and 2.3 and 3.3 mol/l LiPF_6/PC as concentrated electrolyte solutions.

Raman spectra of the electrolyte solutions were obtained by a Model PDP 320 (Photon Design) using a spectrometer equipped with a grating of 900 gr/mm with a 320 mm focus length and a 1064 nm YAG laser as an excitation source.

Theoretical calculations of solvated structures were carried out using DFT with a B3LYP functional and a 6-311+G** basis set. The geometries of all solvation structures were optimized and confirmed to be at their energetically local minimum by Hessian calculations.

3.2.2. Charge and discharge tests

The charge and discharge properties of a graphite electrode were investigated using 2032 coin-type cells with a lithium metal counter electrode. The graphite working electrode was composed of graphite powder as an active material, and styrene-butadiene rubber (SBR) and carboxymethyl cellulose (CMC) as binders (98:1:1 by weight). Charge/discharge measurements were performed at a rate of 0.1 C between 0.01 and 1.5 V for 15 cycles at 30 °C.

After the charge/discharge tests, the coin cell was disassembled in an Ar-filled glove box to collect the working electrode, which was then rinsed in DEC to remove the electrolyte solution and dried under vacuum at room temperature. The composition of the surface film formed on the graphite electrodes was investigated by X-ray photoelectron spectroscopy (Quanter SXM, ULVAC-PHI). In the XPS measurements, the acceleration voltage and the emission current of a monochromatic Al K α X-ray gun were set at 15 kV and 3 mA, respectively.

3.3. Results and discussion

3.3.1. Charge and discharge properties of graphite

It has been reported that 1 mol/l LiPF₆/EC+DEC electrolyte solution is mainly composed of SSIP structures, while almost-saturated 3.3 mol/l LiPF₆/EC+DEC contains CIP and AGG structures¹⁸⁻²². The influence of the salt concentration on the solution structures was studied using PC by Raman spectroscopy, and the results are shown in Figure 3.1. In Figure 3.1 (a), PF stretching vibration for an SSIP structure gives a Raman band at 748 cm⁻¹, and CIP and AGG structures at a slightly higher wavenumber at around 753 cm⁻¹. A band width of the Raman bands reflects the distribution of association / dissociation structures of LiPF₆: that is, the formation of CIP and AGG structures generates a structural distribution of LiPF₆ to give a broader Raman band. In Figure 2.1(b), changes in the band width had an inflection point at 2.3 mol/l and the slope became steeper at higher concentrations. The inflection point of Raman band width to LiPF₆ concentration suggests a significant increase of CIP and AGG; the same conclusion was drawn from the peak intensity ratio which was determined by peak separation analysis (Figure 3.2). Therefore, we used 2.3 and 3.3 mol/l LiPF₆/PC solutions to study the charge/discharge properties of graphite.

It is desirable to prepare a PC-based electrolyte solution with a lower LiPF_6 concentration, such as 1 mol/l LiPF_6/PC solution, to evaluate its stability against reduction of SSIP structure with PC molecules. However, it is impossible to intercalate lithium ions into a graphite electrode in 1 mol/l LiPF_6/PC due to the continuous exfoliation of graphite and the decomposition of $\text{PC}^{32,33}$. Hence, in this study, only 1 mol/l EC+DEC was used to study the electrochemical stability of the SSIP structure on graphite electrode.

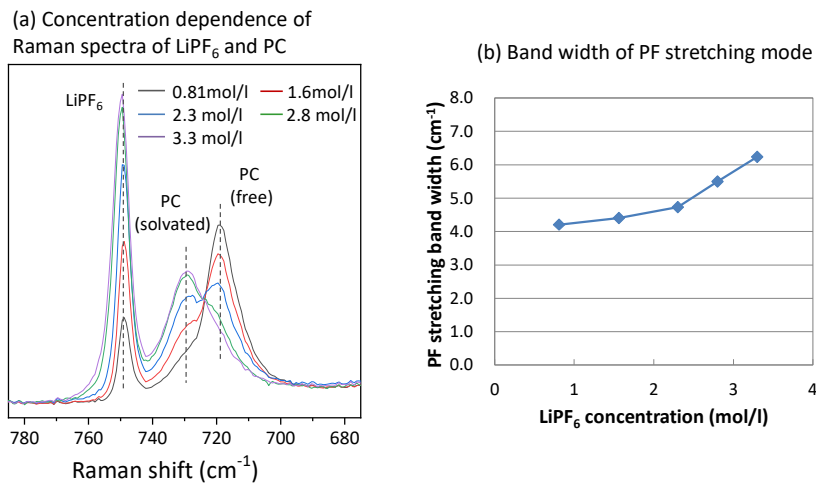


Figure 3.1 (a) Raman spectra of 0.81, 1.6, 2.3, 2.8, and 3.3 mol/l LiPF_6/PC solution and (b) changes in the band width of the P-F stretching vibration at ca. 750 cm^{-1} .

Charge/discharge curves of Li | graphite cells with 2.3 and 3.3 mol/l LiPF_6/PC , and 1 and 3.3 mol/l $\text{LiPF}_6/\text{EC+DEC}$ are shown in Figure 3.3. The variations of charge/discharge capacity, irreversible capacity, and Coulomb efficiency with cycle

number are shown in Figure 3.4. All of the coin cells showed high capacities of about 350 mAh/g, and maintained these levels to the 15th cycle regardless of the kind of solvent and the salt concentration. Differences in charge/discharge performance were reflected in the irreversible capacity (Figure 3.5, Table 3.1); 2.3 mol/l LiPF₆/PC gave the highest irreversible capacity in the initial cycles, while it decreased after the 3rd cycle. It is well known that a reductive decomposition of PC and a continuous exfoliation of graphite occur in low concentration LiPF₆ / PC electrolyte solution³³, and hence a very high irreversible capacities were seen in the initial cycles in 2.3 mol/l LiPF₆ / PC in this study. The irreversible capacities drastically decreased after the 4th cycle in LiPF₆ / PC, regardless of the concentrations, which suggests that a stable SEI was formed in the initial cycles (Figure 3.5).

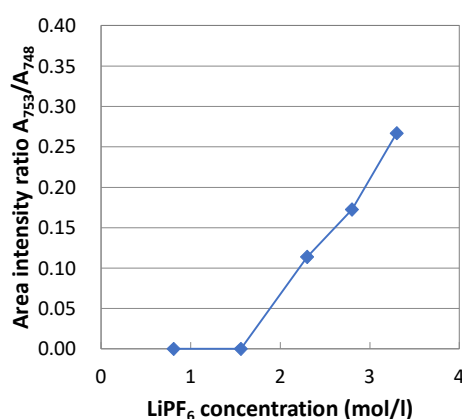


Figure 3.2 Area intensity ratio of 753 cm⁻¹ component (CIP and AGG of LiPF₆) against 748 cm⁻¹ (SSIP)

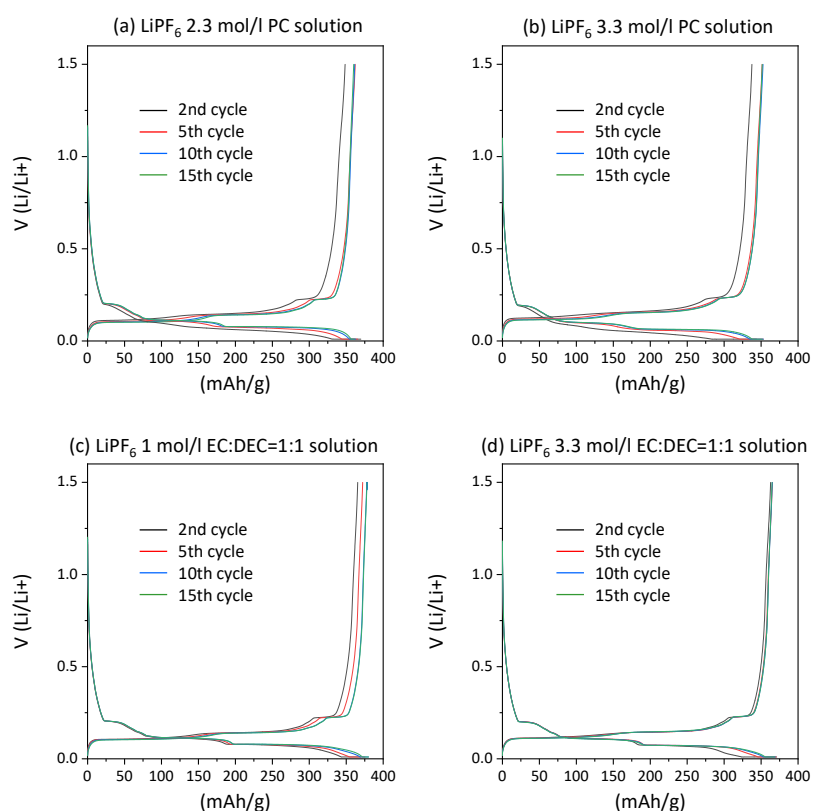


Figure 3.3 Charge/discharge behavior of Li | graphite cells with (a) 2.3 mol/l and (b) 3.3 mol/l LiPF_6/PC , and (c) 1 mol/l and (d) 3.3 mol/l $\text{LiPF}_6/\text{EC}+\text{DEC}$ (1:1 by vol.).

On the other hand, irreversible capacities were still high after the 6th cycle in EC+DEC-based electrolyte solutions. These results imply that the surface films cannot effectively suppress the continuous decomposition of $\text{LiPF}_6 / \text{EC}+\text{DEC}$ electrolyte solutions. In addition, the chemical composition of SEI should be different between EC+DEC- and PC-based electrolyte solutions. The compositional difference in the surface films is discussed later.

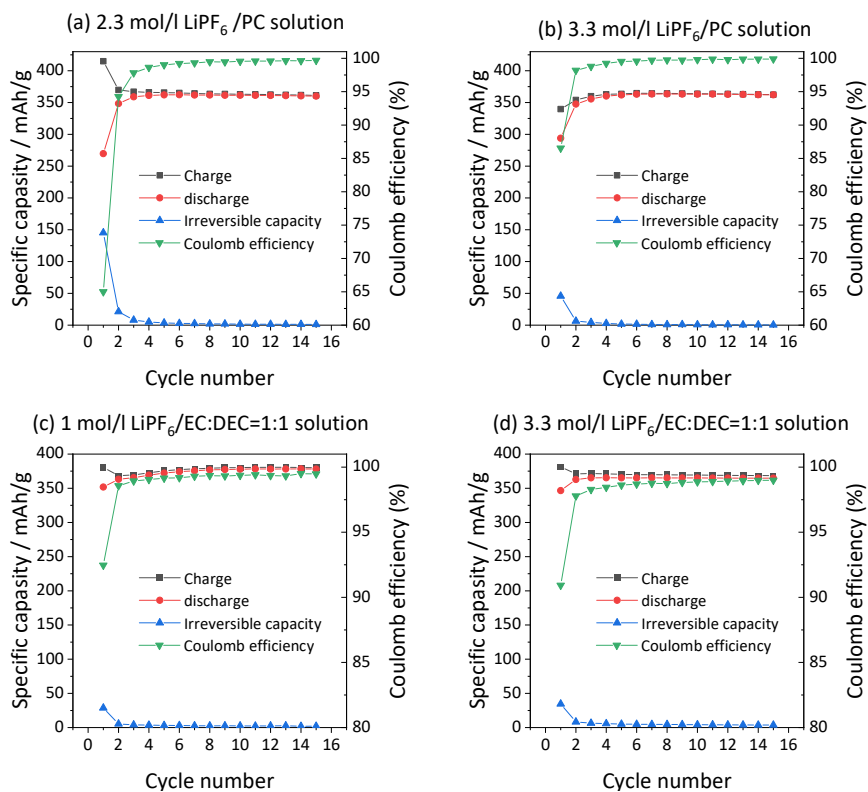


Figure 3.4 Charge / discharge and irreversible capacity, coulomb efficiency of Li | graphite half cell.

Among the electrolyte solutions used in this study, the total irreversible capacity was the lowest for more highly concentrated 3.3 mol/l LiPF₆/PC, and the irreversible capacity in each cycle also remained at the lowest level after the 4th cycle. As for EC+DEC-based solutions, the irreversible capacity was low for 1 mol/l LiPF₆, while more highly concentrated 3.3 mol/l LiPF₆ gave higher irreversible capacity and slightly lower Coulomb efficiency. Thus, there were obvious differences in the dependency of irreversible capacity on the LiPF₆ concentration between PC- and EC+DEC-based electrolyte solutions, which would arise from differences in the solution structures; i.e.,

the electrochemical stability against the reduction of solvated structures varied depending not only on the concentration, but also on the kind of solvent.

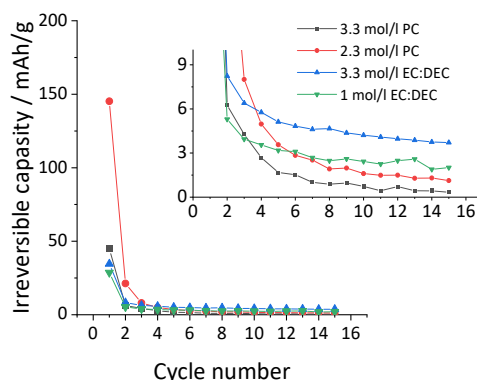


Figure 3.5 Variation of irreversible capacities with cycle number of Li | graphite cells with 2.3 and 3.3 mol/l LiPF₆/PC, and 1 and 3.3 mol/l LiPF₆/EC+DEC (1:1 by vol.).

Table 3.1 Irreversible capacities of Li | graphite cells with 2.3 and 3.3 mol/l LiPF₆/PC, and 1 and 3.3 mol/l LiPF₆/EC+DEC (1:1 by vol.).

Solvent	EC+DEC (1:1 by vol.)		PC	
	1 mol/l	3.3 mol/l	2.3 mol/l	3.3 mol/l
1st	28.7	34.6	145.2	44.9
2nd to 15th	40.5	67.6	55.4	22.4

3.3.2. Solution structure analysis

Raman spectra of the electrolyte solutions were obtained to understand their solvation structures. Figure 3.6 (a) shows the Raman spectra of 2.3 and 3.3 mol/l LiPF₆/PC together with pure PC solvent. PC gave a single Raman band at ca. 720 cm⁻¹, while another peak appeared at ca. 735 cm⁻¹ by dissolving 2.3 and 3.3 mol/l LiPF₆ in PC.

It has been reported that the Raman bands of a solvent split into two components in the electrolyte solution containing lithium salt; one originates from the solvent molecules solvating lithium cations and the other from the solvent molecules that do not interact with lithium cations^{34,35}. The Raman band at ca. 720 cm^{-1} is hence assigned to the ring deformation mode of free PC (designated as “Free”) and the PC molecules solvating lithium cations were detected at 735 cm^{-1} (designated as “Solvated”)³⁶. Similar behaviors were observed for EC in the Raman spectra of $\text{LiPF}_6/\text{EC} + \text{DEC}$ (Figure 3.6 (b)), free and solvating EC molecules were observed at ca. 718 and 730 cm^{-1} , respectively. On the other hand, Raman bands of DEC are known to overlap those of EC, and hence it is generally impossible to distinguish between the solvation structures of DEC and EC. However, in this study, we found that free and solvating DEC molecules gave Raman bands at ca. 525 and 460 cm^{-1} , respectively, both of which are assigned to the O-C-O bending mode as shown in Figure 3.6 (c). These bands enable us to discuss the solvation structure of DEC independently.

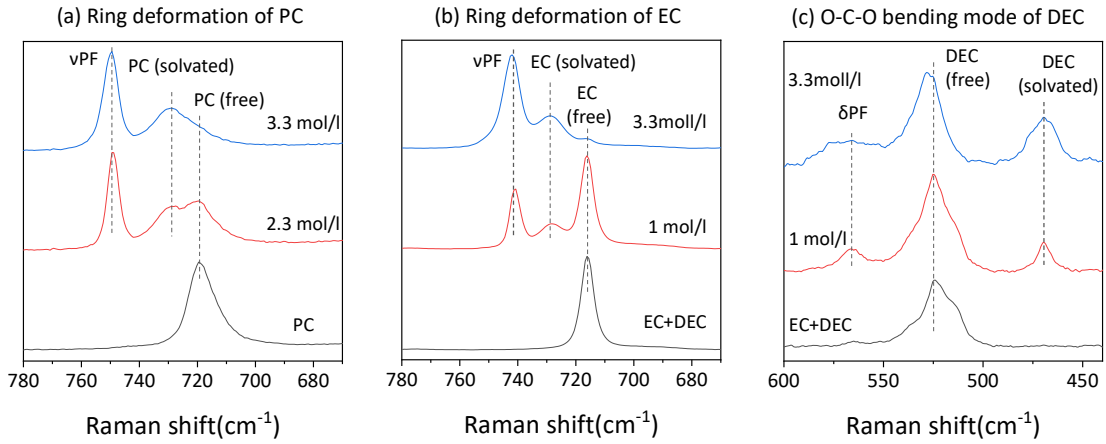


Figure 3.6 Raman spectra (a) a PC solvent, and 2.3 and 3.3 mol/l LiPF₆/PC, (b and c) a mixture of EC+DEC, and 1 and 3.3 mol/l LiPF₆/EC+DEC (1:1 by vol.).

Raman bands of free and solvating solvents are used to estimate the solvation number, which is the number of solvent molecules solvating a lithium cation^{18,32,34}. We denote the integrated Raman band intensity of free and solvating solvent molecules as I_f and I_s , respectively. As for the ring deformation vibration of PC and EC in Figure 3.6 (a) and (b), respectively, the Raman bands of free and solvating molecules overlapped each other, and hence spectral deconvolution was conducted assuming the spectral shape as a Gaussian and/or Lorentzian function to evaluate the integrated intensity of each component (EC+DEC- and PC-based solutions in Figures 3.7 and 3.8, respectively). The solvation number can be determined based on the assumption that free and solvating solvent molecules have an almost equal Raman sensitivity and its integrated intensities are proportional to the number of solvent molecules. Based on

these assumptions, the relative intensity ratio of solvating solvent molecules, $I_r = I_s / (I_s + I_f)$ is correlated with the solvation number as shown in eq.(3-1), where C_s and C_0 are the concentration of a solvating molecule and the total molar concentration of the solvent, respectively. The average solvation number per lithium cation, N_s , is thus given by eq.(3-2), where C_{Li} is the molar concentration of LiPF₆:

$$C_s = I_r \times C_0 = \frac{I_s}{I_s + I_f} \times C_0 \quad (3 - 1)$$

$$N_s = \frac{C_s}{C_{Li}} = \frac{I_s}{I_s + I_f} \times \frac{C_0}{C_{Li}} \quad (3 - 2)$$

Average solvation numbers evaluated from Figure 3.4 are summarized in Table 3.2. The solvation numbers of both 2.3 and 3.3 mol/l LiPF₆/PC solutions are 2-3 molecules, and these values are in good agreement with those reported in the literature^{18,37,38}. As for EC+DEC solutions, about three EC molecules and one DEC molecule coordinated with a lithium cation in the 1 mol/l solution (Table 3.2). In the highly concentrated 3.3 mol/l solution, the total solvation number of EC (1.50) and DEC (0.34) decreases to about two in total, which indicates that EC mainly solvates lithium cation. As estimated from the band intensity ratio I_r , 19 % of EC and 24 % of DEC molecules in 1 mol/l LiPF₆/EC+DEC solvate lithium cations, while 85 % of EC and 35 % of DEC in 3.3 mol/l LiPF₆/EC+DEC solvate lithium cations. Thus, EC is more involved in solvation when the LiPF₆ concentration increases. Since EC ($\epsilon=95$)

has a much higher dielectric constant than DEC ($\epsilon=2.8$), EC molecules should preferentially coordinate with lithium cations and DEC molecules remain free and uncoordinated. The viscosity of each electrolyte solution is summarized in Table 3.3. The viscosity of 3.3 mol/l $\text{LiPF}_6/\text{EC}+\text{DEC}$ solution (113.8 cP) is lower than 272.6 cP of 3.3 mol/l LiPF_6/PC solution when compared at the same molar concentration of LiPF_6 . This perhaps means that solvation structures should consist mainly of lithium ion and EC molecules in the concentrated electrolyte solution, and DEC acts as a diluent to reduce the viscosity.

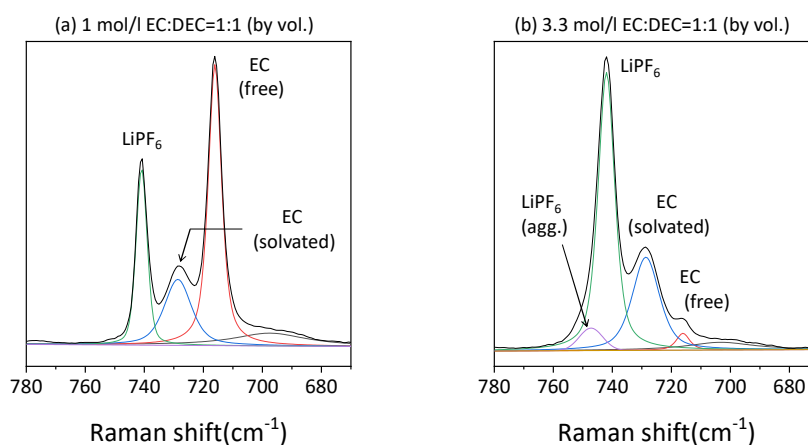


Figure 3.7 Peak-fitting for Raman spectra of (a) 1 and (b) 3.3 mol/l $\text{LiPF}_6/\text{EC}+\text{DEC}$ (1:1 by vol.).

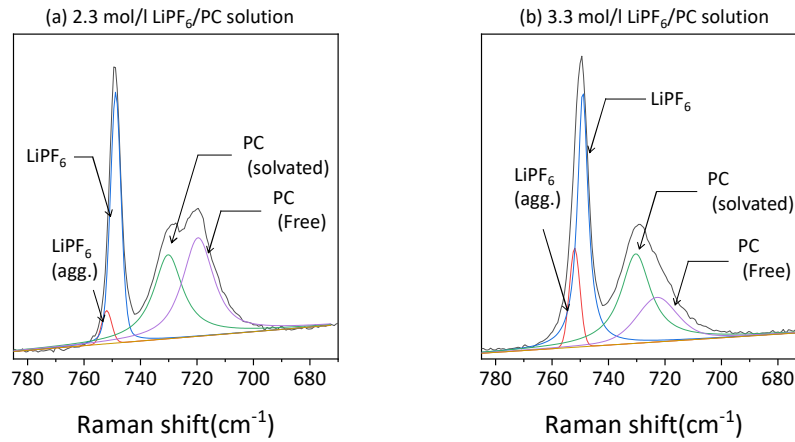


Figure 3.8 Peak fitting for the Raman spectra of (a) 2.3 mol/l, (b) 3.3 mol/l LiPF₆/PC solution.

Table 3.2 Solvation numbers N_s of 2.3 and 3.3 mol/l LiPF₆/PC, and 1 and 3.3 mol/l LiPF₆/EC+DEC (1:1 by vol.).

Solvent	LiPF ₆ molar concentration (mol/l)	$I_r = I_s / (I_s + I_f)$	N_s
PC	2.3	0.557	2.44
	3.3	0.774	2.20
EC	1	0.189	2.55
	3.3	0.847	1.50
DEC	1	0.238	0.94
	3.3	0.351	0.34

Table 3.3 Conductivity and viscosity of electrolyte investigated in this study (measured at 30 °C)

	molar ratio solvent / Li ⁺	conductivity mS/cm	viscosity cP
1 mol/l EC:DEC=1:1 (by vol.)	11.1	8.7	3.8
3.3 mol/l EC:DEC=1:1 (by vol.)	2.8	1.0	113.8
2.3 mol/l PC	4.4	2.7	43.2
3.3 mol/l PC	2.8	0.6	272.6

Solvation structures were modeled using DFT by a B3LYP density functional with a 6-311G+** basis set. Though it has been pointed out that B3LYP does not give completely accurate calculated structures and geometrically relaxed structures like other theoretical calculations³¹, the comparison of the calculated results of compounds with similar chemical structures is considered to be qualitatively valid. The geometrically relaxed structures were calculated using a polarizable continuum model (PCM) where we hypothesized a continuous dielectric media with a dielectric constant of a solvent around the calculated solvated structure. We used $\epsilon=65$ for solvation structures with PC molecules, and $\epsilon=32$ for EC+DEC systems⁴⁰. Here, we calculatedSSIP structures consisting of a lithium cation and four solvent molecules: 4 PC, 4 EC, and 3 EC + 1 DEC, which is a reasonable assumption based on the solvation number for 1 mol/l LiPF₆/EC+DEC (Table 3.2). CIP becomes a major solvation structure when the LiPF₆ concentration increases¹⁸⁻²², and hence we calculated CIP structures of LiPF₆ with three solvent molecules: three PC, three EC, and two EC and one DEC. Similarly, CIP structures with two solvents were also studied: two PC, two EC, and one EC and one DEC. Representative optimized structures are shown in Figure 3.9. The solvation structures of CIP with two solvent molecules were energetically optimized as monodentate and bidentate coordination structures; in the former structure, one fluoride

atom was coordinated to a lithium ion, and in the latter two fluoride atoms coordinated to a lithium ion. The optimized energy for mono- and bidentate solvation structures was almost the same in our calculation. Because a monodentate coordination structure is known to be more stable than a bidentate structure in the optimization calculation for LiPF_6 in solvents⁴¹, the chemical stability of the CIP structure with two solvent molecules was also considered for a monodentate solvation structure.

The stability of chemical species at reductive and oxidative potentials has commonly been discussed using LUMO and HOMO energy levels, respectively. However, LUMO often fails to properly reflect the actual stability against reduction. Hence, here, we used the electron affinity (EA) to evaluate the reductive stability of electrolyte solutions. The EA is defined as the difference ($E_0 - E^-$) in the energy of the neutral solvation structure and the anion radical, where E_0 is the optimized energy for the neutral species, and E^- is the energy calculated for the ionized species^{25,42,43}. EA can predict the stability of chemical species at reductive potentials with high accuracy and less dependence on calculation conditions²⁹. HOMO and LUMO levels and EA for the calculated structures are summarized in Table 3.4.

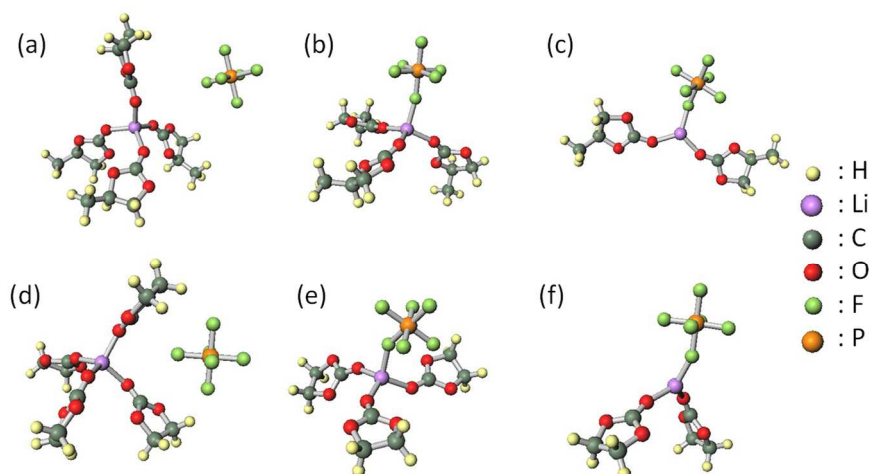


Figure 3.9 Optimized solvation structures of (a) SSIP with four PCs, (b) CIP with three PCs, (c) CIP with two PCs, (d) SSIP with four ECs, (e) CIP with three ECs, and (f) CIP with two ECs.

EA showed very similar values (39-40 kcal/mol) for the SSIP and CIP structures with three solvent molecules, and increased as the solvation number decreased to two molecules, which suggests that highly concentrated electrolyte solutions are expected to be vulnerable to reduction (Figure 3.10). In particular, in this study, the CIP structure with two EC molecules, which is dominant in 3.3 mol/l $\text{LiPF}_6/\text{EC}+\text{DEC}$ solution (Table 3.2), was the most unstable at low potentials.

Table 3.4 HOMO and LUMO levels and EA of solvents and solvated structures

Solvent	Chemical species	Solvation Structure	HOMO [eV]	LUMO [eV]	EA [kcal/mol]
PC	PC	-	-8.6423	0.0925	34.47
	Li ⁺ - 4 PC - PF ₆ ⁻	SSIP	-8.8519	-0.4898	39.56
	LiPF ₆ - 3 PC	CIP	-8.8927	-0.4762	40.21
	LiPF ₆ - 2 PC	CIP	-8.9852	-0.5089	42.18
EC: DEC = 1:1	EC	-	-8.6859	-0.0054	34.66
	DEC	-	-8.2750	0.1660	27.49
	Li ⁺ - 4 EC - PF ₆ ⁻	SSIP	-8.7702	-0.5170	39.30
	Li ⁺ - 3 EC/1 DEC -PF ₆ ⁻	SSIP	-8.6151	-0.5578	39.98
	LiPF ₆ - 3 EC	CIP	-8.9253	-0.5279	39.10
	LiPF ₆ - 2 EC/1 DEC	CIP	-8.6287	-0.5007	39.85
	LiPF ₆ - 2 EC	CIP	-9.0070	-0.5687	43.22
	LiPF ₆ -1 EC/1 DEC	CIP	-8.6913	-0.5442	42.39

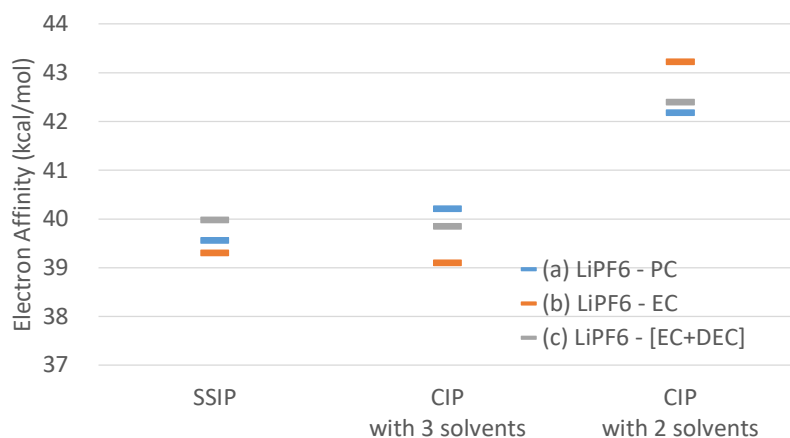


Figure 3.10 EA of solvated structures of (a) LiPF₆/PC, (b) LiPF₆/EC and only EC, and (c) LiPF₆/EC+DEC (including EC molecule(s) with one DEC molecule)

3.3.3 Correlations between theoretical calculation and irreversible capacity of graphite electrode

3.3 mol/l LiPF₆/EC+DEC solution gave a higher irreversible capacity of graphite electrode than 1 mol/l LiPF₆ solution in the initial cycle (Table 3.1), and the sum of the irreversible capacities in the 2nd-15th cycles was the highest among the four electrolyte solutions tested in this study. The CIP structure with two solvent molecules is dominant in the 3.3 mol/l LiPF₆/EC+DEC solution (Table 3.2), and is most likely to decompose reductively at low potentials because the EAs of the CIP structures with two solvent molecules were the highest. Thus, the theoretical predictions agreed well with the experimental results regarding the electrochemical stability of LiPF₆/EC+DEC electrolyte solutions against reduction.

As for PC-based solutions, EA increased as the solvation number decreased (Table 3.2, Figure 3.10), which suggests that the electrolyte solution should become unstable at low potentials as the LiPF₆ concentration increases. However, highly concentrated 3.3 mol/l LiPF₆/PC solution delivered a lower total irreversible capacity in the 1st-15th cycles than 2.3 mol/l solution. To clarify the apparently contradictory results between the irreversible capacity and EA of the solvation structures, the

composition of surface films on graphite electrodes after 15 cycles, which is the origin of the irreversible capacity, was analyzed by XPS.

Figure 3.11 shows XPS F1s and C1s spectra on graphite negative electrode after 15 cycles in different electrolyte solutions, and the compositions of the surface film estimated from the XPS spectra are summarized in Table 3.5. In the F1s region, the observed fluoride peaks were divided into two chemical species to quantify each fluoride compound: one is LiPF_6 peaking at 686 eV and the other is LiF at 684 eV¹⁰. The peak at 684 eV identified as LiF were dominant except for 1 mol/l $\text{LiPF}_6/\text{EC}+\text{DEC}$, and the peak intensity was strongest for 3.3 mol/l LiPF_6/PC (Figure 3.11 (a) and Table 3.5 (a)). The amount of LiF precipitated on the graphite surface was the largest for 3.3 mol/l LiPF_6/PC solution, and almost the same amount of LiF was detected for 3.3 mol/l $\text{LiPF}_6/\text{EC}+\text{DEC}$ and 2.3 mol/l LiPF_6/PC solutions. These results indicate that an inorganic surface film containing LiF should form on the graphite surface in concentrated electrolyte solutions. On the other hand, in the surface films for 1 mol/l $\text{LiPF}_6/\text{EC}+\text{DEC}$ solution, a quite small amount of LiF was detected, which was smaller than that of the LiPF_6 residue remaining on the graphite negative electrodes after rinsed with DEC. This result implies that an organic-rich surface film is formed when the

1 mol/l electrolyte solution containing mainly SSIP is reductively decomposed on graphite. The details are discussed below in the consideration of the C1s spectra.

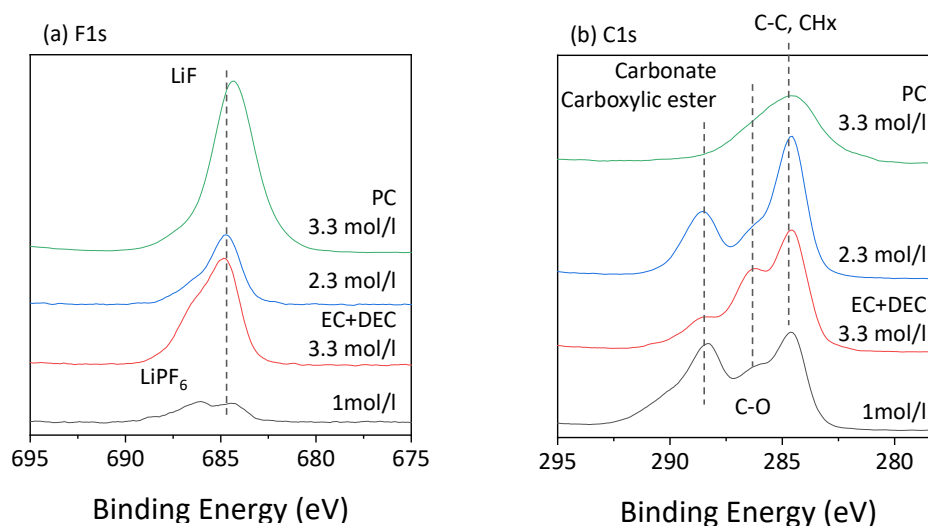


Figure 3.11 XPS spectra of (a) F1s, (b) C1s regions for graphite negative electrodes after 15 cycles in 2.3 and 3.3 mol/l LiPF₆/PC, and 1 and 3.3 mol/l LiPF₆/EC+DEC (1:1 by vol.).

Table 3.5 Atomic composition percentages of (a) whole surface films, and (b) F-containing compounds in the surface films on graphite electrodes after 15 cycles in 2.3 and 3.3 mol/l LiPF₆/PC, and 1 and 3.3 mol/l LiPF₆/EC+DEC (1:1 by vol.).

(a)	(atomic%)				
	Li	C	O	F	P
1 mol/l EC: DEC = 1:1 (by vol.)	16.5	41.5	39.1	2.6	0.4
3.3 mol/l EC: DEC = 1:1 (by vol.)	16.3	42.1	27.8	11.0	2.8
2.3 mol/l PC	20.1	40.5	32.9	5.4	1.1
3.3 mol/l PC	34.9	16.3	12.9	32.9	3.0

(b)	(atomic%)	
	F-P	F- (LiF)
1 mol/l EC: DEC = 1:1 (by vol.)	1.9	0.7
3.3 mol/l EC: DEC=1:1 (by vol.)	5.9	5.1
2.3 mol/l PC	1.7	3.7
3.3 mol/l PC	0.8	32.1

From the XPS spectra of the C1s region in Figure 3.11 (b), carbonates and ester compounds were hardly detected for 3.3 mol/l LiPF₆/PC solution, which shows that PC decomposition does not proceed when the salt concentration reaches near saturation. Considering the low irreversible capacity in the charge/discharge cycles for 3.3 mol/l LiPF₆/PC, an inorganic surface film containing LiF, which is generated from the CIP structures, is chemically stable at reductive potentials, and prevents continuous decomposition of the electrolyte solution. According to the literature, the reductive decomposition of LiPF₆ proceeds through the following reactions to produce LiF⁴⁴, $\text{LiPF}_6 \rightarrow \text{LiF} + \text{PF}_5$, and $\text{LiPF}_6 + 2 \text{Li}^+ + 2 \text{e}^- \rightarrow 3 \text{LiF} + \text{PF}_3$. These reactions seem to be plausible for the highly concentrated LiPF₆/PC because Li⁺ and PF₆⁻ are associated with each other to form CIP and AGG. On the other hand, carbonates and esters were also present on the graphite electrode in 2.3 mol/l LiPF₆/PC solution, which originated from the co-intercalation of PC-solvated lithium ion into the graphite layers accompanied by its decomposition during the initial few cycles. At the same time, the CIP decomposed to form an inorganic-rich surface film containing LiF during the initial

cycles in the concentrated electrolyte solution, as was discussed earlier¹⁰. In our previous study¹⁰, we analyzed the surface films on graphite negative electrodes by XPS combined with Ar ion sputtering, and reported the atomic distributions in a depth direction from the surface of graphite negative electrodes after 15 charge / discharge cycles in the highly concentrated LiPF₆ / PC electrolyte solution. When we removed the surface film by Ar ion sputtering to near the surface of graphite active materials, lithium and fluoride were mainly detected, together with a quite small amount of oxygen that is derived from a PC solvent. These results suggest that LiF-based inorganic components were formed on the graphite active materials in the initial cycles in PC-based concentrated electrolyte solution. After the formation of the stable SEI consisting principally of LiF at the surface of graphite, the continuous decomposition of PC was suppressed. As a result, the irreversible capacities were kept low after the initial cycles for 2.3 and 3.3 mol/l LiPF₆/PC solutions, as shown in Figure 3.5, though the DFT calculations suggested that the CIP structures with fewer solvent molecules should be easily reduced to decompose.

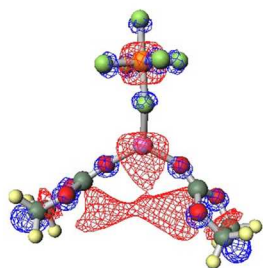
In 1 mol/l LiPF₆/EC+DEC solution, solvates with aSSIP structure are a major component, and EA values of the solvates were higher than those of EC and DEC solvent molecules, as shown in Table 3.3. Hence, the solvent molecules coordinated

with a lithium cation should decompose reductively on a graphite electrode to form a surface film mainly composed of organic components. The irreversible capacity of 1 mol/l $\text{LiPF}_6/\text{EC}+\text{DEC}$ solution is slightly higher than those of 2.3 and 3.3 mol/l LiPF_6/PC solutions in which the LiPF_6 salt preferentially decomposed to form a surface film consisting mainly of LiF. These results suggest that the organic-rich surface film cannot effectively suppress the continuous decomposition of the electrolyte solution, when compared with the LiF-based inorganic surface film that formed in the LiPF_6/PC solutions^{24,45}.

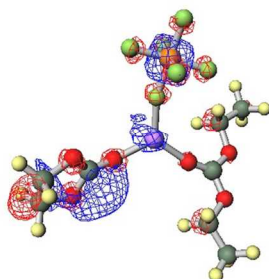
In the highly concentrated $\text{LiPF}_6/\text{EC}+\text{DEC}$, organic surface film containing carbonates, esters, and ethers was formed as well as the inorganic surface film as shown in Figure 3.11 and Table 3.5. This is a different behavior from that seen with PC-based electrolyte solutions. When the LiPF_6 concentration increased from 1 to 3.3 mol/l in EC+DEC, the main component changed from the SSIP to the CIP structure. The CIP structure with two EC molecules has the highest EA, and hence would be the most vulnerable to reduction. In addition, the LUMO of the CIP structure with two EC molecules was clarified to spread both the PF_6^- anion and the two EC molecules by DFT calculations for the spatial distribution of LUMO (Figure 3.12 (a) and (b)). This was quite different from the localized distribution of the LUMO on the PF_6^- anion in the CIP

structure with two PC molecules (Figure 3.12 (c)). Such a difference in the spatial distribution of the LUMO between the EC and PC systems was also seen in the CIP structures with three solvent molecules (Figure 3.13 (a), (b), and (c)). The LUMO was locally distributed on the PF_6^- anion in PC-based solutions, and hence the PF_6^- was reductively decomposed to effectively produce the stable LiF-based inorganic surface film. On the other hand, the explicit LUMO distribution on the EC solvent molecules suggests that EC should decompose easily to form the organic surface film as well on reduction. In addition, a substantial amount of DEC molecules remains free in the EC+DEC electrolyte solutions as shown in Table 3.2, which may swell and dissolve the organic surface film. Once the free DEC swells the surface films, the solvates in the electrolyte solutions would directly reach the graphite surface to decompose reductively. As a result, the organic surface films should gradually convert to LiF-rich surface films in EC+DEC electrolyte solutions. Therefore, the use of EC+DEC solutions resulted in high irreversible capacities until 15 cycles, compared with PC-based solutions.

(a) $\text{LiPF}_6 (\text{EC})_2$



(b) $\text{LiPF}_6 \text{ EC+DEC}$



(c) $\text{LiPF}_6 (\text{PC})_2$

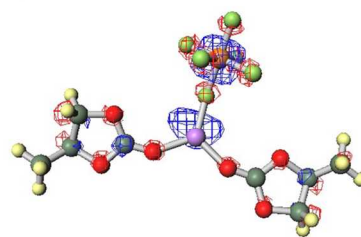
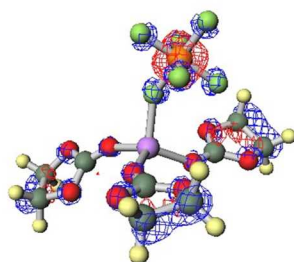
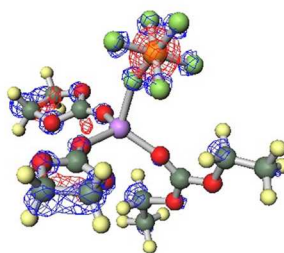


Figure 3.12 LUMO distribution of the CIP structures with two solvent molecules (blue and red indicate the different signs of the isosurface of the wave function)

(a) $\text{LiPF}_6 (\text{EC})_3$



(b) $\text{LiPF}_6 (\text{EC})_2\text{DEC}$



(c) $\text{LiPF}_6 (\text{PC})_3$

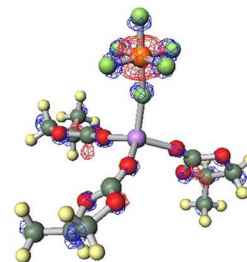


Figure 3.13 LUMO distribution of the CIP structures with three solvent molecules

3.4. Conclusions

The electrochemical stability of PC and EC+DEC solutions with different solvation structures was studied by both experiments and DFT calculations, and the correlation between the reductively decomposition products and charge/discharge characteristics was evaluated. All the electrolyte solutions investigated in this study showed high charge/discharge performance of graphite electrodes, but the irreversible capacity varied depending on the concentration of LiPF_6 and the kind of solvent. In PC-based electrolyte solutions, the SSIP structure was expected to have greater stability against reduction than the CIP structures with fewer PC molecules, and decomposed reductively on graphite negative electrode to form a PC-derived surface film. The CIP structure in the highly concentrated PC-based electrolyte solution had a higher EA, and decomposed to form an inorganic surface film containing LiF on a graphite electrode. The inorganic surface film has greater stability against reduction than a PC-derived one, and can prevent the further decomposition of electrolyte solution in subsequent charge/discharge cycles. Therefore, the irreversible capacity was suppressed in highly concentrated PC-based electrolyte solutions. On the other hand, when the LiPF_6 concentration in EC+DEC was increased to form the CIP structures, the irreversible capacity increased compared with that in the highly concentrated PC-based electrolyte

solution. The EC-containing solvation structures, in particular the CIP structure with two solvent molecules, had a higher EA than that in the PC-based electrolyte solutions, and as a result the reductive decomposition of the solvent molecules and PF_6^- proceeded simultaneously to form a surface film containing both organic and inorganic compounds. This organic-rich surface film has a lower electrochemical stability against reduction than the LiF-rich film that formed in the PC-based electrolyte solution. Therefore, the EC+DEC electrolyte solutions gave higher irreversible capacities than the highly concentrated PC electrolyte solution. These results suggest that the reductive stability of SEI, as well as electrolyte solution itself, should be improved to enhance the durability of graphite electrodes. More importantly, this study indicates that both the chemical composition and physicochemical properties of SEI can be predicted by the more effective utilization of DFT calculation. The predictive characterization of SEI allows us to efficiently design an electrolyte solution that can deliver high performance of negative electrodes such as graphite and silicon.

References

- [1] Goodenough, J. B. Evolution of Strategies for Modern Rechargeable Batteries. *Acc. Chem. Res.* **2013**, *46*, 1053-1061.
- [2] Whittingham, M. Lithium Batteries and Cathode Materials. *Chem. Rev.* **2004**, *104*, 4271-4301.
- [3] Xu, K. Nonaqueous Liquid Electrolytes for Lithium-Based Rechargeable Batteries. *Chem. Rev.* **2004**, *104*, 4303-4417.
- [4] Yamada, Y.; Iriyama, Y.; Abe, T.; Ogumi, Z. Kinetics of Lithium Ion Transfer at the Interface between Graphite and Liquid Electrolytes: Effects of Solvent and Surface Film. *Langmuir* **2009**, *25*, 12766-12770.
- [5] Yamada, Y.; Wang, J.; Ko, S.; Watanabe, E.; Yamada, A. Advances and issues in developing salt-concentrated battery electrolytes. *Nat. Energy* **2019**, *4*, 269-280.
- [6] Yamada, Y.; Yamada, A.; Review - Superconcentrated Electrolytes for Lithium Batteries. *J. Electrochem. Soc.* **2015**, *162*, A2406-A2423.

[7] Qian, Q.; Yang, Y.; Shao, H. Solid electrolyte interphase formation by propylene carbonate reduction for lithium anode. *Phys. Chem. Chem. Phys.* **2017**, *19*, 28772-28780.

[8] Schroder, K.; Celio, H.; Webb, L.; Stevenson, K. Examining Solid Electrolyte Interphase Formation on Crystalline Silicon Electrodes: Influence of Electrochemical Preparation and Ambient Exposure Conditions. *J. Phys. Chem. C* **2012**, *116*, 19737-19747.

[9] Sano, A.; Maruyama, S. Decreasing the initial irreversible capacity loss by addition of cyclic sulfate as electrolyte additives. *J. Power Sources* **2019**, *192*, 714-718.

[10] Aoki, Y.; Oda, S.; Oda, M.; Ogawa, M.; Ishihama, T.; Doi, T.; Inaba, M. Quantitative Analysis of Solid Electrolyte Interphase and Its Correlation with The Electrochemical Performance of Lithium Ion Batteries Using Concentrated LiPF₆/Propylene Carbonate. *J. Electrochem. Soc.* **2021**, *168*, 020530.

[11] Nie, M.; Abraham, D.; Seo, D.; Chen, Y.; Bose, A.; Lucht, B. Role of Solution Structure in Solid Electrolyte Interphase Formation on Graphite with LiPF₆ in Propylene Carbonate. *J. Phys. Chem. C* **2013**, *117*, 25381-25389.

[12] Wang, Y.; Nakamura, S.; Ue, M.; Balbuena, P. B.; Theoretical Studies To Understand Surface Chemistry on Carbon, Anodes for Lithium-Ion Batteries: Reduction Mechanisms of Ethylene Carbonate. *J. Am. Chem. Soc.* **2001**, *123*, 11708-11718.

[13] Wang, Y.; Nakamura, S.; Tasaki, K.; Balbuena, P. B. Theoretical Studies To Understand Surface Chemistry on Carbon Anodes for Lithium-Ion Batteries: How Does Vinylene Carbonate Play Its Role as an Electrolyte Additive?. *J. Am. Chem. Soc.* **2002**, *124*, 4408-4421.

[14] Zhang, W.; Zhang, S.; Fan, L.; Gao, L.; Kong, X.; Li, S.; Li, J.; Hong, X.; Lu, Y. Tuning the LUMO Energy of an Organic Interphase to Stabilize Lithium Metal Batteries. *ACS Energy Lett.* **2019**, *4*, 644 – 650.

[15] Ue, M.; Murakami, A.; Nakamura, S. Anodic Stability of Several Anions Examined by Ab Initio Molecular Orbital and Density Functional Theories. *J. Electrochem. Soc.* **2002**, *149*, A1572-A1577.

[16] Halls, M.; Tasaki, K. High-throughput quantum chemistry and virtual screening for lithium ion battery electrolyte additives. *J. Power Sources* **2010**, *195*, 1472-1478.

[17] Pelj, P.; Girault, H. Electrochemical potential window of battery electrolytes: the HOMO–LUMO misconception. *Energy Environ. Sci.* **2018**, *11*, 2306-2309.

[18] Hwang, S.; Kim, D.; Shin, J. H.; Jang, J. E.; Ahn, K. H.; Lee, C.; Lee, H. Ionic Conduction and Solution Structure in LiPF₆ and LiBF₄ Propylene Carbonate Electrolytes. *J. Phys. Chem. C* **2018**, *122*, 19438-19446.

[19] Marcus, Y.; Hefter, G. Ion Pairing. *Chem. Rev.* **2006**, *106*, 4585-4621.

[20] Buchner, R.; Hefter, G. Interactions and Dynamics in Electrolyte Solutions by Dielectric Spectroscopy. *Phys. Chem. Chem. Phys.* **2009**, *11*, 8984-8999.

[21] Self, J.; Wood, B.; Rajput, N.; Persson, K. The Interplay between Salt Association and the Dielectric Properties of Low Permittivity Electrolytes: The Case of LiPF₆ and LiAsF₆ in Dimethyl Carbonate. *J. Phys. Chem. C* **2018**, *122*, 1990-1994.

[22] Seo, D.; Reininger, S.; Kutcher, M.; Redmond, K.; Euler, W.; Lucht, B. Role of Mixed Solvation and Ion Pairing in the Solution Structure of Lithium Ion Battery Electrolytes. *J. Phys. Chem. C* **2015**, *119*, 14038-14046.

[23] Borodin, O.; Smith, G. Quantum Chemistry and Molecular Dynamics Simulation Study of Dimethyl Carbonate: Ethylene Carbonate Electrolytes Doped with LiPF₆. *J. Phys. Chem. B* **2009**, *113*, 1763-1776.

[24] Xing, L.; Zheng, X.; Schroeder, M.; Alvarado, J.; Cresce, A. W.; Xu, K.; Li, Q.; Li, W. Deciphering the Ethylene Carbonate–Propylene Carbonate Mystery in Li-Ion Batteries. *Acc. Chem. Res.* **2018**, *51*, 282-289.

[25] Tateyama, Y. First-Principles Calculation Study on Solid Electrolyte Interphase (SEI) in Lithium Ion Battery. *J. Comput. Chem. Jpn.* **2019**, *18*, 18-28.

[26] Okuno, Y.; Ushirogata, K.; Sodeyama, K.; Tateyama, Y. Decomposition of the fluoroethylene carbonate additive and the glue effect of lithium fluoride products for the solid electrolyte interphase : an ab initio study. *Phys. Chem. Chem. Phys.* **2016**, *18*, 8643-8653.

[27] Sodeyama, K.; Yamada, Y.; Aikawa, K.; Yamada, A.; Tateyama, Y. Sacrificial Anion Reduction Mechanism for Electrochemical Stability Improvement in Highly Concentrated Li-Salt Electrolyte. *J. Phys. Chem. C* **2014**, *118*, 14091-14097.

[28] Ushirogata, K.; Sodeyama, K.; Futera, Z.; Tateyama, Y.; Okuno, Y. Near-Shore Aggregation Mechanism of Electrolyte Decomposition Products to Explain Solid Electrolyte Interphase Formation. *J. Electrochem. Soc.* **2015**, *162*, A2670-A2678.

[29] Leung, K.; Tenney, C. M. Toward First Principles Prediction of Voltage Dependences of Electrolyte/Electrolyte Interfacial Processes in Lithium Ion Batteries. *J. Phys. Chem. C* **2013**, *117*, 24224-24235.

[30] Leung, K.; Rempe, S. B.; Foster, M. E.; Ma, Y.; Martinez del la Hoz, J. M.; Sai, N.; Balbuena, P. B. Modeling Electrochemical Decomposition of Fluoroethylene Carbonate on Silicon Anode Surfaces in Lithium Ion Batteries. *J. Electrochem. Soc.* **2014**, *161*, A213-A221.

[31] Yamada, Y.; Furukawa, K.; Sodeyama, K.; Kikuchi, K.; Yaegashi, M.; Tateyama, Y.; Yamada, A. Unusual Stability of Acetonitrile-Based Superconcentrated Electrolytes for Fast-Charging Lithium-Ion Batteries. *J. Am. Chem. Soc.* **2014**, *136*, 5039-5046.

[32] Shi, P.; Lina, M.; Zheng, H.; He, X.; Xue, Z.; Xiang, H.; Chen, C. Effect of propylene carbonate-Li⁺ solvation structures on graphite exfoliation and its application in Li-ion batteries. *Electrochimica Acta* **2017**, *247*, 12-18.

[33] Jeong, S.; Inaba, M.; Iriyama, Y.; Abe, T.; Ogumi, Z. Electrochemical Intercalation of Lithium Ion within Graphite from Propylene Carbonate Solutions. *Electrochem. Solid-State Lett.* **2003**, *6*, A13-A15.

[34] Morita, M.; Asai, Y.; Yoshimoto, N.; Ishikawa, M. A Raman spectroscopic study of organic electrolyte solutions based on binary solvent systems of ethylene carbonate with low viscosity solvents which dissolve different lithium salts. *J. Chem. Soc. Faraday Trans.* **1998**, *94*, 3451-3456.

[35] Kondo, K.; Sano, M.; Hiwara, A.; Omi, T.; Fujita, M.; Kuwae, A.; Iida, M.; Mogi, K.; Yokoyama, H. Conductivity and Solvation of Li⁺ Ions of LiPF₆ in Propylene Carbonate Solutions. *J. Phys. Chem. B* **2000**, *104*, 5040-5044.

[36] Åvall, G.; Wallenstein, J.; Cheng, G.; Gering, K. L.; Johansson, P.; Abraham, D. P. Highly Concentrated Electrolytes: Electrochemical and Physicochemical Characteristics of LiPF₆ in Propylene Carbonate Solutions. *J. Electrochem. Soc.* **2021**, *168*, 050521.

[37] Chapman, N.; Borodin, O.; Yoon, T.; Nguyen, C.; Lucht, B. Spectroscopic and Density Functional Theory Characterization of Common Lithium Salt Solvates in Carbonate Electrolytes for Lithium Batteries. *J. Phys. Chem. C* **2017**, *121*, 2135-2148.

[38] Reddy, V.; Smart, M.; Chin, K.; Ratnakumar, B.; Surampudi, S.; Hu, J.; Yan, P.; Prakash, G. ¹³C NMR Spectroscopic, CV, and Conductivity Studies of Propylene

Carbonate-Based Electrolytes Containing Various Lithium Salts. *Electrochem. Solid-State Lett.* **2005**, *8*, A294-A298.

[39] Barnes, T.; Kaminski, J.; Borodin, O.; Miller, III, T F. Ab Initio Characterization of the Electrochemical Stability and Solvation Properties of Condensed-Phase Ethylene Carbonate and Dimethyl Carbonate Mixtures. *J. Phys. Chem. C* **2015**, *119*, 3865-3880.

[40] Wang, F.; Varenne, F.; Ortiz, D.; Pinzio, V.; Mostafavi, M.; Le Caër, S. Degradation of an Ethylene Carbonate/Diethyl Carbonate Mixture by Using Ionizing Radiation. *Chem. Phys. Chem.* **2017**, *18*, 2799-2806.

[41] Takeuchi, M.; Matubayasi, N.; Kameda, Y.; Minofar, B.; Ishiguro, S.; Umebayashi, Y. Free-Energy and Structural Analysis of Ion Solvation and Contact Ion-Pair Formation of Li^+ with BF_4^- and PF_6^- in Water and Carbonate Solvents. *J. Phys. Chem. B* **2012**, *116*, 6476-6487.

[42] Li, X.; Cai, Z.; Sevilla, M. DFT Calculations of the Electron Affinities of Nucleic Acid Bases: Dealing with Negative Electron Affinities. *J. Phys. Chem. A* **2002**, *106*, 1596-1603.

[43] Zhan, C.; Nichols, J.; Dixon, D. Ionization Potential, Electron Affinity, Electronegativity, Hardness, and Electron Excitation Energy: Molecular Properties from Density Functional Theory Orbital Energies. *J. Phys. Chem. A* **2003**, *107*, 4184-4195.

[44] Aurbach, D.; Markovsky, B.; Shechter, A.; Ein-Eli, Y.; Cohen, H. A Comparative Study of Synthetic Graphite and Li Electrodes in Electrolyte Solutions Based on Ethylene Carbonate-Dimethyl Carbonate Mixtures. *J. Electrochem. Soc.* **1996**, *143*, 3809-3820

[45] Zhao, H.; Park, S.; Shi, F.; Fu, Y.; Battaglia, V.; Ross, P.; Liu, G. Propylene Carbonate (PC)-Based Electrolytes with High Coulombic Efficiency for Lithium-Ion Batteries. *J. Electrochem. Soc.* **2014**, *161*, A194-A200.

Chapter 4

Effective approach by computational chemical prediction and experimental verification to elucidate SEI formation mechanism in LiPF_6 , LiFSI and LiBF_4 -containing electrolyte solutions

4.1. INTRODUCTION

There have been many research activities on lithium ion batteries (LIBs) to achieve higher energy density and longer durability and to respond to the increasing demands for portable and automobile energy sources^{1,2}. Various kinds of positive and negative electrode materials have been newly developed so far, and electrolyte solutions have also advanced to utilize these electrode materials as much as possible³. There are a lot of features required for the electrolyte solutions, such as wide potential windows, high ionic conductivity, and chemical stability against reduction and oxidation. One of the most important features is the ability to form a stable surface film, namely, solid

electrolyte interphase (SEI), on the surface of graphite negative electrodes through reductive decomposition of an electrolyte solution in charge/discharge processes⁴⁻⁸.

Electrolyte solutions are generally composed of free ions, a solvent-separated ion pair (SSIP), a contact ion pair (CIP), and an aggregate of an electrolyte salt particularly in a highly concentrated electrolyte solution⁹⁻¹². The stability of electrolyte solutions against reduction and the reaction pathway for SEI formation depends on the solvation structure^{6,13-15}. However, the solvation structure is so complicated that the formation mechanism of SEI, its chemical composition and electrochemical characteristics still remain to be elucidated completely¹⁶⁻¹⁸. The composition of SEI has been analyzed by FT-IR, NMR, and XPS so far¹⁹, but the experimental results cannot yet be correlated with solvation structures of lithium ion and their reaction pathway of SEI formation. Quantum chemical calculation suggests that HOMO and LUMO energies, and their gaps can be used as a measure for the estimation of oxidative and reductive stability, whereas there exists heavy dependence of the energies on basis set when we compare them between different solvation structures with different salts and solvent species²⁰. Ab initio MD calculation is a theoretically promising approach and it can predict not only the reductive stability, but also the reaction pathway, while the computational cost is significantly high^{21,22}.

In this study, we aimed to establish an effective approach by predicting the reductive stability of a solvation structure and SEI formation pathway to comprehensively understand the formation mechanism of SEI on a graphite negative electrode. Three kinds of lithium salts, LiPF_6 , $\text{LiN}(\text{SO}_2\text{F})_2$ (LiFSI) and LiBF_4 were used in combination with a conventional mixture solvent of ethylene carbonate (EC) and diethyl carbonate (DEC). The solvation structure of these electrolyte solutions was experimentally determined, and the electron affinity was evaluated by DFT calculation as a measure of the reductive stability. LUMO distribution in the solvates is also calculated to predict a reaction pathway of SEI formation. These theoretical predictions are verified experimentally through electrochemical measurements and composition analyses of SEI.

4.2. EXPERIMENTAL SECTION

Three kinds of electrolyte solutions with different lithium salts were prepared as follows; commercially available battery grade Ethylene Carbonate (EC) and Diethyl Carbonate (DEC) were mixed in Ar filled glove box (< 1 ppm H_2O) with 1 : 1 by volume, and then 1 mol/l each of LiPF_6 , LiFSI and LiBF_4 was dissolved. Raman spectra of electrolyte solutions were obtained to determine the solvation structures by a Raman

spectrometer Model PDP 320 (Photon Design) equipped with the grating of 900 gr/mm with 320 mm focus length and 1064 nm YAG laser was used as an excitation source.

Theoretical calculations of solvation structures were carried out using DFT with a B3LYP functional and a 6-311+G** basis set. The geometries of all solvation structures were optimized and confirmed to be at their energetically local minimum by Hessian calculations using a polarizable continuum model (PCM) where we hypothesized a continuous dielectric media with a dielectric constant of a solvent around the calculated solvation structure.

The chemical stability of electrolyte solutions was investigated by cyclic voltammetry (CV) using 2032 coin-type two electrode cells. The graphite working electrode was composed of graphite powder as an active material, and styrene-butadiene rubber (SBR) and carboxymethyl cellulose (CMC) as binders (98:1:1 by weight). A counter electrode was a lithium foil. CV measurements of the coin cells with different electrolyte solution were conducted between 2 and 0.01 V at 0.1 mV/s using a VSP potentiostat/galvanostat (Biologics Inc.), and repeated three times at 25 °C. Electrochemical ac impedance measurements were carried out after the 1st and 3rd CV cycle at 25 °C. The voltage was kept at 0.2 V until reaching a steady state, and then

impedance was measured in a frequency range from 100 kHz to 10 mHz with a potential modulation of ± 10 mV.

After CV measurements, the coin cells were disassembled in an Ar-filled glove box to collect the working electrode. It was then rinsed in dimethyl carbonate (DMC) to remove the electrolyte solution, and dried under vacuum at room temperature. The morphological observation and elemental analysis of the graphite negative electrode were conducted by Scanning Electron Microscope (SEM, S-4800, Hitachi High-Tech Corp.) and Energy Dispersive X-ray Spectroscopy (EDX, QUANTAX Flat QUAD System Xflash 5060FQ, Bruker ltd.). Acceleration voltage was set to 0.8 and 5.0 kV for SEM observation and EDX analysis, respectively. The composition of surface films on the graphite electrodes was also investigated by X-ray photoelectron spectroscopy (XPS, Qunatera SXM, ULVAC-PHI). In the XPS measurements, the acceleration voltage and the emission current of a monochromatic Al $K\alpha$ X-ray gun were set at 15 kV and 3 mA, respectively. The samples were transferred from an Ar-filled glove box to SEM-EDX and XPS instruments using special air-tight vessels without any exposure to air and moisture.

4.3. RESULTS AND DISCUSSION

Raman spectra were acquired to understand the solvation structures of electrolyte solutions (Figure 4.1). Free EC molecules and those solvating Li^+ cations show its C-O stretching vibration mode at around 890 and 910 cm^{-1} , which are represented as “Free” and “Solvating EC” in Figure 4.1 (b), respectively. The relative band intensity of “Solvating EC” to “Free EC” is almost the same for 1 mol/l LiPF_6 and LiFSI electrolyte solutions, and hence they possess similar solvation structure. When LiBF_4 is used as an electrolyte salt, the relative intensity of “Solvating EC” to “Free EC” is lower than those of the LiPF_6 and LiFSI solutions, which suggests that the fraction of solvating EC molecules is smaller in the 1 mol/l LiBF_4 electrolyte solution. This is because LiBF_4 is less dissociative than LiPF_6 and LiFSI²³⁻²⁵. The C-O stretching mode of free DEC molecules is observed at 905 cm^{-1} , which is unfortunately superimposed on the C-O stretching mode of solvating EC. However, it does not severely affect the estimation of EC solvation because of the smaller Raman scattering coefficient of DEC than that of EC (Figure 4.2).

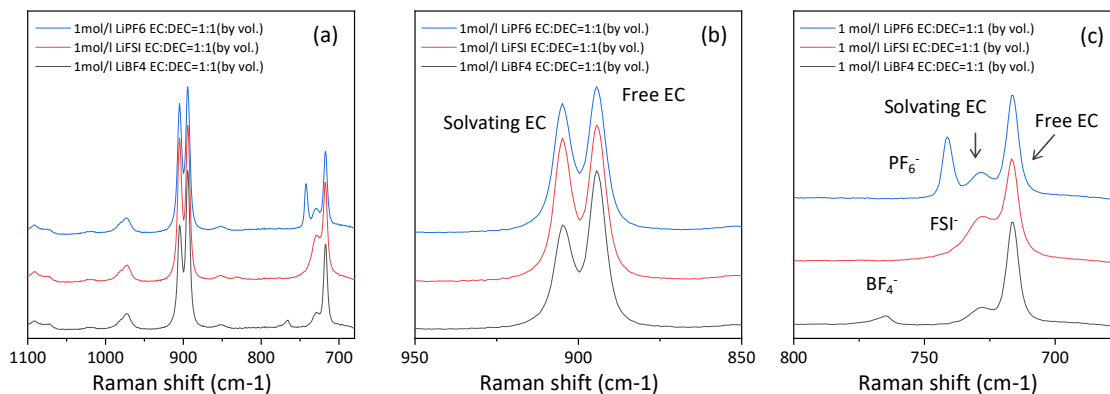


Figure 4.1 Raman spectra of (a) 1 mol/l $\text{LiPF}_6/\text{EC}+\text{DEC}(1:1 \text{ by vol.})$, 1 mol/l $\text{LiFSI}/\text{EC}+\text{DEC}(1:1 \text{ by vol.})$, and 1 mol/l $\text{LiBF}_4/\text{EC}+\text{DEC}(1:1 \text{ by vol.})$, (b) the enlarged views of (b) C-O stretching mode region, and (c) anion and EC ring deformation mode region in (a).

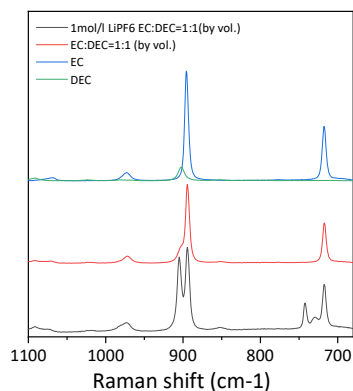


Figure 4.2 Raman spectra of EC, DEC, EC+DEC (1:1 by vol.) and 1 mol/l LiPF_6 electrolyte solution (EC+DEC (1:1 by vol.)).

Solvation structures of electrolyte solutions can be understood in more detail from Raman bands of counter anions. PF_6^- anions give a single and symmetric spectral shape at 740 cm^{-1} , which are attributable to free anions (solvated PF_6^- anions) and/or those

with a SSIP structure in 1 mol/ 1 LiPF₆ electrolyte solution, as was reported in the literatures¹⁰⁻¹². S-N stretching vibration mode of FSI⁻ anions in 1 mol/l LiFSI electrolyte solution shows Raman bands at 720, 730, and 740-760 cm⁻¹, which are identified as SSIP, CIP, and aggregate structures, respectively²⁶. Ring deformation mode of free EC molecules is observed at 715 cm⁻¹ and that for solvating ones is at 728 cm⁻¹^{27,28}. Accordingly, a band for an FSI⁻ anion in a SSIP structure (720 cm⁻¹) is observed between these two Raman bands. Moreover, a band for ring deformation of solvating EC (728 cm⁻¹) overlaps with that for an FSI⁻ anion in a CIP structure (730 cm⁻¹). The relative peak intensity of 730 cm⁻¹ to free EC (715 cm⁻¹) for 1 mol/l LiFSI electrolyte solution is higher than that for 1 mol/l LiPF₆ solution though these two electrolyte solutions possess almost the same solvation structure, as described above. Therefore, the Raman band at 730 cm⁻¹ for 1 mol/l LiFSI electrolyte solution is ascribable not only to the ring deformation mode of solvating EC but also to the stretching mode of FSI⁻ in CIP. These results indicate that FSI⁻ anions with a CIP structure are also present in the LiFSI-containing electrolyte solution, in addition to free anions (solvated FSI⁻ anion) and those with a SSIP structure. In the Raman spectra of 1 mol/l LiBF₄ electrolyte solution, the B-F stretching vibration mode shows broad bands between 760 and 780 cm⁻¹, which suggests a mixture of SSIP, CIP and aggregate structures of LiBF₄ at 762,

770 and 780 cm^{-1} respectively²⁹. The relative area ratios of these peaks are evaluated to be 39, 55, and 6 % for SSIP, CIP, and aggregate structures, respectively (Figure 4.3).

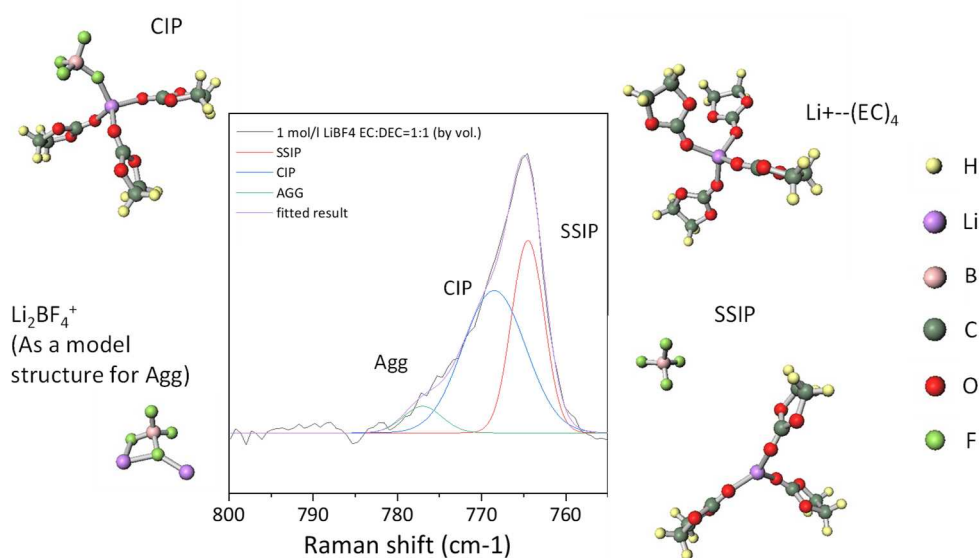


Figure 4.3 Raman spectra of the B-F symmetric stretching vibration band of 1 mol/l $\text{LiPF}_6/\text{EC}+\text{DEC}$ (1:1, by vol.), and peak separation analysis with three components of SSIP, CIP, and aggregate structures (Agg).

The structure of solvates that were determined by Raman spectroscopy was optimized by DFT calculation. Solvation structures were modeled using DFT by a B3LYP density functional with a 6-311G+** basis set. Though B3LYP does not give completely accurate and geometrically relaxed structures like other theoretical calculations³⁰, it is qualitatively valid to compare the calculated results with similar chemical structures. The geometrically relaxed structures were calculated using a

polarizable continuum model (PCM) where we hypothesized a continuous dielectric media with a dielectric constant (ϵ) of a solvent around the calculated solvation structure; that is, ϵ was set to 32 for EC+DEC systems in this study³¹. LiPF₆ and LiFSI dissociate to form free Li⁺-(EC)₄ ions and those with a SSIP structure in the 1 mol/l electrolyte solutions, as was proved from the Raman spectra in Figure 4.1. Hence, 4 EC molecules solvate a Li⁺ cation to form a Li⁺-(EC)₄, and a PF₆⁻ or FSI⁻ anion exists in the vicinity of the solvate to form a SSIP structure (Figure 4.4 (a), (b), (c)). CIP structures are also formed in 1 mol/l LiFSI electrolyte solution, which has 3 (Figure 4.4 (d)) or 2 EC molecules. On the other hand, 1 mol/l LiBF₄ electrolyte solution contains CIP and aggregate structures as well as a SSIP structure, and hence three types of solvation structures were considered; one is SSIP in Figure 4.4 (e), and another is CIP of LiBF₄ with 3 (Figure 4.4 (f)) or 2 EC molecules. The other is Li₂BF₄⁺ with an aggregate structure (Figure 4.4 (g)). All the calculated conformations are representatives for solvation structures, and there possibly exist slightly different conformation for them, whereas the difference in conformation does not affect the order of electron affinity (Figure 4.5).

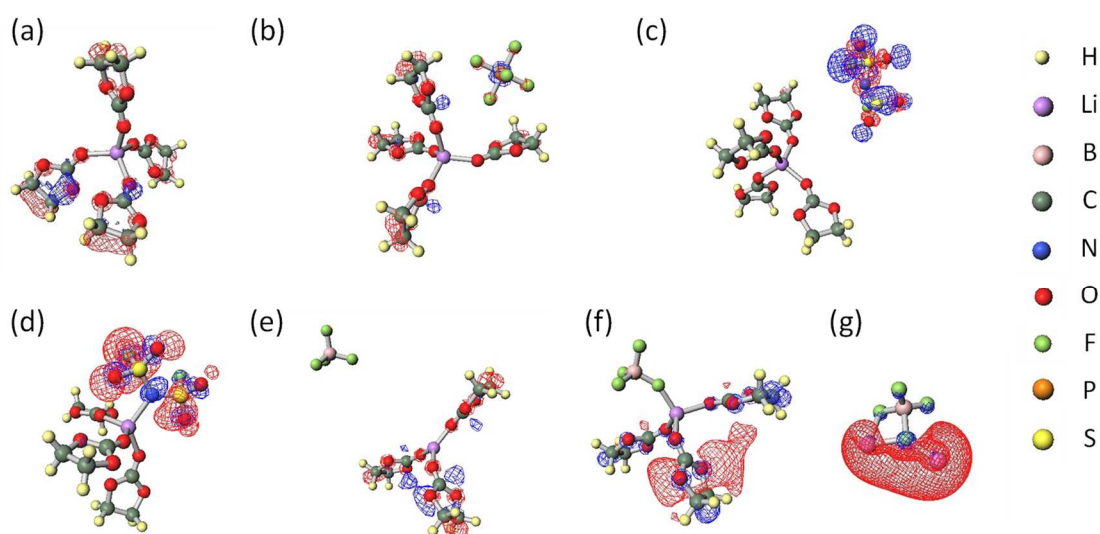


Figure 4.4 Geometrically optimized solvation structures and their LUMO distribution of (a) EC-solvated Li cation, (b) SSIP of 4 EC + LiPF₆, (c) SSIP of 4 EC + LiFSI, (d) CIP of 3 EC + LiFSI, (e) SSIP of 3 EC + LiBF₄, (f) CIP of 3 EC + LiBF₄, (g) Aggregate (Li₂BF₄⁺), isosurface value for LUMO distribution is set to 0.02.

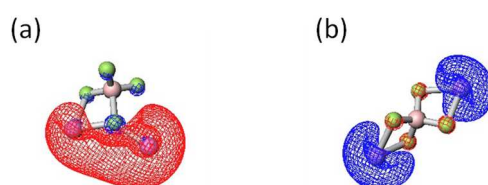


Figure 4.5 Different conformers with aggregate structures. Electron affinity for different conformations of Li₂BF₄⁺, which is models for aggregation, was calculated to check the effect of conformation on electron affinity.

Electron affinity and LUMO distribution of solvates were calculated to evaluate the reductive stability and to elucidate the decomposition reaction pathways of them³¹. Reductive stability of electrolyte solutions is often discussed by LUMO energy level, but it depends on the basis function employed for theoretical calculation. On the other

hand, dependence of electron affinity on the basis set is low³²⁻³⁴, and in fact we have demonstrated that electron affinity can predict the reductive stability of LiPF₆-containing electrolyte solutions with different concentrations³². In addition, the spatial distribution of LUMO can indicate a decomposition pathway of the solvates because LUMO is anti-bonding molecular orbital which accepts an electron upon reduction.

Electron affinity is summarized in Figure 4.6 and Table 4.1. In 1 mol/l LiPF₆ electrolyte solution, free Li⁺-(EC)₄ ions and those with a SSIP structure are dominant, whose electron affinities are close to each other ranging from 39 to 41 kcal/mol. LUMO distributes on the EC molecules in a free Li⁺-(EC)₄ ion (Figure 4.4 (a)), and both on PF₆⁻ anion and EC molecules in a SSIP structure (Figure 4.4 (b)). These results suggest that reductive decomposition reactions should proceed through both EC ring opening and PF₆⁻ anion decomposition. LiFSI-containing solvates with SSIP and CIP structures possess a quite high electron affinity about 85 - 88 kcal/mol, and LUMO distributes almost only on FSI⁻ anion. Therefore, FSI⁻ anions will reductively decompose in preference. 1 mol/l LiBF₄ electrolyte solution has free Li⁺-(EC)₄ ions, SSIP, CIP and aggregate structures. Electron affinity is relatively low for SSIP (25 kcal/mol), and increases as the number of EC molecules decreases; 39 - 42 kcal/mol for CIP, and the highest value of 48 kcal/mol for an aggregate structure. These values indicate that the

aggregate is reductively decomposed in preference to produce BF_4^- anion-derived products. The other solvates, free $\text{Li}^+(\text{EC})_4$ ions and CIP, should be also subject to reductive decomposition because of only a slight difference in electron affinity and the relatively high proportion; the LUMO distributions in free $\text{Li}^+(\text{EC})_4$ ions (Figures 4.4 (e)) and those with a CIP structure (Figures 4.4 (f)) suggest the preferential decomposition of EC molecules.

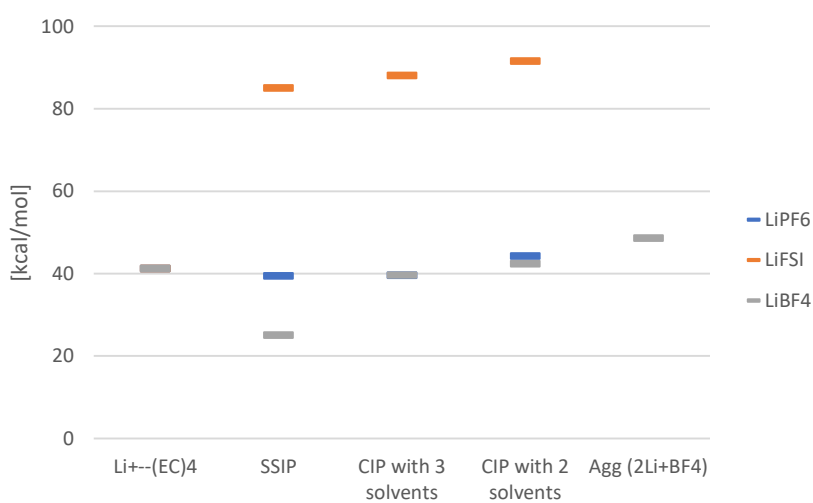


Figure 4.6 Comparison of electron affinity of solvates. The solvent molecules used are EC.

Table 4.1 HOMO, LUMO, their gaps, and electron affinity of solvent and solvates.

Species	Solvation structure	HOMO [eV]	LUMO [eV]	HOMO-LUMO [eV]	Electron Affinity [kcal/mol]
EC	-	-8.686	-0.005	8.68	34.7
DEC	-	-8.275	0.166	8.44	27.5
Li ⁺ -(EC) ₄	-	-9.015	-0.604	8.41	41.3
Li ⁺ - EC ₄ - PF ₆ ⁻	SSIP	-8.757	-0.528	8.23	39.4
LiPF ₆ - EC ₃	CIP	-8.915	-0.520	8.40	39.5
LiPF ₆ - EC ₂	CIP	-9.045	-0.588	8.46	44.2
Li ⁺ - EC ₄ - FSI ⁻	SSIP	-8.291	-0.686	7.61	85.0
LiFSI - EC ₃	CIP	-8.514	-0.784	7.73	88.0
LiFSI - EC ₂	CIP	-8.808	-0.893	7.92	91.5
Li ⁺ - EC ₃ - BF ₄ ⁻	SSIP	-8.664	-0.563	8.10	25.0
LiBF ₄ - EC ₃	CIP	-8.898	-0.512	8.39	39.7
LiBF ₄ - EC ₂	CIP	-8.958	-0.509	8.45	42.3
Li ₂ BF ₄ ⁺	Aggregate	-11.30	-0.963	10.34	47.9

To verify the DFT prediction stated above, cyclic voltammetry was performed using Li | graphite cells (Figure 4.7). During the initial cathodic scan from 3.0 to 0.3 V, a broad cathodic current peak is observed at around 1.2 - 0.5 V for all the electrolyte solutions, indicating the reduction of electrolyte solutions accompanied by formation of SEI on the graphite negative electrode. 1 mol/l LiFSI electrolyte solution gives a peak at 0.6 V (Figure 4.7 (b)), which would result from the decomposition of FSI⁻ anion in SSIP and CIP structures because of their high electron affinities. Such a cathodic current is

not observed in the 2nd cycle, which suggests that a protective SEI can effectively form on the graphite surface and further decomposition reactions are suppressed below a voltage of 0.4 V. On the other hand, a continuous cathodic current was seen until 0.3 V in 1 mol/l LiBF₄ electrolyte solution (Figure 4.7 (c)); the decomposition reaction proceeds until the lower voltages than that for other two electrolyte solutions. These results indicate that protective SEI cannot form facily on graphite electrodes in the LiBF₄-containing electrolyte solution. The SEI formation is followed by Li⁺ intercalation into the graphite at voltages ranging from 0.3 to 0.01 V. The strong cathodic current peaks correspond to the formation of stage structures of Li-graphite intercalation compounds. The anodic currents in the voltage range from 0.01 to 2 V are identified as de-intercalation reactions of Li⁺ cation from graphite.

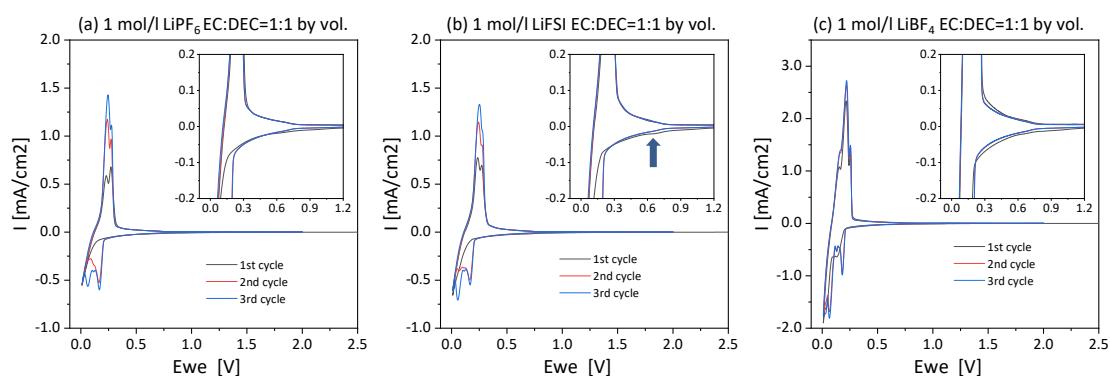
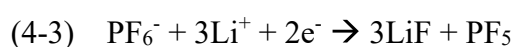
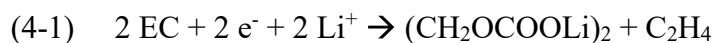


Figure 4.7 Cyclic voltammograms of Li | graphite coin cells using EC + DEC (1 : 1 by vol.)-based electrolyte solutions with (a) 1 mol/l LiPF₆, (b) 1 mol/l LiFSI, and 1 mol/l LiBF₄.

SEM-EDX and XPS measurements were conducted after three CV cycles to prove the reaction pathway of SEI formation that is predicted by DFT calculations. SEM images and elemental distribution of fluoride and oxygen are shown in Figure 4.8. A uniform distribution of oxygen and particles including fluoride less than 500 nm in diameter are observed when LiPF₆ is used as an electrolyte salt. Oxygen derives from the solvent decomposition and fluoride from the decomposition of PF₆⁻. Thus, both solvent and PF₆⁻ anions decompose, as predicted from LUMO distribution, and these results are quite consistent with well-known reaction schemes shown below³⁵.



When LiFSI-containing electrolyte solution was used, particles containing fluoride have smaller sizes than those obtained for LiPF₆-containing one and distributed more homogeneously on the graphite surface. Hence, these particles are formed through reductive decomposition of FSI⁻ anions. In addition, uniform distribution of oxygen suggests that free Li⁺-(EC)₄ ions should reach the graphite surface, and the EC molecules reductively decompose to form oxygen-containing precipitates, such as carbonate / carboxylate.

Quite different results are obtained when LiBF₄ is used as an electrolyte salt. A number of particles as large as 1 μm in diameter, containing fluoride and oxygen, are observed at the surface of graphite. The electron affinity and LUMO distribution do not predict the decomposed compounds containing both fluoride and oxygen; Li₂BF₄⁺ aggregates release fluorine to form LiF, and EC molecules in free Li⁺-(EC)₄ ions and CIP decompose to form oxygen-containing products. In addition, the concentration of fluoride in particulate deposits is quite high. Fluorine should be released from aggregates, but its atomic concentration (Figure 4.8 (c)) is quite higher than expected from the concentration of aggregates in the electrolyte solution (5%). These unexpected results appear to assert the invalidity of DFT calculations for LiBF₄-containing electrolyte solutions.

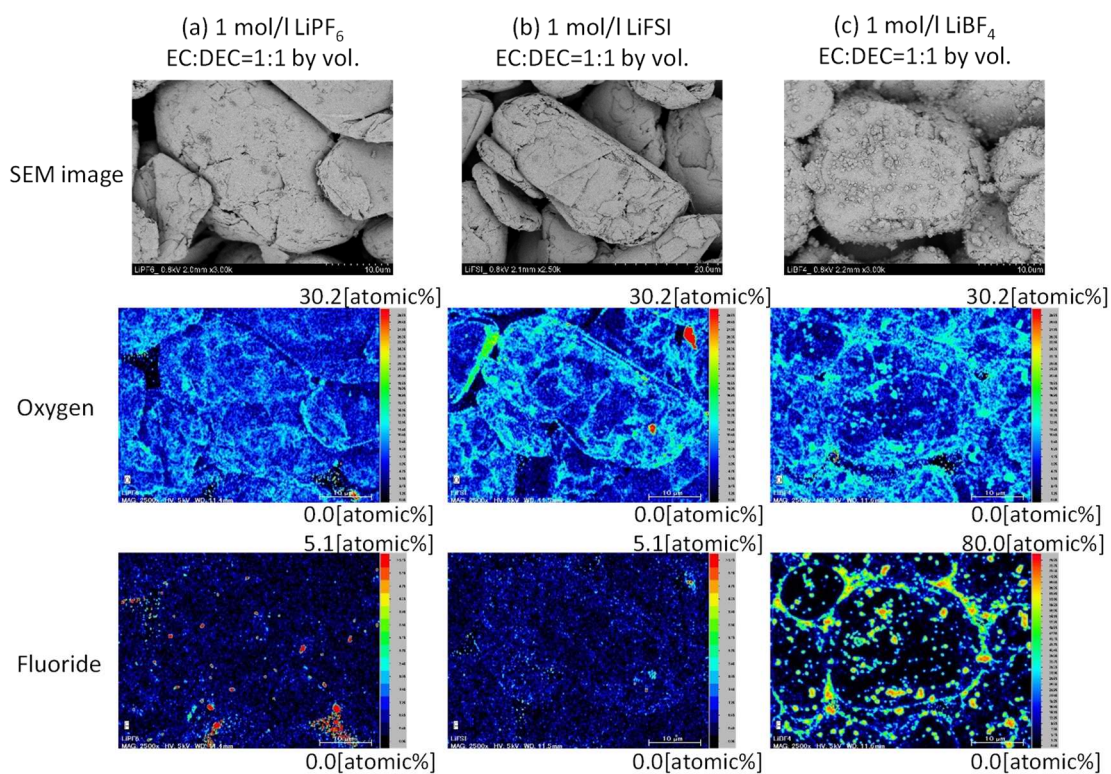


Figure 4.8 (upper) SEM and EDX images of (middle) oxygen and (down) fluorine of graphite negative electrodes after three cycles in EC+DEC (1:1 by vol.) electrolyte solution containing (a) 1 mol/l LiPF₆, (b) 1 mol/l LiFSI, and (c) 1 mol/l LiBF₄

To resolve the inconsistency between theoretical prediction and SEM-EDX results, a chemical structure of SEI on graphite electrodes after CV was further analyzed by XPS. C1s spectra for 1 mol/l LiPF₆ and LiFSI electrolyte solutions were almost the same, indicating the formation of carbonate and carboxylate (Figure 4.9 (a)). These compounds derive from the reductive decomposition of EC, as predicted by DFT calculation of Li⁺-(EC)₄ solvates in both electrolyte solutions and SSIP for the LiPF₆.

On the other hand, C1s spectrum for 1 mol/l LiBF₄-containing electrolyte solution has quite different features compared to the other two solutions; C=O and C-O peaks are mainly detected, while peaks identified as carbonate and carboxylate are very weak. These results suggest that the reductive decomposition of EC similarly occurs in 1 mol/l LiBF₄ electrolyte solution, but the decomposition products are different from those obtained for the other two electrolyte solutions.

Differences among the three electrolyte solutions are also observed in F1s spectra. As for LiPF₆- and LiFSI-containing electrolyte solutions, LiF and a residue of electrolyte salts are detected. Of these two solutions, 1 mol/l LiFSI electrolyte solution gave a stronger signal of LiF on the graphite electrode surface (Figure 4.9 (b)). This is because the solvation structures with an FSI⁻ anion possess a higher electron affinity. On the other hand, when LiBF₄ was used, a very strong B-F signal is mainly observed with a relatively weak signal of LiF. In general, the solubility of LiBF₄ to carbonate solvents is higher than that of LiPF₆³⁶, while a larger amount of a residue exists on the graphite surface after rising with DMC; atomic concentration of fluorine (19.9% for F1s) is about 10 times larger than those for the other two electrolyte solutions, as shown in Table 4.2. Based on these results, the strong B-F signal does not simply derive from a

residue of LiBF_4 , but results from decomposed products that has a different chemical composition from LiBF_4 and possesses the lower solubility in carbonate ester solvents.

$\text{O}1\text{s}$ spectra of graphite electrodes that are cycled in LiPF_6 - and LiFSI -containing electrolyte solutions are quite similar to one another, and the signals are attributed to organic compounds which mainly produced by solvent decomposition (Figure 4.10 (a)). As for the LiBF_4 electrolyte solution, a B-O bond is clearly observed in $\text{O}1\text{s}$ and $\text{B}1\text{s}$ spectra (Figure 4.10 (b)) in addition to the organic compounds. Oxygen derives only from the solvent decomposition in the $\text{Li} | \text{graphite}$ cell, and hence the product needs to react with LiBF_4 to form a B-O bond. Based on the SEM-EDX images (Figure 4.8) and by considering the $\text{F}1\text{s}$ and $\text{O}1\text{s}$ spectra (Figure 4.9), the particulate precipitates on graphite electrodes should contain both B-O and B-F bonds.

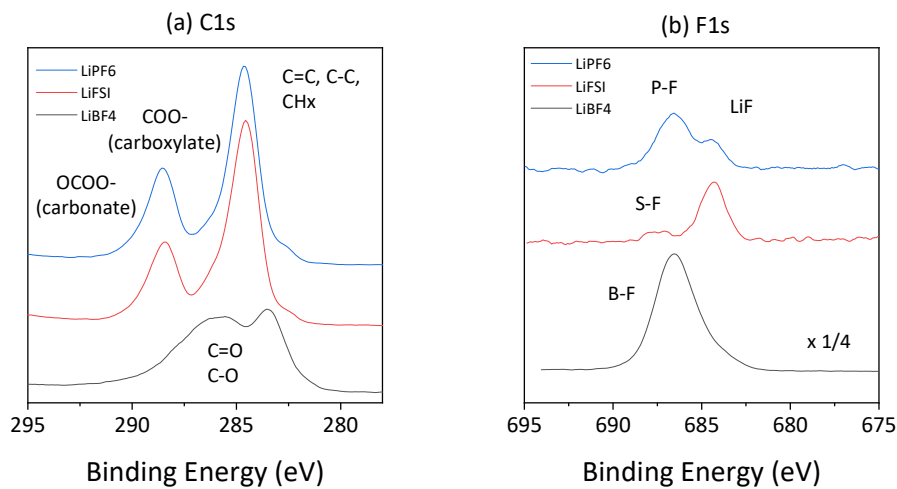


Figure 4.9 (a) $\text{C}1\text{s}$ and (b) $\text{F}1\text{s}$ spectra of graphite negative electrodes after the 3rd CV cycle.

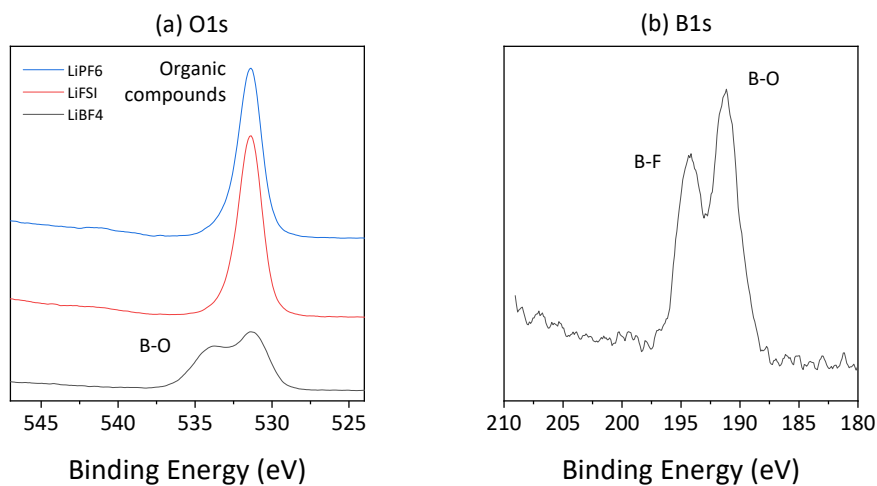


Figure 4.10 (a) O1s and (b) B1s spectra of graphite negative electrodes after the 3rd CV cycle.

Table 4.2 Surface atomic composition of graphite negative electrodes after three cycles between 2 and 0.01 V at 0.1 mV/s.

	(atomic %)								
	Li1s	B1s	C1s	N1s	O1s	F1s	P2p	S2p	Cl2p
LiPF ₆	16.2	–	46.8	–	33.0	2.3	0.7	–	1.0
LiFSI	15.7	–	44.3	1.5	33.3	1.6	–	2.7	0.9
LiBF ₄	22.9	7.4	29.7	–	20.2	19.9	–	–	–

Electron affinity and LUMO distribution predict that EC decomposition proceeds through CIP and/or free Li⁺-(EC)₄ ions in 1 mol/l LiBF₄ electrolyte solution to generate carbonate and carboxylate, as is the case in 1 mol/l LiPF₆ and LiFSI electrolyte

solutions. However, only a smaller amount of carbonate and carboxylate was detected and large particles containing F, O, and possibly B precipitated on the graphite surface. These results were not predicted by DFT calculations. Hence, subsequent reactions should be considered at a graphite electrode in 1 mol/l LiBF₄ electrolyte solution. It is reported that LiBF₄ decomposes to generate LiF and BF₃ through the following reaction

(4-4)^{35,37};

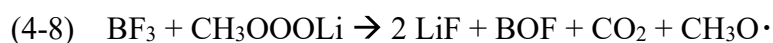
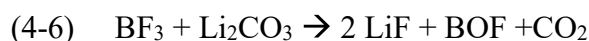


Because BF₃ is a highly reactive Lewis acid, it may easily react with Lewis bases, such as carbonate and carboxylate that dissolve in electrolyte solution and/or precipitate as SEI on the graphite surface. BF₃ is known to form stable carbonate solvent adducts³⁸, such as BF₃-EC, BF₃-DMC, and hence they can revert to LiBF₄ and a solvent by the following reaction (4-5).



Thus, the adducts are involved in equilibrium reactions, and BF₃ does not attack and decompose solvent molecules in the above reactions. It is also reported that BF₃ irreversibly reacts with carbonate and carboxylate in SEI through the following reactions (6), (7), and (8)³⁷. As these reactions proceed, BF₃ is consumed to promote the

reaction (4), and as a result carbonate and carboxylate decompose to form LiF, various gaseous compounds, and methoxy radical in reactions (4-6) - (4-8). Methoxy compounds, such as lithium methoxide, are often pointed out as one of the reaction intermediates in the reductive decomposition process of electrolyte solutions. It causes further decomposition of a carbonate solvent to produce C-O, and C=O bond containing compounds, which was detected by XPS (Figure 4.9 (a))^{39,40}.



BOF, boron fluoride oxide, is a gaseous compound, and hence the reactions (6) ~ (8) are one of the formation reactions of particulate compounds containing oxygen, fluoride, and a B-O bond. Chemical composition of these products is not clear, but they are likely to be inorganic materials, such as $\text{LiB}_x\text{F}_y\text{O}_z$ which is insoluble to carbonate solvents. Thus, carbonate and carboxylate in SEI are not stable in LiBF_4 -containing electrolyte solutions, and further decompose through acid-base reactions (6) ~ (8). The resultant coarse particles have a low protective capability as SEI, and therefore the decomposition reactions would continue interminably to increase the amount of precipitates.

The compositional change of SEI in 1 mol/l LiBF₄ electrolyte solution is verified by electrochemical ac impedance measurements (Figure 4.11). The kinetics of lithium ion transfer between a graphite surface and an electrolyte solution is influenced by two factors; one is solvent species, and the other is the composition of SEI on graphite negative electrodes^{41,42}. Because a mixture solvent system of EC and DEC (1:1, by vol.) is used commonly in this study, the impedance of lithium ion transfer depends on an SEI composition. Two semi-circles are observed in each Nyquist plot (Figure 4.11), assigned to a lithium ion transfer in SEI (R_{SEI}), and lithium ion transfer at graphite interface (R_{CT}). Lithium ion transport resistance in an electrolyte solution is determined at an intercept on a real axis of the semi-circle (designated as R_s). R_{SEI} and R_{CT} are evaluated by use of an equivalent circuit shown in Figure 4.11, and the fitting results are summarized in Table 4.3.

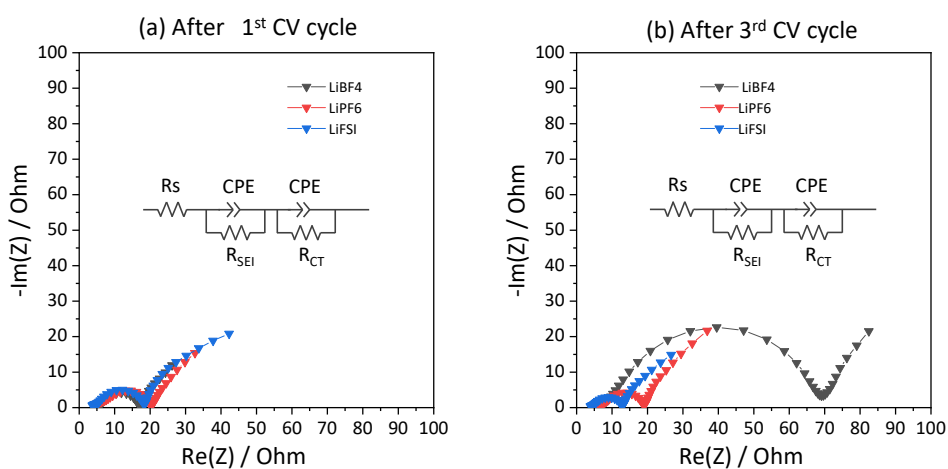


Figure 4.11 Nyquist plots of Li | graphite cells at 0.2 V after the 1st and 3rd CV cycle.

Table 4.3 Fitting results of Nyquist plots shown in Figure 4.11.

	1st cycle			3rd cycle		
	R_s (Ω)	R_{SEI} (Ω)	R_{CT} (Ω)	R_s (Ω)	R_{SEI} (Ω)	R_{CT} (Ω)
LiPF ₆	4.2	4.3	10.8	5.5	4.0	8.1
LiFSI	3.1	3.3	10.5	3.6	2.1	6.4
LiBF ₄	5.0	2.5	8.6	6.2	6.7	53.4

R_{SEI} and R_{CT} shows almost the same value after the initial CV cycle irrespective of electrolyte salt. These results indicate that SEI on the graphite surface possesses electrochemically similar characteristics. After two more cycles, the values of R_{SEI} and R_{CT} remain about the same for a LiPF₆-containing electrolyte solution, and decrease a little bit for LiFSI. As for LiPF₆, both the prediction by DFT calculation and the analyses by SEM-EDX and XPS consistently demonstrated the formation of LiF, carboxylate and carbonate. Such an inorganic/organic-component mixture flawlessly forms a protective SEI during the initial cycle, and thereby R_{SEI} and R_{CT} does not increase in Figure 4.11. On the other hand, the decrease in R_{SEI} and R_{CT} for 1 mol/l LiFSI electrolyte solution implies an increase in lithium-ion conductivity of SEI and that in an interfacial area for lithium ion transfer through SEI, respectively. FSI⁻ anion with a higher electron affinity preferentially decompose to generate LiF, as proved by DFT calculation, SEM-EDX, and XPS, but the inorganic particles cannot form a dense protective film. Accordingly, in the subsequent cycles, the fragmentary SEI is put

together by the formation of organic compounds such as carbonate and carboxylate through further decomposition of EC molecules in free $\text{Li}^+(\text{EC})_4$ ions. In fact, solvent-derived SEI shows higher lithium-ion conductivity than anion-derived one⁴³. Thus, the formation of dense SEI during the first several cycles result in a gradual decrease in R_{SEI} and R_{CT} . Impedance drastically increases during three CV cycles when LiBF_4 is used as an electrolyte salt, which is quite different behavior from those obtained for the other two electrolyte solutions. The increased R_{SEI} would be ascribed to the loss of organic precipitates in SEI, such as carbonate and carboxylate, and the formation of inorganic LiF and $\text{LiB}_x\text{F}_y\text{O}_z$ particles by the reactions (6) ~ (8). Such a sparse inorganic-rich SEI should show low lithium ion conductivity, and have low protective capability. Hence, further decomposition of the electrolyte solution occurs to increase R_{SEI} . In addition, these inorganic particles should cover the electrode active area to impede lithium ion transfer at an electrode/electrolyte solution interface. Therefore, both R_{SEI} and R_{CT} increased in the first three cycles in 1 mol/l LiBF_4 electrolyte solution. Thus, the compositional change of SEI was deduced from the changes in resistance in this study, while calculation of the time evolution in SEI composition by AIMD would also be the most promising candidate to deduce and reveal it in the future⁴⁴.

4.4. CONCLUSIONS

The composition of SEI that forms on negative electrodes is predicted by theoretical calculation of solvates of which the solvation structure is determined experimentally. The resultant electron affinity and LUMO distribution are used to predict reduction reactivity and reduction sites, respectively, of the solvates which constitute the electrolyte solutions. These prediction on SEI are proved experimentally by morphological observation by SEM-EDX, chemical composition analyses by XPS, and electrochemical characterization by impedance spectroscopy. 1 mol/l LiPF₆ and LiFSI electrolyte solutions form a surface film containing carboxylate, carbonate, and LiF, as is predicted by DFT calculation. On the other hand, as for 1 mol/l LiBF₄ electrolyte solution, the experimental results, including a specific increase in internal resistance of R_{SEI} and R_{CT} , can be explained by a theoretically predicted decomposition reaction followed by a subsequent acid-base reaction. Thus, the SEI formation mechanisms and its electrochemical properties are comprehensively understood by the appropriate combination of DFT prediction and experimental analyses at a laboratory level. These are quite effective approaches, and should be applicable to the effective survey of new electrolyte solvents, salts, additives, and their optimal concentrations.

REFERENCES

- [1] Goodenough, J. B.; Kim, Y. Challenges for Rechargeable Li Batteries. *Chem. Mater.* **2010**, *22*, 587–603.
- [2] Tarascon, J.-M.; Armand, M. Issues and Challenges Facing Rechargeable Lithium Batteries. *Nature* **2001**, *414*, 359–367.
- [3] Xu, K. Nonaqueous Liquid Electrolytes for Lithium-Based Rechargeable Batteries. *Chem. Rev.* **2004**, *104*, 4303–4417.
- [4] Verma, P.; Maire, P.; Novak, P. A Review of the Features and Analyses of the Solid Electrolyte Interphase in Li-Ion Batteries. *Electrochim. Acta* **2010**, *55*, 6332–6341.
- [5] Aurbach, D. Review of Selected Electrode–Solution Interactions which Determine the Performance of Li and Li Ion Batteries. *J. Power Sources* **2000**, *89*, 206–218.
- [6] Xu, K.; von Cresce, A. Interfacing Electrolytes with Electrodes in Li Ion Batteries. *J. Mater. Chem.* **2011**, *21*, 9849–9864.
- [7] Niehoff, P.; Passerini, S.; Winter, M. Interface Investigations of a Commercial Lithium Ion Battery Graphite Anode Material by Sputter Depth Profile X-ray Photoelectron Spectroscopy. *Langmuir* **2013**, *29*, 5806–5816.

[8] Schechter, A.; Aurbach, D.; Cohen, H. X-ray Photoelectron Spectroscopy Studies of Lithium Surfaces Prepared in Several Important Electrolyte Solutions. A Comparison with Previous Studies by Fourier Transform Infrared Spectroscopy *Langmuir* **1999**, *15*, 3334–3342.

[9] Marcus, Y.; Hefter, G. Ion Pairing. *Chem. Rev.* **2006**, *106*, 4585–4621.

[10] Self, J.; Wood, B. M.; Rajput, N. N.; Persson, K. A. The Interplay between Salt Association and the Dielectric Properties of Low Permittivity Electrolytes: The Case of LiPF₆ and LiAsF₆ in Dimethyl Carbonate, *J. Phys. Chem. C* **2018**, *122*, 1990-1994.

[11] Chapman, N.; Borodin, O.; Yoon, T.; Nguyen, C. C.; Lucht, B. L. Spectroscopic and Density Functional Theory Characterization of Common Lithium Salt Solvates in Carbonate Electrolytes for Lithium Batteries, *J. Phys. Chem. C* **2017**, *121*, 2135–2148.

[12] Hwang, S.; Kim, D. H.; Shin, J. H.; Jang, J. E.; Ahn, K. H.; Lee, C.; Lee, H. Ionic Conduction and Solution Structure in LiPF₆ and LiBF₄ Propylene Carbonate Electrolytes. *J. Phys. Chem. C* **2018**, *122*, 19438–19446.

[13] Delp, S. A.; Borodin, O.; Olguin, M.; Eisner, C. G.; Allen, J. L.; Jow, T. R. Importance of Reduction and Oxidation Stability of High Voltage Electrolytes and

Additives. *Electrochim. Acta.* **2016**, 209, 498–510.

[14] von Cresce, A.; Borodin, O.; Xu, K. Correlating Li⁺ Solvation Sheath Structure with Interphasial Chemistry on Graphite. *J. Phys. Chem. C* **2012**, 116, 26111–26117.

[15] Xu, K.; von Cresce, A. Interfacing Electrolytes with Electrodes in Li Ion Batteries. *J. Mater. Chem.* **2011**, 21, 9849–9864.

[16] von Cresce, A.; Xu, K. Preferential Solvation of Li⁺ Directs Formation of Interphase on Graphitic Anode. *Electrochem. Solid-State Lett.* **2011**, 14, A154–A156.

[17] Yamada, Y.; Koyama, Y.; Abe, T.; Ogumi, Z. Correlation between Charge–Discharge Behavior of Graphite and Solvation Structure of the Lithium Ion in Propylene Carbonate-Containing, Electrolytes. *J. Phys. Chem. C* **2009**, 113, 8948–8953.

[18] Winter, M. The Solid Electrolyte Interphase – The Most Important and the Least Understood Solid Electrolyte in Rechargeable Li Batteries. *Z. Phys. Chem.* **2009**, 223, 1395–1406.

[19] Aoki, Y.; Oda, S.; Oda, M.; Ogawa, M.; Ishihama, T.; Doi, T.; Inaba, M. Quantitative Analysis of Solid Electrolyte Interphase and Its Correlation with The Electrochemical Performance of Lithium Ion Batteries Using Concentrated

LiPF₆/Propylene Carbonate. *J. Electrochem. Soc.* **2021**, 168, 020530.

[20] Tateyama, Y. First-Principles Calculation Study on Solid Electrolyte Interphase (SEI) in Lithium Ion Battery. *J. Comput. Chem. Jpn.* **2019**, 18, 18-28.

[21] Sodeyama, K.; Yamada, Y.; Aikawa, K.; Yamada, A.; Tateyama, Y. Sacrificial Anion Reduction Mechanism for Electrochemical Stability Improvement in Highly Concentrated Li-Salt Electrolyte. *J. Phys. Chem. C* **2014**, 118, 14091-14097.

[22] Ushirogata, K.; Sodeyama, K.; Futera, Z.; Tateyama, Y.; Okuno, Y. Near-Shore Aggregation Mechanism of Electrolyte Decomposition Products to Explain Solid Electrolyte Interphase Formation. *J. Electrochem. Soc.* **2015**, 162, A2670-A2678.

[23] Seo, D. M.; Borodin, O.; Han, S. D.; Ly, Q.; Boyle, P. D.; Henderson, W. A. Electrolyte Solvation and Ionic Association I. Acetonitrile-Lithium Salt Mixtures: Intermediate and Highly Associated Salts. *J. Electrochem. Soc.* **2012**, 159, A553–A565.

[24] Seo, D. M.; Borodin, O.; Han, S.-D.; Boyle, P. D.; Henderson, W. A. Electrolyte Solvation and Ionic Association II. Acetonitrile-Lithium Salt Mixtures: Highly Dissociated Salts. *J. Electrochem. Soc.* **2012**, 159, A1489–A1500.

[25] Seo, D. M.; Borodin, O.; Balogh, D.; O’Connell, M.; Ly, Q.; Han, S. D.; Passerini,

S.; Henderson, W. A. Electrolyte Solvation and Ionic Association III. Acetonitrile-Lithium Salt Mixtures—Transport Properties. *J. Electrochem. Soc.* **2013**, 160, A1061-A1070.

[26] Wang, J.; Yamada, Y.; Sodeyama, K.; Chiang, C.; Tateyama, Y.; Yamada, A. Superconcentrated electrolytes for a high-voltage lithium-ion battery. *Nature Communications*. **2016**. 7:12032 DOI: 10.1038/ncomms12032.

[27] Morita, M.; Asai, Y.; Yoshimoto, N.; Ishikawa, M. A Raman spectroscopic study of organic electrolyte solutions based on binary solvent systems of ethylene carbonate with low viscosity solvents which dissolve different lithium salts. *J. Chem. Soc. Faraday Trans.* **1998**, 94, 3451-3456.

[28] Klassen, B.; Aroca, R.; Nazri, M.; Nazri, G. A. Raman Spectra and Transport Properties of Lithium Perchlorate in Ethylene Carbonate Based Binary Solvent Systems for Lithium Batteries. *J. Phys. Chem. B* **1998**, 102, 4795–4801.

[29] Seo, D.; Boyle, P.; Allen, J.; Han, D.; Jónsson, E.; Johansson, P.; Henderson, W. Solvate Structures and Computational/Spectroscopic Characterization of LiBF₄ Electrolytes. *J. Phys. Chem. C*, **2014**, 118, 18377–18386.

- [30] Yamada, Y.; Furukawa, K.; Sodeyama, K.; Kikuchi, K.; Yaegashi, M.; Tateyama, Y.; Yamada, A. Unusual Stability of Acetonitrile-Based Superconcentrated Electrolytes for Fast-Charging Lithium-Ion Batteries. *J. Am. Chem. Soc.* **2014**, 136, 5039-5046.
- [31] Wang, F.; Varenne, F.; Ortiz, D.; Pinzio, V.; Mostafavi, M.; Le Caër, S. Degradation of an Ethylene Carbonate/Diethyl Carbonate Mixture by Using Ionizing Radiation. *Chem. Phys. Chem.* **2017**, 18, 2799-2806.
- [32] Aoki, Y.; Oda, M.; Kojima, S.; Ishihama, T.; Nagashima, T.; Doi, T.; Inaba, M. Predictive Characterization of SEI Formed on Graphite Negative Electrodes for Efficiently Designing Effective Electrolyte Solutions. *ACS Appl. Energy Mater.* **2022**, 5, 1085-1094.
- [33] Goodenough, J. B. Evolution of Strategies for Modern Rechargeable Batteries. *Acc. Chem. Res.* **2013**, 46, 1053-1061.
- [34] Okuno, Y.; Ushirogata, K.; Sodeyama, K.; Tateyama, Y. Decomposition of the fluoroethylene carbonate additive and the glue effect of lithium fluoride products for the solid electrolyte interphase: an ab initio study. *Phys. Chem. Chem. Phys.* **2016**, 18, 8643-8653.

[35] Aurbach, D.; Markovsky, B.; Shechter, A.; Ein-Eli, Y.; Cohen, H. A Comparative Study of Synthetic Graphite and Li Electrodes in Electrolyte Solutions Based on Ethylene Carbonate-Dimethyl Carbonate Mixtures. *J. Electrochem. Soc.* **1996**, 143, 3809-3820.

[36] Self, J.; Fong, D.; Persson, A. Transport in Superconcentrated LiPF₆ and LiBF₄/Propylene Carbonate Electrolytes. *ACS Energy Lett.* **2019**, 4, 2843–2849.

[37] Andersson, A.; Herstedt, M.; Bishop, A.; Edstrom, K. The influence of lithium salt on the interfacial reactions controlling the thermal stability of graphite anodes, *Electrochimica Acta.* **2002**, 47, 1885-1898.

[38] Eisele, L.; Laszczynski, N.; Schneider, M.; Lucht, B.; Krossing, I. Preparation of BF₃ Carbonates and their Electrochemical Investigation as Additives in Lithium Ion Batteries. *J. Electrochem. Soc.*, **2020**, 167, 060514.

[39] Gachot, G.; Ribiere, P.; Mathiron, D.; Grugeon, S.; Armand, M.; Leriche, J. B.; Pilard, S.; Laruelle, S. Gas Chromatography/Mass Spectrometry As a Suitable Tool for the Li-Ion Battery Electrolyte Degradation Mechanisms Study. *Anal. Chem.* **2011**, 83, 478–485

[40] Electrolyte decomposition and solid electrolyte interphase revealed by mass spectrometry. Fang, C.; Tran, T-N.; Zhao, Y; Liu, G. *Electrochimica Acta*. **2021**, 399, 139362

[41] Yamada, Y.; Iriyama, Y.; Abe, T.; Ogumi, Z. Kinetics of Lithium Ion Transfer at the Interface between Graphite and Liquid Electrolytes: Effects of Solvent and Surface Film. *Langmuir* **2009**, 25, 12766-12770.

[42] Xu, K.; von Cresce, A.; Lee, U. Differentiating Contributions to “Ion Transfer” Barrier from Interphasial Resistance and Li⁺ Desolvation at Electrolyte/Graphite Interface. *Langmuir*. **2010**, 26, 11538–11543.

[43] Benitez, L.; Seminario, J. SEI Ion Diffusivity through the Solid Electrolyte Interphase in Lithium-Ion Batteries. *J. Electrochem. Soc.*, **2017**, 164, E3159-E3170

Chapter 5

General conclusions and publication list

5.1 General conclusions

In Chapter 2, we have established the qualitative and quantitative analysis of surface film formed on the electrode, and it was confirmed that those results can be correlated with electrochemical performance, such as irreversible capacity, and interfacial resistance. The charge and discharge performance of graphite negative and $\text{LiNi}_{0.5}\text{Co}_{0.2}\text{Mn}_{0.3}\text{O}_2$ (NCM523) positive electrodes in highly concentrated 4.45 mol/kg LiPF_6/PC electrolyte solution was investigated to clarify the chemical species in the surface film formed on both electrode surfaces, and compared with those obtained with conventional 1 mol/l $\text{LiPF}_6/\text{EC} + \text{DMC}$ electrolyte solution. For the graphite negative electrode, the total electrons consumed to form surface film was well correlated with irreversible capacity, and total mole number and chemical species of the surface film

were also correlated with interfacial resistance. In the conventional electrolyte solution, the reductive decomposition of solvents progressed preferentially, while LiPF_6 decomposed to form surface film in the concentrated electrolyte solution. While both organic- and inorganic-based surface films can achieve high coulombic efficiency and high capacity retention over charge/discharge cycles, the inorganic-based surface film resulted in a significant increase in interfacial resistance. As for the NCM523 positive electrode in the concentrated electrolyte solution, the formation of inorganic-based surface film and a remarkable increase in interfacial resistance were observed clearly, as with the graphite electrode. However, there was no direct correlation among mole number of chemical species in surface films formed, their chemical composition and interfacial resistance. The increase in interfacial resistance is estimated due to the crystal structural changes proceeded at the surface of NCM523.

In chapter 3, solid electrolyte interphase (SEI) formed on graphite in highly concentrated electrolyte solutions was thoroughly characterized by a combined experimental and computational study. The comprehensive understanding revealed that a chemical composition of SEI, as well as the chemical species unstable to reduction, can be predicted by a profound understanding of density functional theory (DFT) calculation results of the solvates containing a counter anion. Highly concentrated

LiPF₆/carbonate ester electrolyte solutions were prepared using two kinds of carbonate ester solvents to obtain quite different types of SEI and different charge/discharge behavior of graphite negative electrodes. The solvation structures were determined by Raman spectroscopy to evaluate electron affinity and LUMO of the solvates containing a PF₆⁻ anion by DFT calculation. The chemical composition of SEI was quantitatively analyzed by X-ray photoelectron spectroscopy (XPS), and the results were consistent with a prediction based on the calculation. In addition, the stability of the SEI against reduction was clarified by correlating the chemical composition with the charge/discharge behavior. These results indicate that electrolyte solutions can be efficiently designed by predicting the physicochemical properties of SEI through the more effective utilization of DFT calculation.

In chapter 4, we have tried to verify the validity of the approaches established in chapter 2 and 3. Here, we have applied them to confirm the dependence on electrolyte salts. Solvation structures of ethylene carbonate (EC)-based electrolyte solutions containing 1 mol/l LiPF₆, LiN(SO₂F)₂ (LiFSI), or LiBF₄ are experimentally determined, and their electron affinity and LUMO distribution are calculated by Density Functional Theory (DFT). The stability of electrolyte solutions against reduction can be evaluated using electron affinity of the solvates, and the formation mechanism of solid electrolyte

interphase (SEI) can be predicted by their LUMO distributions. The calculation results suggest that 1 mol/l LiPF_6 and LiFSI electrolyte solutions should form SEI consisting of carbonate and carboxylate which derives from solvent decomposition, and LiF originating from anion decomposition. These predictions are verified experimentally by SEM-EDX and XPS measurements. On the other hand, intriguingly, the reductive decomposition of 1 mol/l LiBF_4 electrolyte solution does not simply proceed as theoretically predicted, and the subsequent reactions of SEI need to be considered; further decomposition of the organic SEI and formation of inorganic particles containing lithium, fluoride, oxygen, and boron. These results are consistent with an increase in resistances of SEI and interfacial lithium ion transfer at graphite negative electrode. Thus, a combination of DFT prediction and experimental analysis is proved to be a effective approach to reveal SEI formation mechanisms, and can be utilized as a versatile approach to develop new solvents, electrolyte salts, and additives, and to design electrolyte solutions with appropriate concentration.

5.2 Future perspectives

In this study, the reduction and decomposition reactions that proceed at the negative electrode were mainly investigated, and it was shown that a combination of experiments and theoretical calculations can provide a lot of insight on the reaction at the interphase of electrolyte solution and electrodes. It is expected that the oxidative stability and reaction mechanism of electrolyte solutions at the positive electrode should be estimated using similar approaches. In Chapter 2, we have shown that extraction and surface analyses conducted on negative electrodes can be performed experimentally also on positive electrode, and it will be interesting to interpret the results combining with theoretical calculations. Here, it is necessary to predict oxidation stability using ionization potentials rather than electron affinity used for reduction stability. In the same way, other solvents than carbonate, such as ethers and sulfones, which have been difficult to put into practical use in conventional electrolytes, can also be the target to be studied. By analyzing the solvation structure and estimating its chemical stability, we believe it will be possible to get many insights on the reactions that proceed at the interface between the electrode and the electrolyte.

5.2 Publication list

Chapter 2

Quantitative analysis of solid electrolyte interphase and its correlation with the electrochemical performance of lithium ion batteries using concentrated LiPF₆/propylene carbonate, Yasuhito Aoki, Shiho Oda, Mami Oda, Miyuki Ogawa, Taihei Ishihama, Takayuki Doi, and Minoru Inaba, *J. Electrochem. Soc.* 168 020530 (2019)

Chapter 3

Predictive characterization of SEI formed on graphite negative electrodes for efficiently designing an effective electrolyte solutions, Yasuhito Aoki, Mami Oda, Sachiko Kojima, Taihei Ishihama, Tsuyoshi Nagashima, Takayuki Doi, and Minoru Inaba, *ACS Appl. Energy Mater.*, 5, 1085 (2022)

Chapter 4

Effective approach by computational chemical prediction and experimental verification to elucidate SEI formation mechanism in LiPF₆, LiFSI and LiBF₄-containing electrolyte solutions, Yasuhito Aoki, Mami Oda, Sachiko Kojima, Yu Yamaga, Taihei Ishihama, Tsuyoshi Nagashima, Takayuki Doi, and Minoru Inaba, *J. Phys. Chem. C.*, 127, 69 (2023)

5.3 Other published works by the author

- S₁-S₀ vibronic spectra of benzene clusters revisited. II. The trimer, Toshifumi Iimori, Yasuhito Aoki, and Yasuhiro Ohshima, *J. Chem. Phys.* 117, 3675 (2002)
- Influence of humidification on deterioration of gas diffusivity in catalyst layer on polymer electrolyte fuel cell, Yusuke Hiramitsu, Hitoshi Sato, Hiroyuki Hosomi, Yasuhito Aoki, Takahiro Harada, Yoko Sakiyama, Yoshitsugu Nakagawa, Kenji

Kobayashi, Michio Hori, *J. Power Sources*, 195, 435 (2010)

- Thermal stability and kinetics of delithiated LiCoO₂, Yoshitomo Furushima, Chika Yanagisawa, Takeshi Nakagawa, Yasuhito Aoki, Naoki Muraki, *J. Power Sources*, 196, 2260 (2011)
- Safety characteristics of chemically delithiated cathode active material, Yasuhito Aoki, Chika Yanagisawa, Takeshi Nakagawa, Yoshitomo Furushima, Yuichi Hasegawa, Mami Oda, *ECS Transaction*. 69, 47 (2015)
- Electrochemical lithiation performance and characterization of silicon-graphite composites with lithium, sodium, potassium, and ammonium polyacrylate binders, Zhen-Ji Han, Kiyofumi Yamagiwa, Naoaki Yabuuchi, Jin-Young Son, Yi-Tao Cui, Hiroshi Oji, Akinori Kogure, Takahiro Harada, Sumihisa Ishikawa, Yasuhito Aoki, Shinichi Komaba, *Phys. Chem. Chem. Phys.*, 17, 3783 (2015)
- Effect of water on solid electrolyte interphase formation in Li-ion batteries, Masahiro Saito, Manabu Fujita, Yasuhito Aoki, Masanobu Yoshikawa, Keisuke Yasuda, Ryoya Ishigami, Yoshinori Nakata, *Nuclear Instruments and Methods in Physics Research B*, 371, 273 (2016)
- Chemical and structural changes of 70 Li₂S-30 P₂S₅ solid electrolyte during heat treatment, Yasuhito Aoki, Kengo Ogawa, Takeshi Nakagawa, Yuichi Hasegawa, Yoko Sakiyama, Toshikatsu Kojima, Mitsuharu Tabuchi, *Solid State Ionics*, 310, 50 (2017)
- Physicochemical Features of Fluorinated Ethyl Acetate-Based Highly Concentrated Electrolyte Solutions and Their Effects on Electrochemical Properties of LiNi_{0.8}Co_{0.1}Mn_{0.1}O₂ Positive Electrodes, Takayuki Doi, Ryo Fujii, Yasuhito Aoki, Tsuyoshi Nagashima, Kyosuke Takehara, and Minoru Inaba, *J. Phys. Chem. C*, 125, 12578 (2021)
- Effective formation of superior surface films on Si negative electrodes in highly concentrated fluorinated carbonate ester solvent/diluent electrolyte solution system, Ryo Okada, Yasuhito Aoki, Mami Oda, Mahiro Nakazawa, Minoru Inaba, and Takayuki Doi, *ACS Appl. Energy Mater.*, 6, 546 (2023).

Those two works above were conducted with members in Professor Doi's group.

- The Possibility of Intermediate-Temperature (120 °C)-Operated Polymer Electrolyte Fuel Cells using Perfluorosulfonic Acid Polymer Membranes, Katsuyoshi Kakinuma, Hitoshi Taniguchi, Takayuki Asakawa, Toshihiro Miyao, Makoto Uchida, Yasuhito Aoki, Tsuyoshi Akiyama, Akihiro Masuda, Nobuyuki Sato, Akihiro Iiyama, *J. Electrochem. Soc.*, 169, 044522 (2022)

Acknowledgements

This thesis is a compilation of studies on electrochemical stability of electrolyte solutions with various solvents and electrolyte salts and their concentration, which was carried out by the author under the supervision of Professor Minoru Inaba and Takayuki Doi at Department of Molecular Chemistry and Biochemistry, Doshisha University during 2020 – 2022.

The author wishes to express his hearty gratitude to Professor Minoru Inaba for his warm and continuous supports, instructions and encouragements throughout the course of the present work in spite of the extreme difficulties in running the lab under the pandemic of Covid19. The author also wishes to express his sincere thanks to Professor Takayuki Doi for his guidance on how to conduct academic research as a corporate researcher, based on his deep knowledge and experience in electrochemistry. Their guidance gave me an opportunity to reconfirm the basic attitude as a researcher. The author is greatly indebted to Professor Yoshifumi Kimura and Professor Takuya Goto, Graduate School of Engineering, Doshisha University for their helpful comments and discussions.

The author is grateful to all members of Professor Inaba's laboratory, especially to Professor Doi's group members, Mr. Taihei Ishihama, Mr. Tsuyoshi Nagashima for their excellent contributions to this work.

Furthermore, the author gratefully acknowledges to Senior Vice President of Toray Research Center Inc., Dr. Masanobu Yoshikawa, General Managers, Dr. Hirofumi Seki, Dr. Keiko Matsuda. The author shows his great gratitude to them for their continuous support to conduct my research in parallel with my work. The author also would like to thank Ms. Mami Oda, Ms. Sachiko Kojima, Ms. Miyuki Ogawa, and Ms. Yu Yamaga of Toray Research Center for their great supports and advices in promoting my work.

Finally, the author would like to give special thanks to his wife and his sons and his parents for their continuous encouragements. This thesis could never have been completed without their assistance and supports

Yasuhito Aoki

March 2023